USGS
science for a changing world

Prepared in cooperation with the Department of the Navy, Naval Facilities Engineering Command, Northwest

Variable-Density Groundwater Flow and Contaminant Transport, Operable Unit 1, Naval Base Kitsap, Keyport, Washington

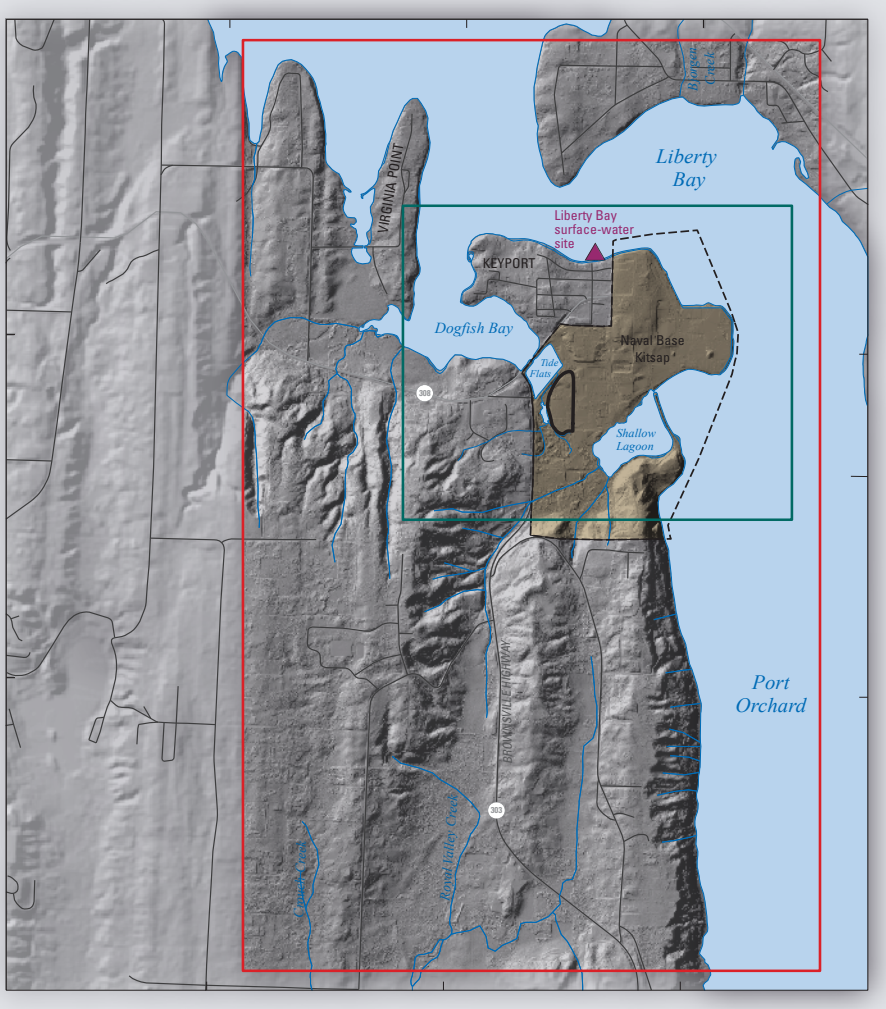

Scientific Investigation Report 2020-5066

U.S. Department of the Interior
U.S. Geological Survey

Cover: Map showing location of study area topography and surface drainage, transport domain and Operable Unit 1, Naval Base Kitsap, Keyport, Washington.

Variable-Density Groundwater Flow and Contaminant Transport, Operable Unit 1, Naval Base Kitsap, Keyport, Washington

By Richard M. Yager, Wendy B. Welch, Alexander Headman, and Richard S. Dinicola

Prepared in cooperation with the Department of the Navy, Naval Facilities Engineering Command, Northwest

Scientific Investigations Report 2020–5066

U.S. Department of the Interior
U.S. Geological Survey

U.S. Department of the Interior
DAVID BERNHARDT, Secretary

U.S. Geological Survey
James F. Reilly II, Director

U.S. Geological Survey, Reston, Virginia: 2020

For more information on the USGS—the Federal source for science about the Earth, its natural and living resources, natural hazards, and the environment—visit https://www.usgs.gov or call 1–888–ASK–USGS.

For an overview of USGS information products, including maps, imagery, and publications, visit https://store.usgs.gov/.

Any use of trade, firm, or product names is for descriptive purposes only and does not imply endorsement by the U.S. Government.

Although this information product, for the most part, is in the public domain, it also may contain copyrighted materials as noted in the text. Permission to reproduce copyrighted items must be secured from the copyright owner.

Suggested citation:
Yager, R.M., Welch, W.B., Headman, A., and Dinicola, R.S., 2020, Variable-density groundwater flow and contaminant transport, Operable Unit 1, Naval Base Kitsap, Keyport, Washington: U.S. Geological Survey Scientific Investigations Report 2020–5066, 58 p., https://doi.org/10.3133/sir20205066.

ISSN 2328-0328 (online)

Acknowledgments

The authors acknowledge Carlotta Cellucci (Remedial Project Manager for Naval Facilities Engineering Command, Northwest) and Michael Meyer (Battelle Memorial Institute) for their assistance in providing historical reports and data to U.S. Geological Survey authors. We thank Chuck Heywood and Eric Swain (U.S. Geological Survey) for comments and discussions that sharpened our thinking and presentation.

This page left intentionally blank

Contents

Figures

Tables

Conversion Factors

U.S. customary units to International System of Units

Multiply	By	To obtain
	Length	
inch (in.)	2.54	centimeter (cm)
foot (ft)	0.3048	meter (m)
mile (mi)	1.609	kilometer (km)
	Area	
acre	0.4047	hectare (ha)
square foot (ft^2)	0.09290	square meter (m^2)
square mile (mi^2)	2.590	square kilometer (km^2)
	Volume	
gallon (gal)	3.785	liter (L)
gallon (gal)	0.003785	cubic meter (m^3)
cubic foot (ft^3)	0.02832	cubic meter (m^3)
	Flow rate	
foot per second (ft/s)	0.3048	meter per second (m/s)
foot per day (ft/d)	0.3048	meter per day (m/d)
cubic foot per second (ft^3/s)	0.02832	cubic meter per second (m^3/s)
cubic foot per day (ft^3/d)	0.02832	cubic meter per day (m^3/d)
gallon per minute (gal/min)	0.06309	liter per second (L/s)
gallon per day (gal/d)	0.003785	cubic meter per day (m^3/d)

	Mass	
ounce, avoirdupois (oz)	28.35	gram (g)
pound, avoirdupois (lb)	0.4536	kilogram (kg)
ton, short (2,000 lb)	0.9072	metric ton (t)
ton, long (2,240 lb)	1.016	metric ton (t)
	Density	
pound per cubic foot (lb/ft^3)	16.02	kilogram per cubic meter (kg/m^3)
pound per cubic foot (lb/ft^3)	0.01602	gram per cubic centimeter (g/cm^3)
	Hydraulic conductivity	
foot per day (ft/d)	0.3048	meter per day (m/d)
	Hydraulic gradient	
foot per mile (ft/mi)	0.1894	meter per kilometer (m/km)
	Transmissivity	
foot squared per day (ft^2/d)	0.09290	meter squared per day (m^2/d)

Temperature in degrees Celsius (°C) may be converted to degrees Fahrenheit (°F) as:

$$°F = (1.8 \times °C) + 32.$$

Temperature in degrees Fahrenheit (°F) may be converted to degrees Celsius (°C) as:

$$°C = (°F - 32) / 1.8.$$

Datums

Vertical coordinate information is referenced to the North American Vertical Datum of 1988 (NAVD 88).

Horizontal coordinate information is referenced to North American Datum of 1983 (NAD 83).

Altitude, as used in this report, refers to distance above the vertical datum.

Supplemental Information

Specific conductance is given in microsiemens per centimeter at 25 degrees Celsius (µS/cm at 25 °C).

Concentrations of chemical constituents in water are given in either milligrams per liter (mg/L) or micrograms per liter (µg/L).

Abbreviations

1,1-DCA	1,1-dichloroethane
1,1-DCE	1,1-dichloroethene
1,1,1-TCA	1,1,1-trichloroethane
CA	chloroethane
CVOC	chlorinated volatile organic compounds
DOD	U.S. Department of Defense
EPA	U.S. Environmental Protection Agency
FD	finite difference
PCE	tetrachloroethene
ppm	parts per million
SWB	soil water balance
TCE	chloroethene compounds trichloroethene
cis-DCE	cis-1,2-dichloroethene
trans-DCE	trans-1,2-dichloroethene
TVD	total-variation-diminishing
USGS	U.S. Geological Survey
VC	vinyl chloride

Variable-Density Groundwater Flow and Contaminant Transport, Operable Unit 1, Naval Base Kitsap, Keyport, Washington

By Richard M. Yager, Wendy B. Welch, Alexander Headman, and Richard S. Dinicola

Abstract

Chlorinated volatile organic compounds (CVOCs) have migrated to groundwater beneath a former 9-acre landfill at Operable Unit 1 (OU-1) on Naval Base Kitsap, which was active from the 1930s through 1973 on the Keyport Peninsula, in Kitsap County, Washington. Biodegradation of CVOCs at OU-1 limits the mass of dissolved-phase CVOCs in groundwater that discharges to surface water, but contaminant concentrations up to 630 milligrams per liter persist in localized areas, likely from the dissolution of residual, non-aqueous phase liquids. Variable-density groundwater-flow and contaminant-transport models were developed using the SEAWAT-Version 4 computer program to simulate the direction and rate of groundwater flow in a 5.9 square-mile (mi^2) - area surrounding the Keyport Peninsula, to estimate the CVOC mass in groundwater and the rate of mass loading, and to assess possible remedial activities at OU-1.

The study area is underlain by Quaternary deposits consisting of alternating glacial and interglacial sediments ranging from 500 to 1,500 feet (ft) thick. A hydrogeologic model delineated a sequence of 10 units including a relatively thin package (less than 100 ft) of recent sediments (Vashon Stade and younger) beneath the Keyport Peninsula that are underlain by the much thicker (more than 300 ft) Clover Park Aquitard, which overlies a confined, sea-level aquifer.

A shallow lagoon, tide flats, marsh (including a pond and outlet creek), and Dogfish Bay (a segment of Liberty Bay connected to Puget Sound) adjacent to OU-1 are the principal areas of groundwater discharge. Water levels in these surface-water bodies fluctuate in response to semi-diurnal tidal cycles. Daily ranges in water-level fluctuations range from 10.5 ft in Dogfish Bay to 0.5 ft in the marsh. Groundwater-level response to tidal fluctuations in and near OU-1 is as much as 7.3 ft.

Three-dimensional (3D), constant-density groundwater flow was simulated using MODFLOW-2005 and MODFLOW-NWT models that were run alternately in an iterative sequence to converge on a common numerical solution. MODFLOW-2005 employed the HUF2 package to represent thin, discontinuous hydrogeologic units beneath OU-1, and the aquifer system was treated as confined to obtain the numerical solution for hydraulic head. MODFLOW-NWT was employed to obtain a hydraulic head distribution while treating the aquifer system as unconfined, but it does not support the HUF2 package. The water table computed by the MODFLOW-NWT model was used to specify as inactive the model cells in the MODFLOW-2005 model that were above the simulated water table, thereby reducing the saturated thickness in the confined simulation.

The groundwater-flow model utilized a variably spaced grid with 15 model layers, 120 rows, and 88 columns; cell widths ranged from 25 ft near OU-1 to 500 ft near model boundaries. Ten model layers of equal thickness represent the Quaternary Vashon Stade or younger deposits, while the bottom four model layers represents the Clover Park Aquitard and deeper units. The top model layer represents surface water. The groundwater-flow simulation included a steady-state period that provided initial conditions to a 31-day transient period that represented approximately 30 tidal cycles. Tidal fluctuations in seawater were approximated by a diurnal function that ranged from a single low-tide stage to a high-tide stage, corrected for the specific gravity of seawater. Water levels in the tide flats and the marsh pond and its outlet were specified as the average high, low, and mean levels measured during July and August 2018.

Model boundaries coincide with the grid of a previously developed regional Kitsap Peninsula groundwater-flow model, which was used to set head and flow boundaries in model layers representing the permeable interbeds within the Clover Park Aquitard and an underlying aquifer. Hydraulic heads at model boundaries within the Quaternary Vashon sediments were assigned to maintain the simulated water table below land surface. Groundwater discharge to surface water and groundwater withdrawals from deep wells were represented as internal boundaries, and net outflow from shallow groundwater withdrawals and infiltration from septic systems was included in the estimated recharge values. Recharge values computed by a Soil-Water Balance (SWB) model for the model domain were adjusted during model calibration.

Two alternative models (A and B) with differing storage properties were constructed to assess the ramifications of representing changes in storage from the fluctuating water

with the confined numerical model. In Model A, a specific storage (S_s) value of 2.0×10^{-6} ft^{-1} was assigned to all hydrogeologic units, while in Model B, the S_s value of the uppermost unit (Qvr sediments) was increased to 0.1 to approximate an unconfined storage value associated with specific yield. A multiplicative scaling factor based on the Qvr unit thickness was applied in Model B to reduce the S_s values where the unit spanned multiple model layers. Unconfined storage near the water table at OU-1 was underestimated in Model A and overestimated in Model B.

Values of hydraulic conductivities and recharge were adjusted in both models A and B during calibration to match 99 observations of 4 types of data: groundwater levels (69), water-level fluctuations in wells in response to tides (26), vertical hydraulic gradients (3) and streamflow (1). Pseudo water-table altitudes computed by MODFLOW-NWT were also specified at 23 upland locations. Observation weights accounted for differences in units or ranges of measurements such that the observations were weighted equally. Parameter values were initially estimated in the confined transient MODFLOW-2005 Model And then updated in the unconfined steady-state MODFLOW-NWT model. The MODFLOW-NWT water table was then used to update inactive model cells in the MODFLOW-2005 simulation, and parameter estimation was reapplied. This procedure was continued until the volumetric water budgets of both simulations were nearly equal.

A total of 24 parameter values were specified, of which 15 were estimated through nonlinear regression using UCODE in Model A and 16 were estimated in Model B. The remaining parameters were estimated through trial and error or assigned from literature values. The average recharge rate computed by the SWB model (16.7 inches per year [in/yr]) was reduced to 4.2 in/yr in Model A (comparable to the rate of 4 in/yr estimated for the northern part of the Kitsap groundwater-flow model) and 6.7 in/yr in Model B. This difference indicates that the SWB model likely overestimates recharge in uplands where relatively permeable soils at land surface are underlain by lower permeability sediments at depth. In these areas, infiltration through the soil profile likely discharges as interflow to local drainage, rather than entering the groundwater-flow system.

The standard error in model fit in both models A and B was similar for groundwater levels and pseudo water-table altitudes (7.8 and 11.1 ft, respectively), but better for water-level fluctuations in Model A (1.0 ft) than in Model B (1.3 ft). The directions of the three vertical hydraulic-gradient observations were simulated correctly, with errors ranging from 25 to 66 percent, but simulated base flow to a perennial stream 70 percent less than the measured value in Model A and 40 percent less in Model B. The simulated hydraulic-head distribution in both models indicates that OU-1 is just north of a regional discharge area that limits groundwater flow from the landfill toward uplands located south and west of the tide flats and the marsh. Simulated vertical groundwater flow is downward beneath the uplands and upward beneath the lowlands and surface-water bodies.

Two SEAWAT simulations of steady-state, variable-density flow and transient solute transport were conducted for both models A and B in a 1.3 mi^2 domain surrounding the Keyport Peninsula. A 5,000-yr simulation with a single solute (seawater) established the initial distribution of seawater for a 50-year simulation with two solutes (seawater and CVOCs). Both simulations used the design and parameter distributions from the corresponding groundwater-flow model. The transport model domain extends from surface water to the upper part of the Clover Park Aquitard.

Seawater concentrations in both transport simulations ranged from 0 percent for fresh water (specific gravity 1.0) to 100 percent for seawater (specific gravity 1.022). Constant-concentration boundaries were specified in model layer 1 to represent seawater. An implicit finite-difference (FD) method with upstream weighting was used in the single-solute simulation which has 100-day time steps in the 5,000-year simulation. The predicted distributions of seawater equilibrated and the simulated transition zone between fresh water and seawater was about 100 ft wide near the tide flats west of OU-1 in Model A, where saline water overlies fresh water at shallow depths, and 125 ft in Model B.

Inflow of CVOCs at OU-1 was represented in dual-solute simulations through mass-loading rates (MT^{-1}) at seven persistent contaminant sources, adjusted to reproduce the maximum observed CVOC concentrations in 2017. The expected biodegradation of CVOCs, initially neglected in the transport simulation, was addressed in an alternative transport simulation. The total-variation-diminishing (TVD) method was used to minimize numerical dispersion using 0.5-day time steps in the 50-yr simulation. The predicted CVOC plume stabilized at a contaminant mass of 256 kilograms (kg) and a mass-loading rate of 150 grams per day (g/d) in Model A. Most of the contaminant mass (134 g/d) discharged to small creeks draining the southern edge of OU-1, while the remainder discharged to the marsh and tide flats. A northern plume with 30 percent of the CVOC mass migrated toward the marsh pond and creek, and a southern plume with 70 percent of the mass that migrated toward small creeks south of OU-1. The predicted CVOC mass was 310 kg with a mass-loading rate of 73 g/d in Model B, in which groundwater flow through deeper sediments beneath OU-1 was restricted by higher vertical anisotropy. The two contaminant plumes intermingled and were diverted westward to Dogfish Bay by higher hydraulic conductivity values in Model B, and less CVOC mass (48 g/d) discharged to the small creeks and more mass discharged to the marsh pond and creek (7.8 g/d) and the tide flats (160 mg/d).

Results of groundwater-flow and contaminant-transport simulations in both models A and B indicate that geologic and hydraulic barriers limit the migration of CVOCs from the former landfill at OU-1, including the low-permeability Clover Park Aquitard, upward hydraulic gradients beneath the Keyport Peninsula, underflow from upland areas south of OU-1, and the density difference between fresh and saline water beneath the tide flats and in Dogfish Bay. Uncertainty

in the rates of recharge and hydraulic properties produces uncertainty in the estimated mass-loading rate of CVOCs at OU-1. Higher rates of recharge and groundwater flow require larger mass-loading rates to maintain a stable configuration of the contaminant plume.

Reductive dechlorination of CVOCs at OU-1 was represented in an alternative 50-yr transport simulation using a first-order, removal rate-constant of 10^{-3} d^{-1} that corresponds to a half-life of 850 days, as computed from the CVOC contaminant mass (256 kg) predicted by the transport simulation with Model B and an estimated biodegradation rate (150 g/d). A stable 77-kg CVOC plume formed within 10 years of migration, and one half of the CVOC mass was lost through biodegradation (75 g/d). Nearly all the remainder (71 g/d) was discharged by the southern plume to a small creek south of OU-1. The areas of the northern and southern plumes were 67 percent and 32 percent less, respectively, than the areas computed by the original transport simulation.

Both models A and B provide an adequate fit to hydraulic and contaminant data, but additional data are required to determine which model more accurately predicts actual contaminant migration at OU-1. Both models predict similar contaminant masses and biodegradation rate constants. Model predictions differ in terms of some of the hydraulic parameters and in the CVOC mass-loading rates and contaminant plume configurations. While Model B better represents the effects of tidal fluctuations on unconfined storage and uses recharge rates closer to the SWB estimated rates, Model A better predicts the groundwater-level response to tidal fluctuations.

Two alternative 50-yr, contaminant-transport simulations with Model A assessed the sensitivity of predicted CVOC migration to the depiction of tidal fluctuations. Mean tides were lowered in seawater, the tide flats, and Marsh Creek in a 50-yr steady-state simulation with the total-variation-diminishing (TVD) solver to match average water levels measured during July and August 2018. Diurnal tidal fluctuations were also represented in a 50-yr transient simulation with the finite difference solver that computed 600 repetitions of a 31.05-day transient period. Both alternative representations of tidal fluctuations had a small effect on the simulated CVOC plumes, because the period of the fluctuations (12 hr) is rapid compared with the groundwater velocity (20 ft/yr) beneath OU-1, so tidal fluctuations only slightly alter groundwater-flow paths.

Three 50-yr, steady-state contaminant-transport simulations with Model A predicted the effects of potential source-control scenarios on the contaminant plumes by reducing CVOC mass-loading rates by factors of 50, 90, and 99 percent, respectively. Under each scenario the mass of CVOCs decreased rapidly and then slowly approached a new dynamic equilibrium. The reductions of CVOC mass in groundwater were 46, 86, and 95 percent, respectively, but sizes of the contaminant plumes were largely unchanged.

Introduction

Chlorinated volatile organic compounds (CVOCs) have migrated to groundwater beneath a former 9-acre landfill at Operable Unit 1 (OU-1) of Naval Base Kitsap in Kitsap County, Washington. Naval Base Kitsap is located on the Keyport Peninsula, which protrudes into an extension of Puget Sound called Liberty Bay (fig. 1). The three predominant groundwater contaminants are the chloroethene compounds trichloroethene (TCE), cis-1,2-dichloroethene (cis-DCE), and vinyl chloride (VC); six other contaminants of concern include the chloroethene and chloroethane compounds tetrachloroethene (PCE), trans-1,2-dichloroethene (trans-DCE), 1,1,1-trichloroethane (1,1,1-TCA), 1,1-dichloroethane (1,1-DCA), chloroethane (CA) and 1,1-dichloroethene (1,1-DCE). Recently another solvent 1-4 dioxane was also detected at the site (Department of the Navy, 2015). A need for remedial action was identified because some of the contaminants present a potential risk to humans, primarily through drinking contaminated groundwater or through ingesting seafood harvested from contaminated surface water (URS Consultants, Inc., 1998).

The U.S. Navy began a cooperative effort with the U.S. Geological Survey (USGS) in 1995 to evaluate the effectiveness of natural attenuation processes for removing and controlling the migration of CVOCs in groundwater at OU-1 through field and laboratory studies conducted from 1996 through 2000 (Dinicola and others, 2002). Additional collection of geochemical and contaminant concentration data was conducted by the USGS from 2001 through 2004 (Dinicola, 2006). The USGS studies demonstrated that biodegradation of CVOCs in shallow groundwater at OU-1 is substantial and prevents most of the mass of dissolved-phase CVOCs in groundwater beneath the landfill from discharging to surface water (Dinicola, 2006). However, dissolved-phase contaminant concentrations in the hundreds of milligrams per liter continue to persist in localized areas of OU-1. These data indicate that residual sources of chloroethenes in the form of non-aqueous phase liquid remain at the site, and that biodegradation is only partly effective at reducing the dissolved-phase contaminants that are generated from these sources.

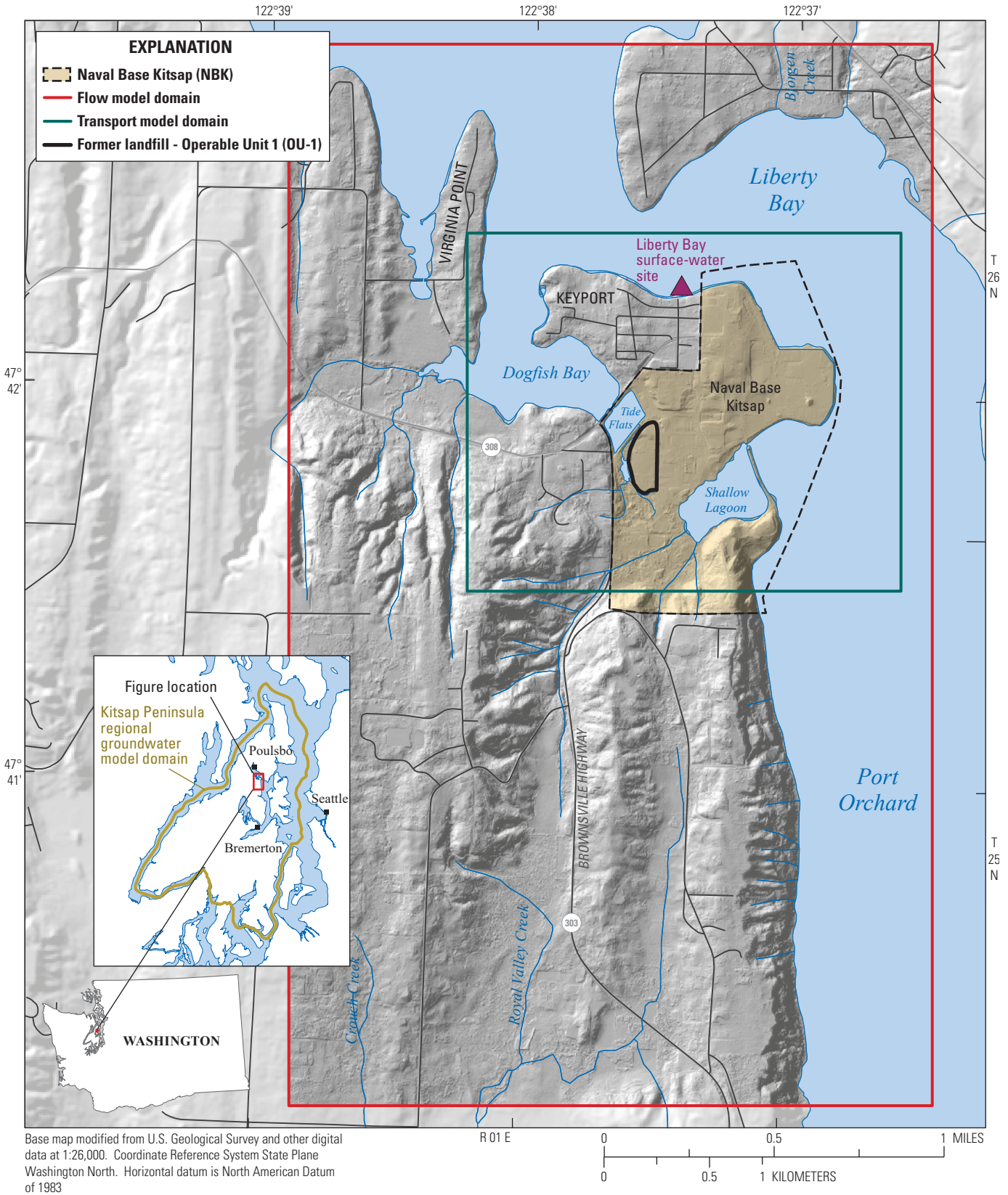

Base map modified from U.S. Geological Survey and other digital data at 1:26,000. Coordinate Reference System State Plane Washington North. Horizontal datum is North American Datum of 1983

Figure 1. Location of study area showing topography and surface drainage, transport domain and Operable Unit 1, Naval Base Kitsap, Keyport, Washington.

In 2018, an additional USGS effort was begun to simulate variable-density groundwater flow and contaminant transport in the vicinity of OU-1 using a revised hydrogeologic model of the site and a refined delineation of persistent contaminant sources, based on data collected by the U.S. Navy in 2016 and 2017 (Battelle Memorial Institute, 2018). The groundwater flow and contaminant transport models were developed using SEAWAT-Version 4, a computer program based on MODFLOW and MT3DMS to simulate three-dimensional, variable-density groundwater flow coupled with multi-species solute transport (Langevin and others, 2007). These models were used to simulate the direction and rate of groundwater flow near OU-1, estimate the CVOC mass in groundwater and the rate of mass loading, and assess possible remedial activities at OU-1. Additional tasks were undertaken in support of the model development, including measurements of the timing and magnitude of water-level changes in response to tides and estimates of groundwater recharge on and around the Keyport Peninsula.

Purpose and Scope

This report describes the hydrogeology in the vicinity of the Keyport Peninsula, including a discussion of the surficial geology and the hydrologic setting. The report includes generalized geologic sections that show the principal hydrogeologic units that underlie the study area. The report also presents measured water-level changes in response to tides and the estimation of groundwater recharge using the Soil Water-Balance (SWB) model (Westenbroek and others, 2010). The report documents the design and calibration of a three-dimensional, groundwater-flow model that was used to simulate the pattern and rate of groundwater flow and to estimate values of hydraulic properties of the hydrogeologic units that control the flow of groundwater. The report also documents the design of variable-density, groundwater flow and contaminant transport models that were used to simulate the migration of CVOCs from localized sources at OU-1. Applications of additional model simulations are presented to show the effects of tidal fluctuations and biodegradation on the migration of CVOCs. Finally, applications of model simulations are presented that predict the fate of contaminants at OU-1 after three hypothesized reductions of localized sources through potential remedial activities.

Previous Studies

Geologic, water-level, and contaminant-concentration data are available from site characterization studies and long-term monitoring conducted for the U.S. Navy using direct-push and auger drilling and groundwater sampling from monitoring wells (Department of the Navy, 2015; Battelle Memorial Institute, 2018). CVOC mass-degradation rates and fluxes to surface water were calculated by Dinicola and others (2002) and Dinicola (2006) from contaminant concentrations and water-level contour maps. A three-dimensional characterization of hydraulic head and groundwater flow rates in the 575 square mile (mi^2) area surrounding the Keyport Peninsula is available from a steady-state, numerical groundwater-flow model of the Kitsap Peninsula developed by Frans and Olsen (2016).

Contaminant History

The landfill at OU-1 is on the narrow strip of land connecting the Keyport Peninsula to the mainland and is adjacent to tide flats that are an extension of Dogfish Bay, which is a segment of Liberty Bay (figs. 1 and 2). The OU-1 landfill is unlined at the bottom and was constructed in a marsh. The landfill was the primary disposal area for domestic and industrial wastes generated by Naval Base Kitsap from the 1930s through 1973. Paints, thinners, solvents, acids, dried sludge from a wastewater-treatment plant, and other industrial wastes were disposed in the landfill (Department of the Navy, 1993).

The most concentrated disposal area for waste paints and solvents was at the southern end of the landfill where the maximum total CVOC concentrations in groundwater were over 100 milligrams per liter (mg/L) in 2017 (fig. 3). The term "total CVOCs," as used in this report, is the sum of the positively detected concentrations (in either mass or moles per unit volume) of six chloroethene and three chloroethane compounds of concern at OU-1. Total CVOC concentrations were less, but still over 10 mg/L in the central part of the landfill in 2017. Results from long-term monitoring indicate that the extent of the CVOC plume in groundwater at OU-1 has been relatively stable, and that a phytoremediation remedy employed at both the northern and southern ends of the landfill has not been as effective as originally anticipated (Department of the Navy, 2015). Non-aqueous phase liquids in the subsurface are assumed responsible for both the persistence and magnitude of CVOC concentrations in these "hotspots," locations where CVOC concentrations are substantially higher than in surrounding areas. Additional characterization of the hotspots in 2017 through vertical profiling using direct-push sampling revealed maximum CVOC concentrations of 630 mg/L as much as 28 ft below land surface in the southern part of OU-1, and 120 mg/L more than 15 ft below land surface in the central part of OU-1.

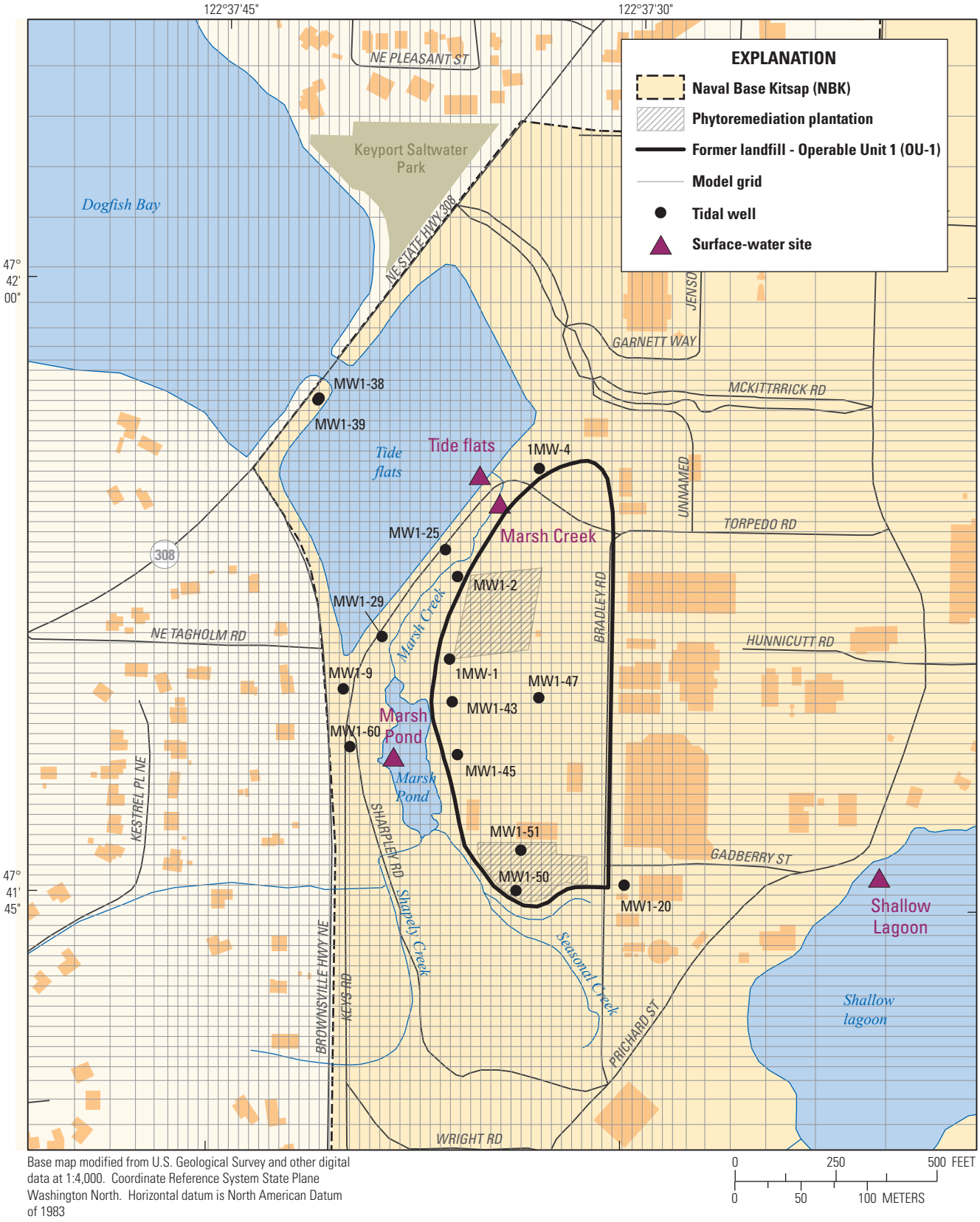

Base map modified from U.S. Geological Survey and other digital data at 1:4,000. Coordinate Reference System State Plane Washington North. Horizontal datum is North American Datum of 1983

Figure 2. Locations of former landfill and data-collection sites used to monitor tidal fluctuations at Operable Unit 1, Naval Base Kitsap, Keyport, Washington.

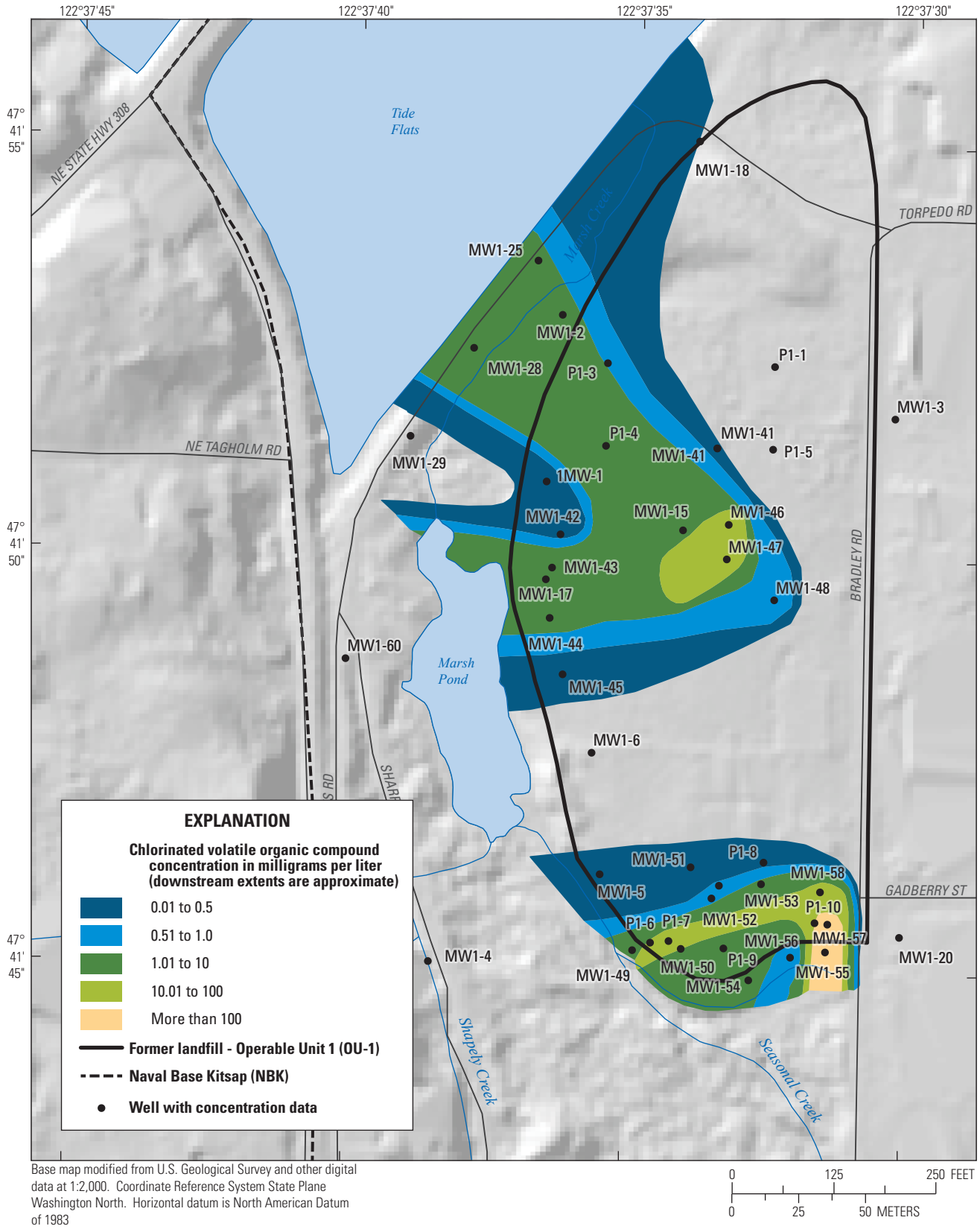

Figure 3. Generalized extent of total concentrations of chlorinated volatile organic compounds (CVOCs) in groundwater at Operable Unit 1, Naval Base Kitsap, Keyport, Washington, 2004, and locations of persistent hotspots in 2017. [Concentrations reflect the likely maximums expected at any depth based on 2017 data (Battelle Memorial Institute, 2018).]

Description of Study Area

Groundwater flow was simulated in a 5.9 mi² area surrounding the Keyport Peninsula extending from Liberty Bay to the uplands 2 mi south of the peninsula. The area includes Virginia Point, a residential area with domestic wells located 0.6 mi northwest of OU-1 across Dogfish Bay. Study area boundaries were delineated to coincide with the model grid of the Kitsap Peninsula used by Frans and Olsen (2016), so simulated groundwater levels from their model could be used to set boundary conditions for the Keyport models. Variable-density groundwater flow and contaminant transport was simulated within a smaller 1.3 mi² transport domain within the larger 5.9 mi² study area that is centered on OU-1 and surrounds the Keyport Peninsula (fig. 1).

Geologic Setting

A summary of the major Quaternary events on the Kitsap Peninsula surrounding Naval Base Kitsap is given below and is based on the work of Garling and others (1965), Vaccaro and others (1998), Jones (1999) and Welch and others (2014). Plate tectonics and Pleistocene glaciations are the two major processes that have shaped the present-day Puget Lowland. The advance and retreat of continental glaciers in the Pleistocene Epoch of the Quaternary Period beginning over 100,000 years ago left behind as much as 3,000 ft of unconsolidated deposits in the Puget Lowland with 500–1,500 ft of unconsolidated deposits commonly found beneath the Kitsap Peninsula. Underlying these unconsolidated deposits are Tertiary bedrock units consisting primarily of sedimentary claystone, siltstone, sandstone, beds of coal, and volcanic rocks.

The Puget Lobe of the Cordilleran ice sheet advanced and retreated several times into the Puget Lowland from the mountains of British Columbia since the beginning of the Quaternary Period and left behind a complex sequence of alternating glacial and interglacial sediments. The Vashon Stade of the Fraser Glaciation (12,000–18,000 years ago) was the most recent and extensive of the major advances that covered the Kitsap Peninsula. The sequence of glacial deposits in each glacial interval typically contains advance outwash sand and gravels, overlain by glacial till (poorly sorted mixture of indurated clay, silt, sand and gravel) and covered by recessional outwash sand and gravels. Each major glacial interval was followed by an extended interglacial period where fluvial, lacustrine, bog and marsh deposition dominated. Interglacial deposits typically consist of clay, silt, or discontinuous lenses of sand and gravel or peat. Since the end of the last glaciation, erosion has been the dominant geomorphic process affecting the Kitsap Peninsula. Alluvial sediments, typically sands and gravels, have been deposited by streams in valleys and marsh deposits formed in low-lying poorly drained areas.

Hydrogeologic Units

For this study, unconsolidated deposits were described by a hydrogeologic model that grouped the deposits into ten hydrogeologic units consisting of aquifers and confining units (table 1; figs. 4 and 5) that were based on lithologic (depositional facies, grain size, and sorting) and hydrologic characteristics, and relative stratigraphic position. Generally, in the Puget lowland, saturated glacial outwash or coarse-grained interglacial deposits form aquifers, whereas deposits such as till and fine-grained interglacial deposits form confining units. The hydrogeologic units defined in this study are similar to units defined by previous investigations of the Kitsap Peninsula (Welch and others, 2014) and the Keyport Peninsula (URS Consultants Inc., 1997); however, they have been reinterpreted for this study, and the extents or thicknesses of individual units are not directly comparable. Drillers' logs for wells containing descriptions of lithology were the primary source of information for the definition of hydrogeologic units in the vicinity of the Keyport Peninsula. The hydrogeologic analysis was conducted using a geographic information system (GIS) that included locations and lithologic information for more than 300 wells, surficial hydrogeology from Welch and others (2014), and lidar-derived digital land-surface altitudes.

Unit 1. Unit 1 is present at land surface and is primarily composed of Vashon recessional outwash (Qvr), artificial fill and topsoil found near OU-1, and surficial alluvial deposits. This unit consists of silt, sand, and gravel deposits that closely follow river valleys and the shoreline, as well as modified land/artificial fill composed of heterogeneous material ranging from clay to gravel and trash. The average thickness of Unit 1 throughout the study area is about 8 ft and is 10 ft beneath OU-1.

Unit 2. Unit 2 consists of recent marsh and estuary deposits (Qm) which are composed of uncompacted silt or silty sand that generally underlie Unit 1 and are distinguished in drillers' logs by dark organic material. Unit 2 extends from Dogfish Bay, underlies the tide flats and OU-1, and extends eastward beneath the shallow lagoon. The average thickness of Unit 2 throughout the study area is 14 ft and is 6 ft beneath OU-1. Unit 2 was divided into marsh (Qmarsh) and estuary (Qestuary) units for the purpose of estimating hydraulic conductivity in model calibration.

Unit 3. Unit 3 is present at land surface throughout much of the study area and consists primarily of Vashon till (Qvt). The till is a dense mix of sand and gravel in a clay matrix. Unit 3 mantles the hilltops south of the Keyport Peninsula and is not present at OU-1. The average thickness of Unit 3 throughout the study area is 32 ft but varies spatially from a thin veneer on hilltops to more than 150 ft near Port Orchard.

Unit 4. Unit 4 primarily consists of Vashon advance outwash (Qva). Unit 4 is found beneath Unit 3 throughout the study area and is exposed at land surface along coastal bluffs and hillsides. It consists of well-sorted sand or sand

Table 1. Hydrogeologic units defined in this study and correlation between hydrogeologic units and model layers of the Keyport and Kitsap groundwater flow models and previous investigations.

[**U.S. Geological Survey Kitsap Model**: From Welch and others (2014). **Stratigraphic units**: From URS Consultants, Inc., 1997, table 3-2. **Abbreviations:** —, not applicable]

Keyport model (this report)			U.S. Geological Survey Kitsap model	Stratigraphic units
Transport model	**Flow model**	**Hydrogeologic model**	**Hydrogeologic units**	**Unit identifier and hydrostatigraphy**
Layer 1–Water	Layer 1–Water	—	—	—
Layer 2–11 Qv sediments	Layer 2–11 Qv sediments	Unit 1 (Qvr, fill)	Qvr, Vashon recessional aquifer	A, fill and topsoil Er, recessional aquifer
		Unit 2 (Qm)		B, marsh C, estuary
		Unit 3 (Qvt)	Qvt, Vashon till confining unit	Et, Vashon till
		Unit 4 (Qva)		Ea, Upper aquifer H1, Upper aquifer
		Unit 5 (Qvsemi)	Qva, Vashon advance aquifer	H2, middle aquitard
		Unit 6 (Qvinter)		H4, intermediate aquifer Jo, intermediate aquifer
Layer 12	Layer 12	Unit 7 (QC1up)	QC1, upper confining unit	Km, Clover Park aquitard
—	Layer 13	Unit 8 (QC1pi)	QC1pi, permeable interbeds	Ks, Clover Park coarse-grained zone
	Layer 14	Unit 9 (QC1low)	QC1, upper confining unit	Km, Clover Park aquitard
	Layer 15	Unit 10 (QA1)	QA1, sea-level aquifer	—

and gravel with lenses of silt and clay. The average thickness of Unit 4 throughout the study area is 40 ft but is only 6 ft beneath OU-1.

Unit 5. Unit 5 is a laterally discontinuous sandy silt with some clay (Qvsemi) that only occurs in the area surrounding OU-1. Unit 5 forms a semi-confining layer between Units 4 and 6 that can only be distinguished from those units by its finer grain size. The average thickness of Unit 4 throughout the study area is 8 ft and is 6 ft beneath OU-1.

Unit 6. Unit 6 consists of sand, gravel, and silt deposits (Qvinter) in the area surrounding OU-1 that overlies a continuous clay layer known locally as the Clover Park Aquitard, Lawton Clay (Battelle Memorial Institute, 2017) or QC1 (Welch and others, 2014). The average thickness of Unit 6 throughout the study area is 12 ft and is 11 ft beneath OU-1.

Units 7, 8 and 9. The Clover Park Aquitard is divided into three parts: the upper clay (Unit 7), the permeable interbeds (Unit 8), and the lower clay (Unit 9). Units 7 and 9 (QC1) are thick and laterally extensive consisting of early Vashon, low-permeability lacustrine silt and clay and underlying interglacial fine-grained deposits. Units 7 and 9 are present throughout the study area with average thicknesses of 232 ft and 121 ft beneath OU-1 for Unit 7, and average thicknesses of 92 ft and 60 ft within OU-1 for Unit 9. The permeable interbeds (QCpi) in Unit 8 are locally continuous deposits of sand and gravel that lie between Units 7 and 9 (fig. 6). The average thickness of Unit 8 where it exists in the study area is 65 ft.

Unit 10. Unit 10 is a confined aquifer commonly referred to as the sea-level aquifer (QA1) or Salmon Springs Drift (Welch and others, 2014) that is present beneath most of study area. Unit 10 consists primarily of sand and gravel with silt interbeds and is the lowermost unit represented in the groundwater-flow model.

Hydrologic Setting

The topography of the study area indicates that surface water in the northern two-thirds of the area drains northward to Liberty Bay, while the southern third drains southward to Royal Valley and Crouch Creek (fig. 1). Steep bluffs border the eastern edge of the study area along Port Orchard where groundwater discharges through springs at discrete locations. Groundwater level data are sparse in the uplands, but the direction of groundwater flow probably parallels the direction of surface-water drainage. A small perennial stream drains part of the uplands to a shallow lagoon on the east side of the Keyport Peninsula.

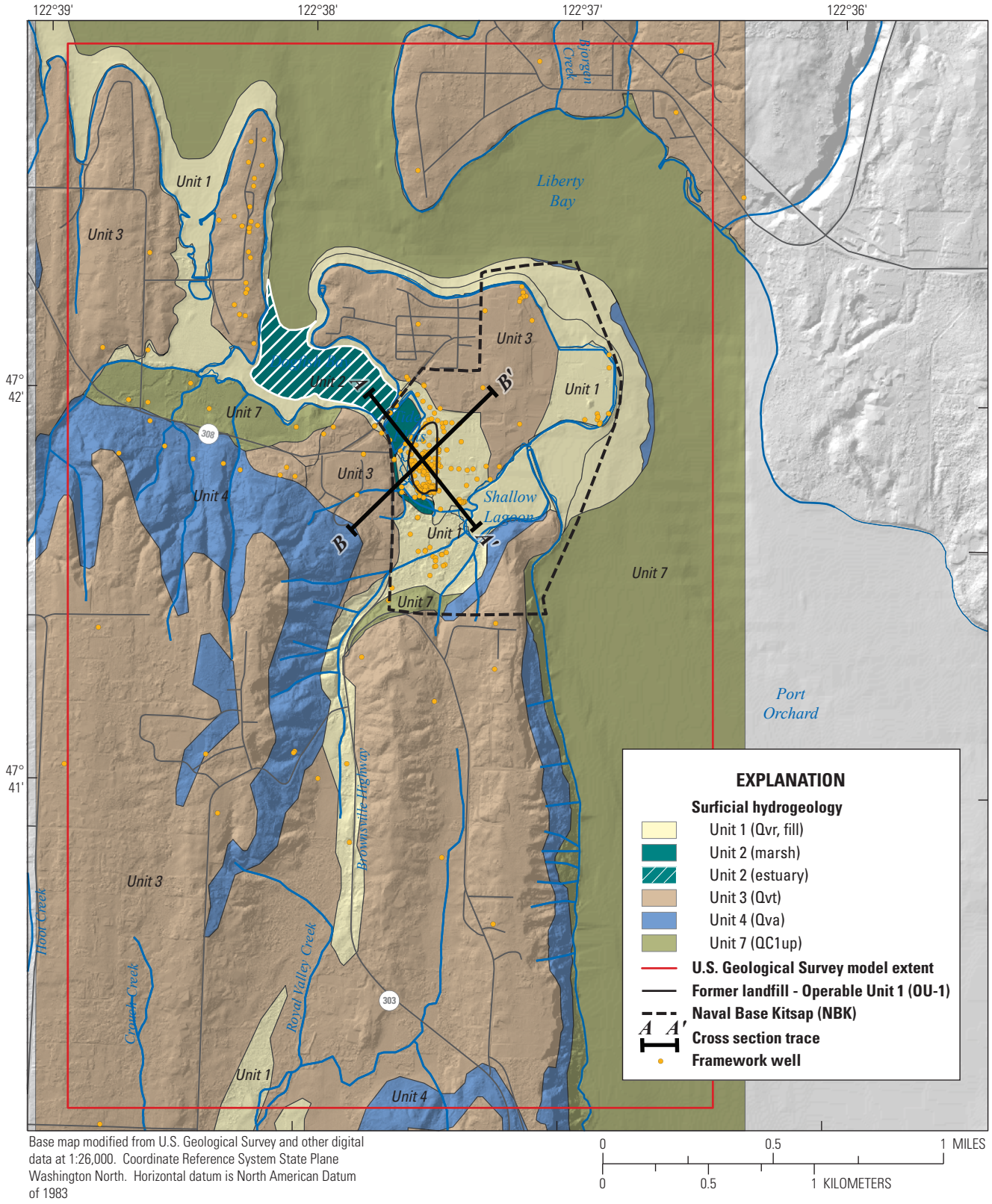

Figure 4. Surficial hydrogeology, cross section traces, and framework well locations near Operable Unit 1, Naval Base Kitsap, Keyport, Washington.

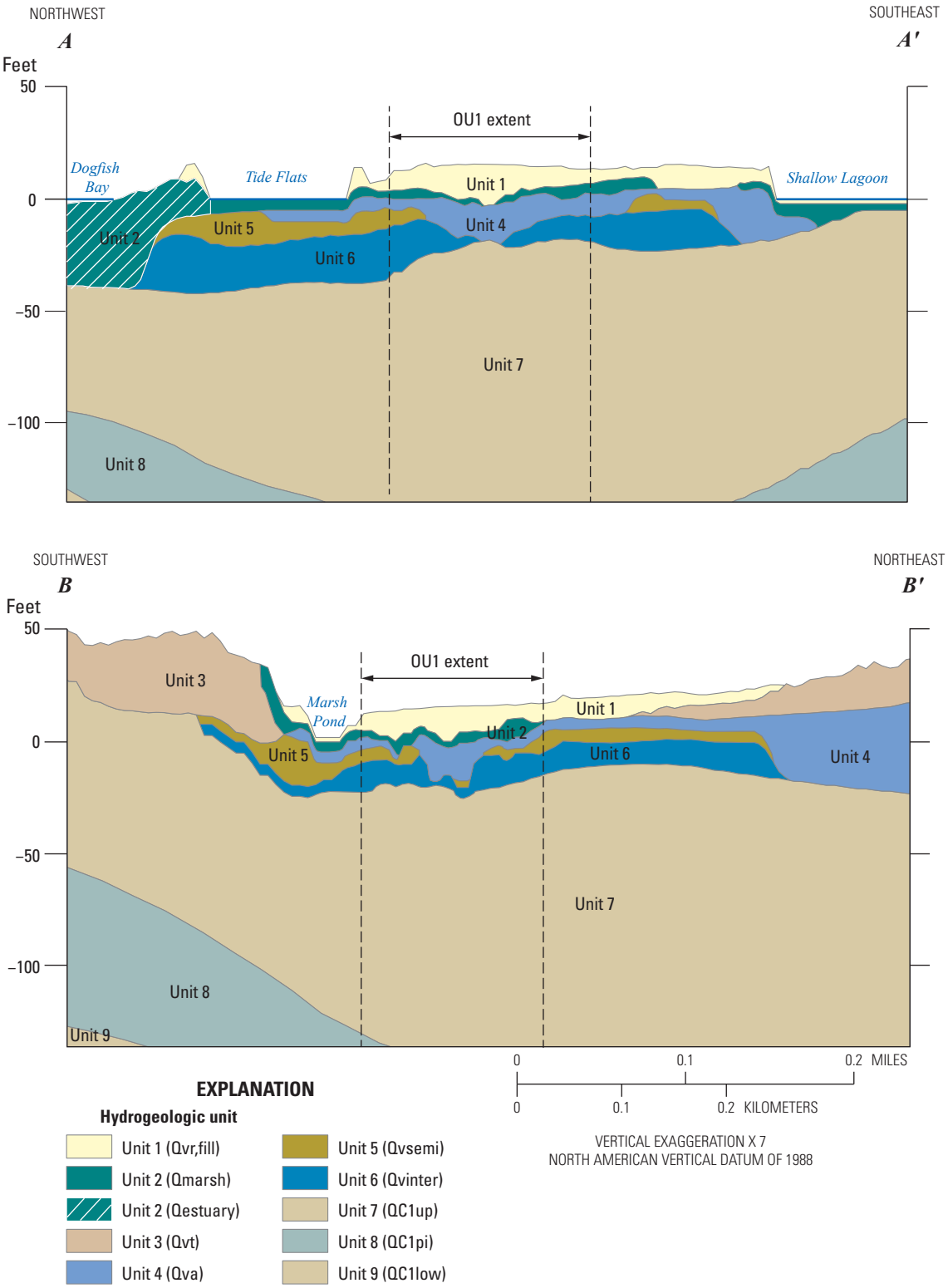

Figure 5. Generalized geologic sections near Operable Unit 1, Naval Base Kitsap, Keyport, Washington.

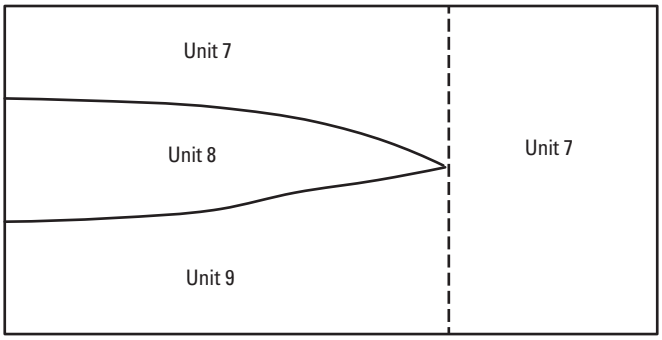

Figure 6. Relationship between Units 7, 8, and 9 beneath Operable Unit 1, Naval Base Kitsap, Keyport, Washington.

Two creeks flow into the marsh where the Keyport Peninsula connects to the mainland. A single perennial creek (referred to as Marsh Creek) drains a perennial pond in the marsh and discharges into the tide flats of Dogfish Bay (fig. 2). Marsh Creek flows through a culvert and tide gate and into the tide flats. Water exchange between the tide flats and Dogfish Bay is constrained by a weir in the State Route 308 causeway that has a sill elevation of 0.3 ft. During high tides, water levels in the tide flats are at the same water-level altitude as Dogfish Bay, but during low tides the water level in Dogfish Bay is lower than the sill elevation and the water level in the tide flats. Also, the tide gate at Marsh Creek outlet automatically closes during higher tides and prevents seawater from flowing upstream beyond the marsh pond, resulting in a higher water level in the tide flats than in the marsh. During periods of no surface-water runoff, there is perennial freshwater inflow into the marsh derived from groundwater discharge.

The shallow lagoon, the marsh (including the pond and associated creeks), the tide flats, and Dogfish Bay are the principal areas of groundwater discharge near OU-1. Shallow groundwater at OU-1 originates as recharge from precipitation that falls on OU-1, in addition to lateral flows from the Keyport Peninsula to the northeast and from the Kitsap Peninsula uplands to the southwest, and vertical flow from the underlying aquifer of Unit 10 (QA1). Groundwater level data collected by the Navy and USGS (Welch and others, 2014; URS Consultants Inc., 1998) indicate that groundwater flow northeast of OU-1 converges with flow from the southwest, and then flows beneath the landfill toward the marsh. Some groundwater discharges to the shallow lagoon southeast of OU-1, but the flow divide between discharge areas in the marsh and shallow lagoon is located to the southeast of OU-1. In general, hydraulic gradients indicate groundwater flow is vertically downward beneath most of the Kitsap Peninsula and the uplands to the southwest, and flow is upward beneath the Keyport Peninsula and marsh. Deep wells drilled below the Clover Park Aquitard (QC1) for Navy and public supplies were reported to be artesian.

Water-Level Response to Tidal Fluctuations

The water-level response to tidal fluctuations in the vicinity of OU-1 was measured by Opatz and Dinicola (2019) to determine optimal times to sample groundwater flowing from the landfill. Groundwater and surface-water levels were measured at 19 monitoring wells and 5 adjacent surface-water sites to provide 15-min time-series data from July 12, 2018, to August 8, 2018, a period that included both neap and spring tides. Data from 15 of those wells and all 5 surface-water sites were used during model calibration (figs. 1 and 2). The five surface-water sites included Liberty Bay on the north side of the Keyport Peninsula, the tide flats, the pond in the marsh and its outlet creek, and the shallow lagoon.

Daily tidal fluctuations in Liberty Bay follow a semi-diurnal pattern that includes two high tides and two low tides each day, with a higher and lower high tide and a higher and lower low tide (fig. 7). The sequence of the high-high, low-high, high-low, and low-low tides within a tidal cycle changes over the course of a year. The means of the high-high tides and the low-low tides were computed from the 2017 predicted tides for Liberty Bay (National Oceanic and Atmospheric Administration [NOAA] station 9445719 at Poulsbo, Washington; fig. 1;National Oceanic and Atmospheric Administration, 2020), and were corrected to the North American Vertical Datum of 1988 (NAVD88) datum at the site (Opatz and Dinicola, 2019) for comparison to surface water and groundwater levels near the Keyport Peninsula. The mean high-high tide in Liberty Bay was 7.94 ft NAVD88 and the mean low-low tide was -2.54 ft, resulting in a mean range of 10.53 ft. The mean tide in Liberty Bay in 2017 was 5.24 ft NAVD88.

Water-level data for surface-water bodies near the Keyport Peninsula (fig. 8) indicate that the daily tidal fluctuation in Liberty Bay ranged from 9 to 16 ft during the observed period. The daily tidal cycle had a mean length of 24.84 hr. The semi-diurnal tidal pattern was reflected in water-levels measured in the tide flats and Marsh Creek, with the minimum water level in the tide flats restricted to 0.3 ft by the sill that connects the tide flats to Dogfish Bay, yielding a daily water-level fluctuation range in the tide flats of only 7–8 ft. The daily range in water-level fluctuation in Marsh Creek was only about 1.5 ft, and the water level in the marsh pond showed less than 0.5 ft fluctuations in response to tides around a mean pond elevation of 6.0 ft. The water-level response to tides in the shallow lagoon was greatly attenuated by a sill at the lagoon outlet and was only discernible at the highest tides.

Groundwater-level response to tidal fluctuations at the 19 monitoring wells ranged from 7.3 ft at MW1-39 to 0.1 ft at MW1-50 and MW1-51 (table 2). Four wells (MW1-10, MW1-20, MW1-41, and P1-10) exhibited a groundwater-level response to tidal fluctuations less than 0.1 ft. The lag in groundwater-level response ranged from 15 min at MW1-39 to 255 min at MW1-50, with the lag time increasing with diminishing groundwater-level response (fig. 9). Groundwater-level data collected at high and low tides during a previous

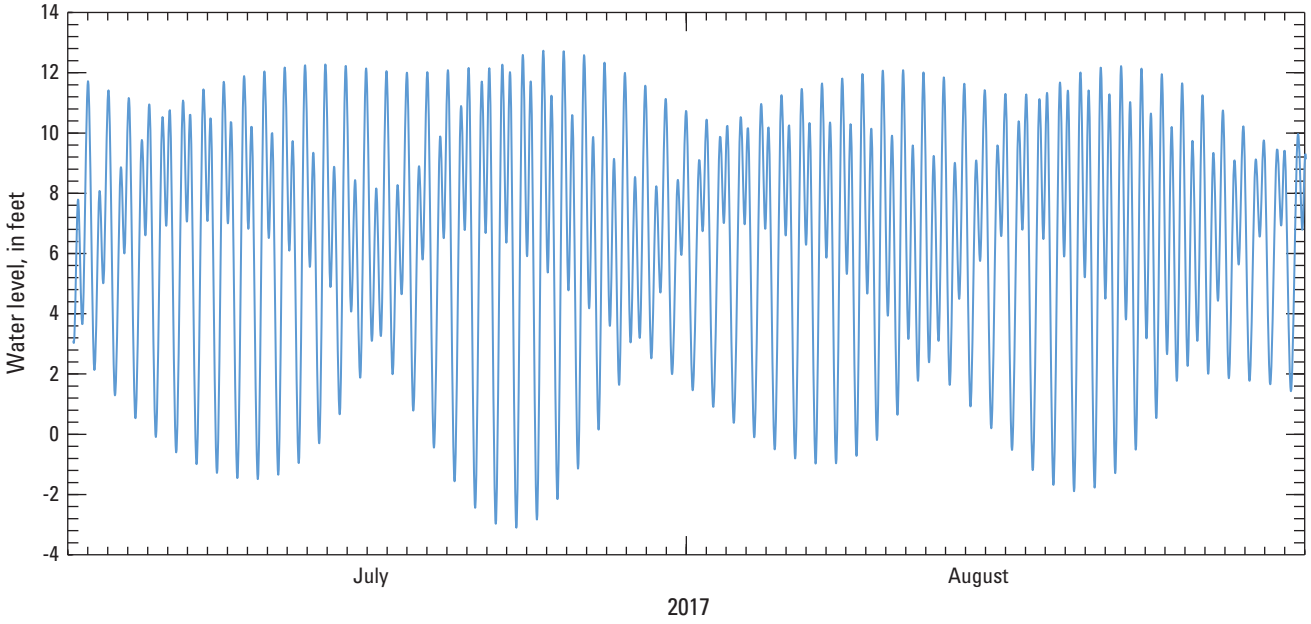

Figure 7. Predicted tides for Liberty Bay at Poulsbo, Washington (station 9445719), in July and August 2017.

study (URS Consultants, Inc., 1997) indicated responses to tidal fluctuations ranging from 5.1 to 0.5 ft in an additional 14 monitoring wells (table 2).

The horizontal propagation of changes in groundwater level from tidal fluctuations in Dogfish Bay to the monitoring wells is governed by the hydraulic diffusivity of the aquifer sediments, as determined using the equation:

$$(D = K/S_s) \quad (1)$$

where

K is the hydraulic conductivity [LT^{-1}], and ‘
S_s is the specific storage [T^{-1}].

The hydraulic diffusivity is related to the period of the tidal fluctuations and the attenuation in amplitude of the fluctuations at an observed distance x from the shoreline. The hydraulic diffusivity can be calculated from the following equation (Keller and others, 1989; Yager and Kappel, 1998), given as a solution by Carslaw and Jaeger (1959) to the governing equation for one-dimensional flow induced through isotropic and homogeneous media by a fluctuating head boundary approximated as sinusoidal function:

$$D = \left[\frac{x^2\pi}{T_0}\right]\left[ln\left(\frac{a}{A}\right)^{-2}\right] \quad (2)$$

where

T_0 is the period of the fluctuations, and
a/A is the attenuation of the original amplitude A.

The hydraulic diffusivity was computed for the 12 wells where fluctuations in groundwater levels were greater than 0.1 ft, assuming a 12-hr period in tidal fluctuation. Values of D ranged from 2.2×10^5 to 18×10^5 feet squared per day (ft^2/d), with a geometric mean value of 5.4×10^5 ft^2/d (table 2).

Recharge

The magnitude and distribution of groundwater recharge in the 5.9 mi^2 study area was computed using national spatial datasets and the SWB model (Westenbroek and others, 2010), which calculates spatial and temporal variations in recharge based on climatological data, and soil and landscape properties. The SWB model is a deterministic model that uses gridded data and physically based parameters to apportion water derived from daily precipitation and snowmelt into surface runoff, evapotranspiration (*ET*), recharge, and water storage in the soil column. Recharge is computed as surplus water in excess of the soil field capacity (*storage*), a product of available water capacity and root depth in the soil column.

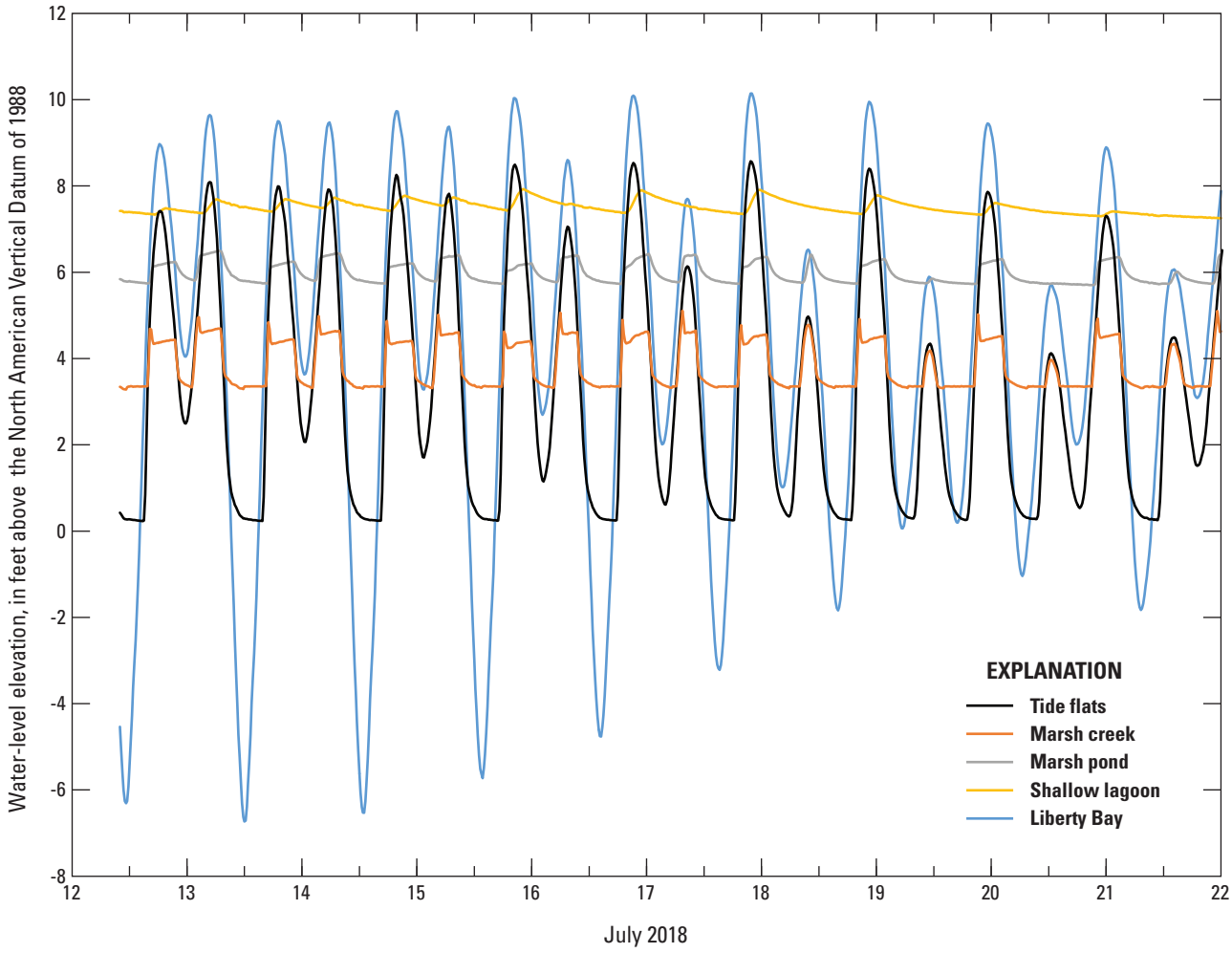

Figure 8. Surface water levels in Liberty Bay, the tide flats, the marsh pond and creek, and the shallow lagoon measured from July 12 to 22, 2018, at Operable Unit 1, Naval Base Kitsap, Keyport, Washington.

SWB calculates water-balance components in the following equation using a modified Thornthwaite Mather soil-water-balance approach at daily time steps in a grid of model cells:

$$recharge = (precipitation + snowmelt + inflow) - (interception + outflow + ET) - \Delta storage \quad (3)$$

where

outflow (Surface runoff) is determined by the National Resource Conservation (NRCS) curve numbers (Miller and White, 1998; Natural Resources Conservation Service, 2018) that have been modified for the Pacific Northwest by Gendasezek and Welch (2018);

inflow (runoff from upgradient adjacent cells) is computed using runoff directions determined with a flow-direction grid derived from a digital elevation model (DEM);

Interception is the specified amount of precipitation that is trapped and transpired by vegetation; and

ET (evapotranspiration) was computed using the method of Hargreaves and Samani (1985).

The SWB model constructed for the study area utilizes a 25-ft grid spacing, contains 8,652 model cells and requires five spatially distributed datasets including: daily climate data (precipitation, maximum and minimum air temperature), land cover, flow direction, hydrologic soil group and available soil-water capacity (app. 1). Daily calculations of the water-balance components were made for the period 1980–2015. The daily recharge rates were then summed and averaged to obtain spatially distributed, mean-annual recharge rates for the study area. The recharge rates reflect the spatial distribution of land cover and soil properties in the study area (fig. 10). The average recharge rate computed for the study area was 16.7 in/yr.

Table 2. Groundwater level response to tidal fluctuations in monitoring wells at Operable Unit 1, Naval Base Kitsap, Keyport, Washington.

[**Abbreviations:** ft, foot; ft²/d, square feet per day]

Well identifier	Groundwater level response (ft)	Hydraulic diffusivity (10^5 ft²/d)
From Opatz and Dinicola (2019)		
1MW-1	0.9	5.4
1MW-4	1.0	3.6
MW1-2	2.7	9.9
MW1-9	0.3	3.0
MW1-25	4.1	12.0
MW1-29	3.4	18.0
MW1-38	6.8	2.2
MW1-39	7.3	2.5
MW1-43	0.6	5.7
MW1-45	0.3	5.9
MW1-47	0.4	6.1
MW1-50	0.1	-
MW1-51	0.1	-
MW1-60	0.2	4.0
From URS Consultants, Inc. (1997)		
MW1-18	1.4	-
MW1-21	0.5	-
MW1-22	0.9	-
MW1-23	2.2	-
MW1-28	3.5	-
MW1-30	5	-
MW1-32	0.5	-
MW1-34	0.6	-
MW1-36	5.1	-
MW1-37	5.1	-
MW1-40	1.5	-
PW1535HWY308	0.5	-

Simulation of Constant-Density Groundwater Flow

Constant-density groundwater flow and contaminant transport within the Keyport study area were simulated using three MODFLOW-based models. Three-dimensional (3D) groundwater flow in the entire 5.9 mi² study area was simulated using both MODFLOW-2005 (Harbaugh, 2005) and MODFLOW-NWT (Niswonger and others, 2011) during model calibration, as described below. Three-dimensional, variable-density groundwater flow and contaminant transport in the 1.3 mi² transport domain surrounding OU-1 were simulated using SEAWAT-Version 4 (Langevin and others, 2007), a computer program that combines a modified version of MODFLOW-2000 (Harbaugh and others, 2000) with MT3DMS (Zheng and Wang, 1999). The model input, output, and executable files are available from Yager (2020).

The 3D constant-density, transient groundwater-flow model was calibrated using the parameter-estimation program UCODE (Poeter and Hill, 1998) to groundwater-level responses in 26 wells during a generalized 31-day period that represented 30 tidal cycles. A steady-state simulation that provided initial conditions to the 31-day transient period was also included in model calibration to match groundwater levels observed in 69 wells. Steady-state, groundwater levels for 54 of the 69 wells at or near OU-1 were determined by averaging 5 rounds of measurements (each including measurements at low tide and high tide) made from August 1995 through September 1996 (URS Consultants Inc., 1997). Steady-state, groundwater levels for the other 15 wells farther from OU-1 were approximated from one or two measurements made during well installation, or at various times over the past few decades (URS Consultants Inc., 1997, app. A). The calibrated constant-density, groundwater-flow model was the basis for the SEAWAT variable-density, contaminant-transport models applied to the transport domain surrounding OU-1, discussed further on.

Model Design

The design of the 3D groundwater-flow model was based on the 3D hydrogeologic model presented earlier. The model domain encompasses 5.9 mi² and is divided into a variably spaced grid with 120 rows and 88 columns; cell widths ranged from 25 ft near OU-1 to 500 ft near Model Boundaries (fig. 1). The 15 model layers contain a total of 135,477 active cells. The bottom four model layers correspond to the bottom four hydrogeologic units represented in the geologic model [the Clover Park Aquitard (Unit 7; QC1) to the sea-level aquifer (Unit 10; QA1), table 1], while the upper six hydrogeologic units that represent Quaternary Vashon Stade (Qv) or younger deposits (referred to as Qv sediments herein) were subdivided into 10 model layers to better represent flow through the surficial sediments beneath OU-1. The top model layer (1) represents surface water, including the shallow lagoon, the marsh pond and its outlet, the tide flats, and the open marine waters of Dogfish and Liberty Bays and Port Orchard. The active model domain excludes the land area north of Liberty Bay, with the exception of the bottom model layer (15), which represents the sea-level aquifer (Unit 10; QA1) and extends throughout the model domain.

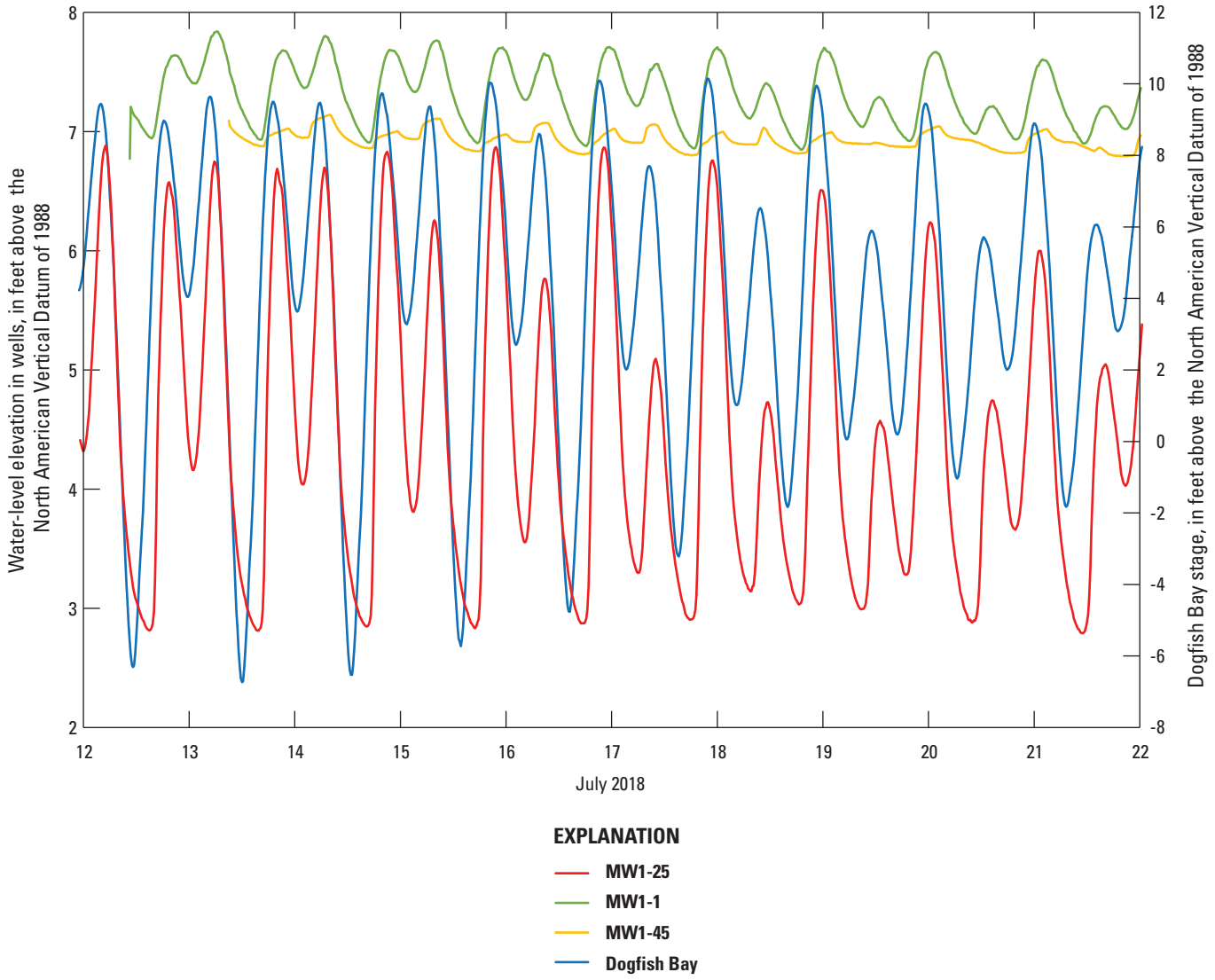

Figure 9. Water-level response to tidal fluctuations at selected monitoring wells from July 12 to 22, 2018, at Operable Unit 1, Naval Base Kitsap, Keyport, Washington.

Hydrogeologic-Unit Flow (HUF2) Package

The HUF2 package (Anderman and Hill, 2000) was used for representing the thin discontinuous hydrogeologic units that are common beneath OU-1. The method entails incorporating hydraulic properties for the upper six hydrogeologic units described in the previous section (table 1) into flow-model layers 2–11. The six units do not extend throughout the model domain and are discontinuous at various locations. The HUF2 package assigns hydraulic properties associated with each hydrogeologic unit to the appropriate flow-model layer based on the depth interval occupied by the unit. The HUF2 package then determines the number of hydrogeologic units that intersect each flow-model layer and computes an average property value for each model cell. An alternative method for representing discontinuous hydrogeologic units would have entailed assigning each unit to a separate flow-model layer. Very large vertical hydraulic-conductivity values and small layer thicknesses would then be specified in model cells where the hydrogeologic units are missing to minimize the loss of hydraulic head while simulating flow across these cells. Application of this alternative method would have required the use of very small time steps in the variable-density flow and contaminant transport simulations described further on, however, and would have resulted in unreasonably long simulation times. One limitation of the HUF2 package is that its application is limited to MODFLOW-2000-based models, such as SEAWAT Version 4, because the package is not currently supported in more recent versions of MODFLOW, such as MODFLOW-NWT.

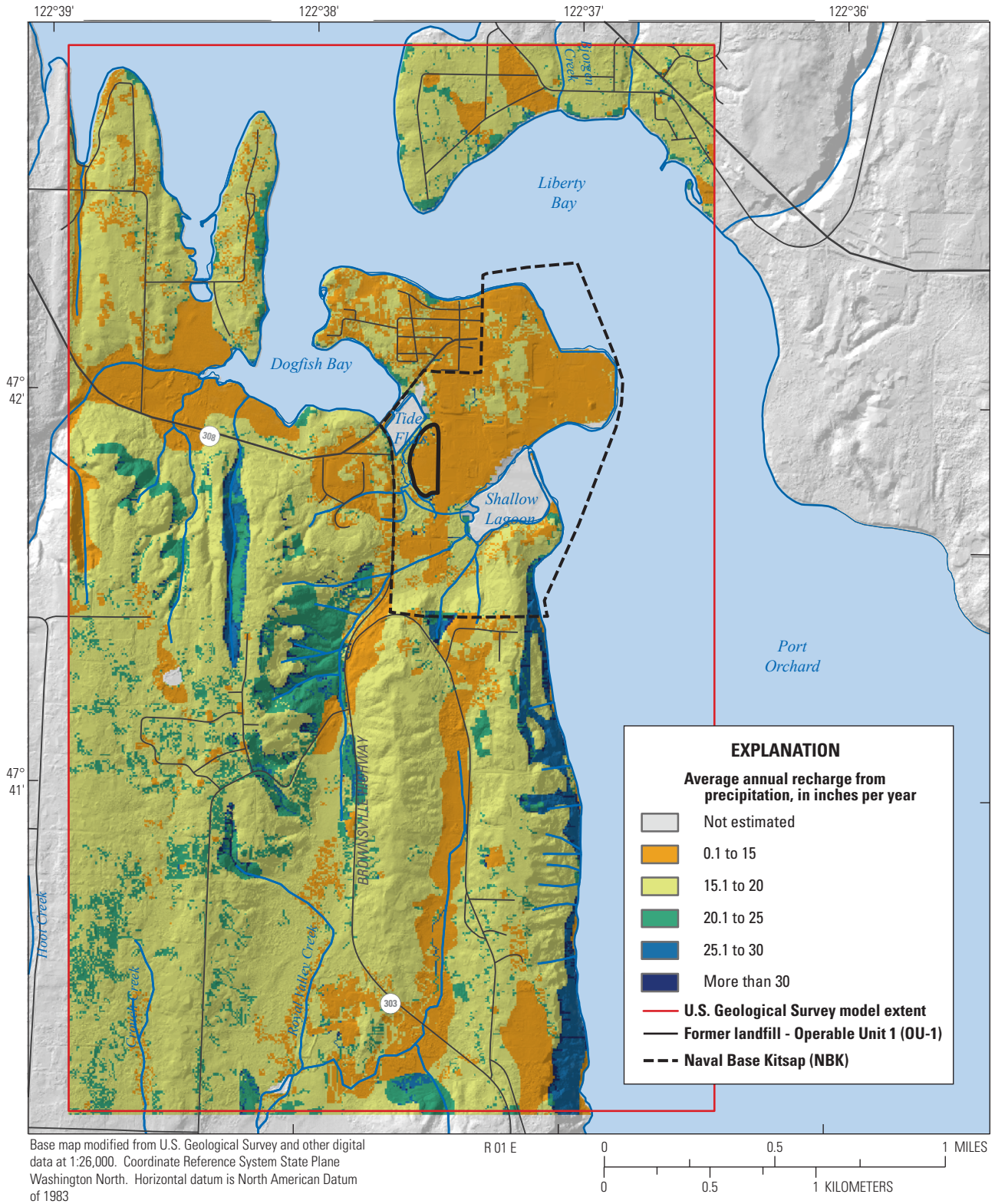

Figure 10. Distribution of average annual recharge from precipitation based on the Soil-Water Balance model near Keyport, Washington.

The thicknesses of the 10 model layers representing Qv sediments, which are equal within each vertical stack of model cells, were obtained by dividing the total thickness of Qv sediments at each grid cell by 10. This method resulted in a minimum model-layer thickness of 3 ft beneath OU-1. The maximum thickness of these flow-model layers ranged from 17 ft beneath the Keyport peninsula to 18 ft thick beneath the uplands to the south. Hydraulic properties associated with each hydrogeologic unit were estimated during model calibration.

Surface Water

The groundwater-flow simulation consists of a steady-state period followed by a 31.05-day transient period divided into 30 daily tidal cycles. Each semi-diurnal tidal cycle was simplified to a diurnal tidal cycle and employed five stress periods to represent the approximate 25-hr tidal cycle in the open and connected waters of Dogfish and Liberty Bays and Port Orchard. Tidal fluctuations were approximated by a trapezoidal function with a period of 1.035 days (24.84 hr) that ranged from a single low-tide stage to a high-tide stage (fig. 11). The high and low tide stages were computed as the respective means of the high-high and low-low tides predicted for Liberty Bay at Poulsbo, Washington, in 2017, as presented earlier. This approximation ignores the intermediate high and low tides that are observed in the data, but allowed the groundwater-flow and contaminant-transport simulations to be conducted in a reasonable amount of time.

Water levels were specified for Dogfish and Liberty Bays and Port Orchard in model layer 1 at the beginning and end of each stress period as either a low, high, or mean (average of high and low) tide using the Time-Variant Specified-Head (CHD) package (Harbaugh, 2005) and corrected for the specific gravity of seawater (1.022) (Collias and others, 1974) (fig. 12*A*). Stress periods were divided into either two or four time steps, and water levels at each time step were interpolated by the CHD package from the specified water levels. This approximation overestimates the stage in Dogfish Bay during the tidal cycle but simplifies the specification of this boundary and permits the completion of a 50-yr transient transport simulation discussed further on. The mean tide predicted for Liberty Bay at Poulsbo, Washington, in 2017 was specified for Dogfish and Liberty Bays and Port Orchard during the steady-state period.

Mean and low tides were lower than the sediment surface at the top of the hydrogeologic model for some model cells that are exposed at the lower tide stages (for example, in mud flats surrounding Dogfish Bay). The minimum water level in these cells was specified as equal to the sediment-surface elevation and was assigned in model layer 2. The tide flats are an extension of Dogfish Bay and experience the same mean and high tides. At low tide, however, the water level in the tide flats was specified as 0.3 ft, the elevation of the sill connecting the two water bodies. Water levels in the marsh pond and its outlet were specified as the average high, low, and mean tides measured during July and August 2018 (table 3) using the Flow and Head Boundary (FHB) package. The water level in the shallow lagoon was specified as a constant value of 7.2 ft with the CHD package, based on measurements by Opatz and Dinicola (2019). The FHB and CHD packages function similarly, but the application of the CHD package allowed constant-concentration boundaries to be specified for several water bodies in the variable-density and contaminant transport simulations described further on.

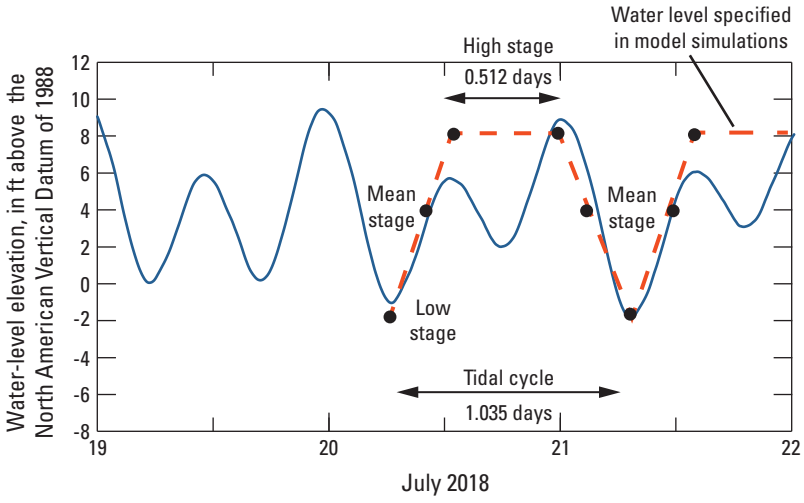

Figure 11. Tidal fluctuation in Dogfish Bay from July 19 to 22, 2018, and tidal fluctuation in Keyport groundwater-flow model.

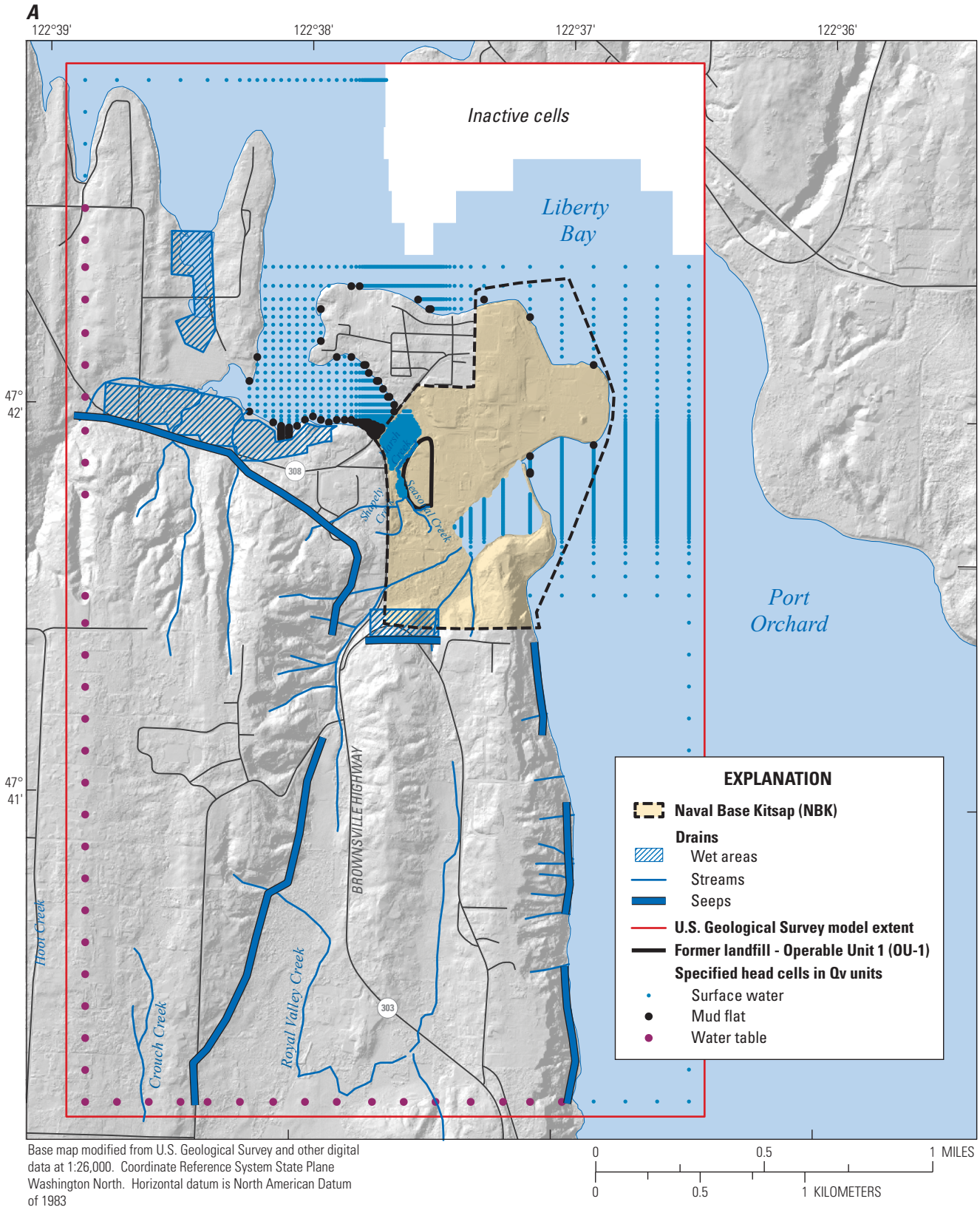

Figure 12. Boundaries specified within Keyport, Washington, groundwater-flow model domain: *A*, Surface water and Vashon Stade (Qv) units, and *B*, sea-level aquifer (QA1) unit.

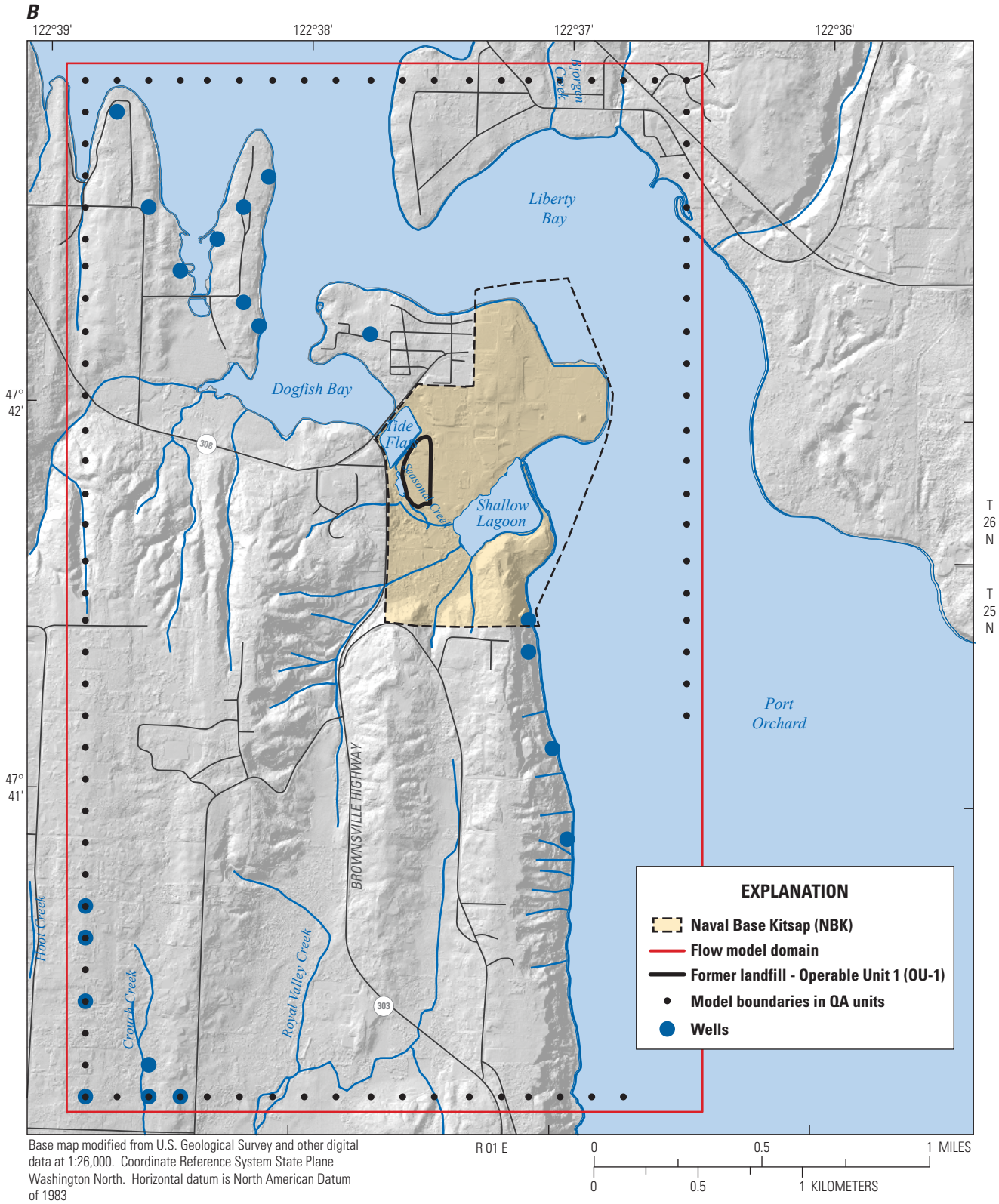

Figure 12.—Continued

Table 3. Water levels specified for surface water bodies at high, low, and mean tides.

Surface-water body	Tidal stage		
	High	Mean	Low
Dogfish and Liberty Bays and Port Orchard	[1]7.94	[1]5.24	[1]-2.54
Tide flats	[1]7.94	[1]5.24	0.3
Marsh outlet	4.65	3.98	3.3
Marsh pond	6.4	6.1	5.8

[1]Water levels are corrected for seawater density in model simulation.

Domain Boundaries

Model domain boundaries coincide with the model grid of the 3D Kitsap groundwater-flow model of Frans and Olsen (2016), but they do not correspond to natural hydrologic boundaries. Hydraulic heads and flow rates computed by the Kitsap model were used to set head and flow boundaries in the Keyport model in two model layers below the top of the Clover Park Aquitard (Unit 7: QC1) with the FHB package. Hydraulic heads were specified at domain boundaries in model layers 13 and 15 representing the permeable interbeds (Unit 8; QC1pi) within the Clover Park Aquitard and the sea-level aquifer (Unit 10; QA1), respectively (fig. 12*B*). Vertical flows exchanged between the sea-level aquifer and deeper model layers in the Kitsap model were also specified with the FHB package in model layer 15. Hydraulic heads computed by the Kitsap model were adjusted during calibration of the Keyport model to better match observed water levels in wells screened in the sea-level aquifer.

The Kitsap model was calibrated to water-level data over a much larger area than the Keyport model, and it predicts water levels above land surface along a large portion of the Keyport model boundary, particularly where the uplands slope downward to the edge of Dogfish and Liberty Bays and Port Orchard. Hydraulic heads were specified along southern and western grid boundaries of the Keyport model in a single model layer within the Qv sediments. The elevation and head at these boundary cells were computed as the top of the Clover Park Aquitard (Unit 7; QC1) plus one-third of the thickness of the Qv sediments. This boundary maintained the simulated water table in the Qv sediments below land surface.

Hydraulic heads were also specified with the CHD package along northern and eastern grid boundaries where the model domain intersects Liberty Bay and Port Orchard. Heads specified at these locations in the top model layer (1) correspond to the high, low, and mean tide stages. Heads were specified in model layer 12 (Unit 7; QC1) using values computed from the Kitsap model for the upper part of the Clover Park Aquitard. The remainder of the model domain boundaries were specified as no flow.

Surface Drainage

Groundwater discharge to surface drainage at land surface (fig. 12*A*) was represented by drains using the Drain (DRN) package which requires specification of the elevation and hydraulic conductance (discharge per foot of head difference between groundwater and the drain, ft^2/d) of each boundary cell. Perennial streams delineated in the USGS National Hydrography Dataset (U.S. Geological Survey, 2014) were represented in model layer 2 using the bottom elevation of the layer and a conductance value of either 20 or 10 ft^2/d for the main channels or tributaries, respectively. The small creek draining the southern edge of OU-1 and the ditch along the Brownsville Highway west of the marsh were also represented as drains using elevations scaled from site-scale topographic maps and conductance values of 10 ft^2/d.

Groundwater seeps in the uplands were represented as drains with large conductance values (100 ft^2/d) to minimize resistance to flow. Elevations of seeps along the bluffs at the eastern edge of the uplands above Port Orchard were set at the bottom of the Qv sediments in model layer 11 (fig. 12*A*). Drain elevations at land surface were specified in model layer 2 for two wet areas along the south shore of Dogfish Bay. In addition, three lines of seeps were represented as drains in the Qv sediments where coarse-grained sediments of the Vashon advance aquifer (Unit 4; Qva) pinch out above the fine-grained sediments of till (Unit 3; Qvt). The elevations of these drains were specified as the top of the Unit 4.

Groundwater Withdrawals

Groundwater withdrawals from Welch and others (2014) were specified at 20 pumped wells with the Well (WEL) package (fig. 12*B*). Groundwater withdrawals from 16 of the wells were specified in model layer 15 (Unit 10; QA1) and the remainder in model layer 13 (Unit 8; QC1p). Groundwater withdrawals from shallow domestic wells screened in Qv sediments and infiltration from domestic septic systems were not represented explicitly but are accounted for by representing net outflow (withdrawals minus infiltration) from these domestic systems in the estimated recharge values.

Recharge

Recharge computed by the SWB model (app. 1) was applied to model layer 2 with the Recharge (RCH) package. The model domain was divided into five areas based on the surficial geology to enable the adjustment of the recharge values during model calibration (fig. 13). Areas where coarse-grained sediments (Units 1 and 4; Qvr and Qva) were present at land surface were grouped together, as were areas where fine-grained sediments were present (Unit 3; Qvt). The fine-grained sediment areas were divided further into two groups corresponding to upland and lowland areas. A fourth recharge area was delineated where the Clover Park Aquitard (Unit 7;

QC1) is present at land surface; recharge in these areas was set to the vertical-hydraulic conductivity specified for Unit 7. A fifth recharge area was delineated during model calibration around a small knoll in the lower part of the uplands southwest of Keyport Peninsula. The computed SWB recharge in this area was decreased by a factor of 0.1 in this area to limit water levels computed by the groundwater-flow simulation to below land surface, as described further on.

Model Calibration

The Keyport groundwater-flow model was calibrated by adjusting values of hydraulic properties to match 99 observations of four types of data: groundwater levels (69), water-level fluctuations in wells that respond to tides (26), vertical hydraulic gradients (3) and streamflow (1). Eleven groundwater level observations were in the QCpi and QA1 units, while the remainder were in Qv sediments. In addition, pseudo water-table altitudes were specified at 24 locations to compensate for the lack of data in the uplands and to ensure the predicted water table was below land surface (fig. 14). Estimation of the pseudo water-table altitudes is described below. A total of 24 parameter values were specified in the model (table 4), 15 of which were estimated through nonlinear regression using UCODE (Poeter and Hill, 1998), a computer program that uses weighted least squares to minimize model residuals (difference between observed and simulated data). Model sensitivities corresponding to the remaining nine parameters were too small to allow estimation by regression, and values were assigned by trial and error, or taken from the literature.

Weights assigned to most observations included in the regression were chosen to account for differences in units (for example, groundwater levels and streamflow) or ranges of measurements (for example, 60 ft for groundwater levels and 7 ft for water-level fluctuations) and adjusted such that the observations had equal weight in the regression. Water-level fluctuations and vertical hydraulic-gradient measurements were weighted slightly larger than groundwater levels, and pseudo water-table altitudes were weighted slightly smaller. Downward hydraulic gradients were computed from the differences in groundwater levels measured in two pairs of wells screened in shallow and deep Qv sediments at the base of uplands south of the Keyport Peninsula (fig. 14). The vertical hydraulic gradient at a third location on the Keyport Peninsula was estimated from a water-table map prepared for the Qv sediments and results from the Kitsap groundwater flow model, which indicated an upward gradient beneath the peninsula and Liberty Bay. A single measurement of flow was recorded in the perennial stream that drains to the shallow lagoon on March 2019 following a period with little surface runoff.

Iterative Calibration Approach

Model calibration involved the application of two simulations that were run alternately in an iterative sequence: a combined steady-state and transient simulation using MODFLOW-2005 and a steady-state simulation using MODFLOW-NWT. The use of the HUF2 package necessitated the application of MODFLOW-2005, but that program requires the aquifer system to be treated as confined to obtain a numerical solution for hydraulic head in the study area, where steep slopes in the uplands transition abruptly to the level topography of the lowlands. When the aquifer system is treated as unconfined, the numerical solvers available in MODFLOW-2005 cannot converge to a solution for hydraulic head and dry cells (with heads below the cell bottoms) propagate throughout the model domain. Treating the aquifer system as confined overestimates underflow from the uplands to the lowlands, however, because the saturated thickness of each model layer is artificially increased. In contrast, the MODFLOW-NWT program can better simulate the transition in hydraulic head from the uplands to the lowlands while treating the aquifer system as unconfined. In the unconfined MODFLOW-NWT simulation, model layers above the water table are dry and the corresponding model cells are inactive. Therefore, underflow is computed using a more realistic value of saturated thickness. Unfortunately, the numerical solver in MODFLOW-NWT is not supported in the SEAWAT Version 4 program that was later used to simulate variable-density flow and contaminant transport, which necessitated the iterative procedure described below.

Parameter values were estimated initially from a confined transient simulation using MODFLOW-2005 and then updated in the unconfined steady-state simulation using MODFLOW-NWT. This entailed importing values for horizontal and vertical hydraulic-conductivity and recharge directly into the MODFLOW-NWT model, which does not support application of the HUF2 package. The water table computed by the MODFLOW-NWT simulation was then used to specify as inactive the model cells in the MODFLOW-2005 simulation that were above the simulated water table. Parameter estimation was then reapplied to the MODFLOW-2005 simulation, and the procedure was continued until the volumetric water budgets of both simulations were nearly equal. The pseudo water-table altitudes used in model calibration were taken from the water table computed by the MODFLOW-NWT simulation and updated after each iteration of this procedure.

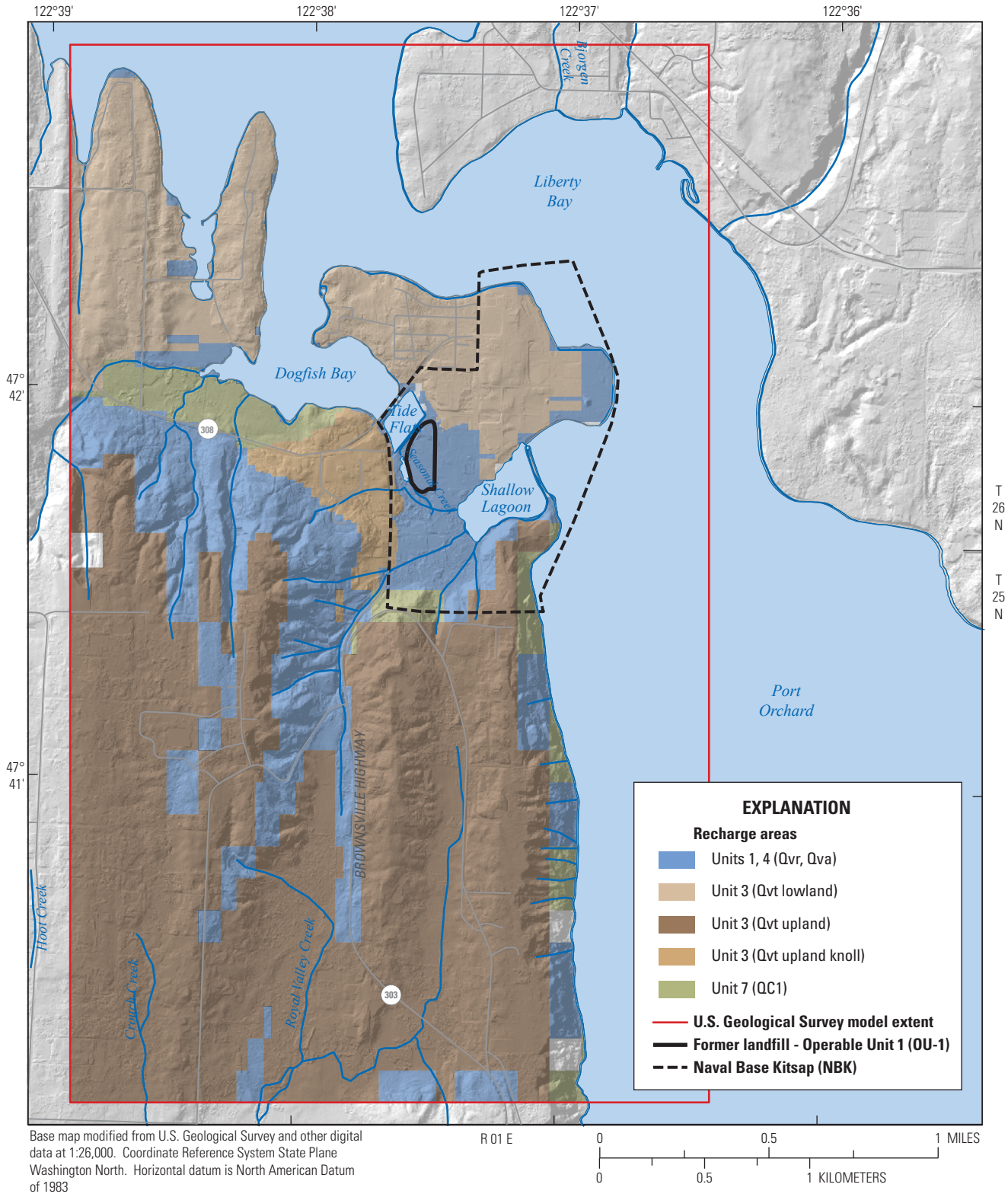

Figure 13. Recharge areas based on surficial geology delineated for model calibration, Naval Base Kitsap, Keyport, Washington.

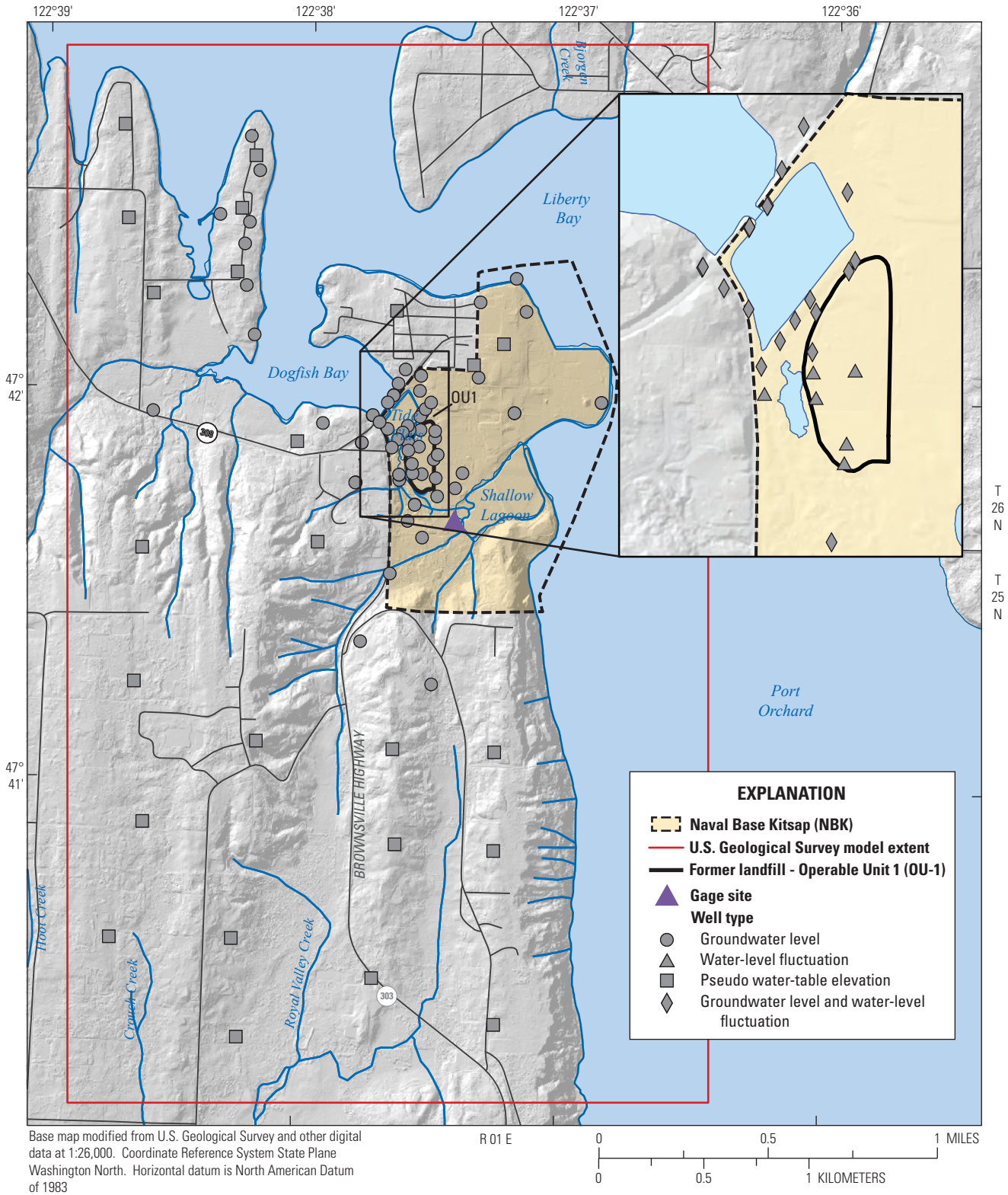

Figure 14. Observations used in model calibration, Naval Base Kitsap, Keyport, Washington.

Table 4. Parameter values in Keyport, Washington, groundwater-flow models A and B, specified or estimated through model calibration.

[**Bold** values signify coefficient of variation less than 100 percent. **Abbreviations:** ft/d, foot per day; –, not applicable]

Parameter	Assigned value	Model A		Model B	
		Estimated value	Coefficient of variation (percent)	Estimated value	Coefficient of variation (percent)
Hydraulic conductivity (ft/d)					
Operable Unit 1(Qvr)	–	0.9	–	**8.2**	83
Operable Unit 2 (Qm):					
Qmarsh	–	**0.18**	44	0.25	–
Qestuary	–	1	–	19	–
Operable Unit 3(Qvt):					
Lowland	–	**0.66**	51	**0.07**	94
Upland	–	**0.15**	34	**0.24**	80
Knoll	–	**10**	51	10 [3]	–
Operable Unit 4(Qva):					
Lowland	–	0.9	–	0.9	–
Upland	–	1.7	–	**2**	90
Unit 5(Qvsemi)	0.1	–	–	–	–
Unit 6 (Qvinter)	–	1	–	**3.1**	86
Units 7 & 9 (QC1)	0.01	–	–	–	–
Unit 8 (QC1pi)	–	1.7	–	1.7	–
Unit 10 (QA1)	–	50	70	50	–
Anisotropy, ratio of horizontal to vertical hydraulic conductivity					
Coarse-grained units:	2	–	–	–	–
Units 1, 4, 6 & 8 (Qvr, Qva, Qvinter, QC1pi)					
Unit 2 (Qm)	5	–	–	1.5	–
Unit 3(Qvt)	–	**26**	41	**53**	61
Unit 5(Qvsemi)	2	–	–	**4.6**	92
Units 7 & 9 (QC1)	100	–	–	–	
Recharge factor					
Coarse-grained units:					
Units 1 & 4 (Qvr & Qva)	–	**0.65**	53	1.2	–
Unit 3 (Qvt):					
Lowland	–	0.17	–	0.23	–
Upland	–	**0.22**	52	**0.38**	99
Knoll	0.1	–	–	–	–
Unit 7 (QC1)	1.0E-04	–	–	–	–
Storage (ft_{-1})					
All units[1]	2.0E-06	–	–	–	–
Unit 1 (Qvr)[2]	0.1			–	–

[1]Except Unit 1 in Model B

[2]Model B only

[3]Specified in Model B

Representation of Storage Values

The assumption of confined conditions in the transient MODFLOW-2005 simulation does not represent the exchange of groundwater to and from storage that would occur near a fluctuating water table under unconfined conditions. However, hydraulic diffusivity (D) values computed from the observed groundwater fluctuations in wells near OU-1 indicate that the measured well responses occur under confined conditions. Assuming an expected hydraulic conductivity value for the aquifer sediments of 1 ft/d, the specific storage (S_s) computed from the geometric mean D value of 5.35×10^{5} ft^2/d is 1.9×10^{-6} ft^{-1}, a value within the range of S_s values estimated for unconsolidated material (1.0×10^{-6} to 2×10^{-5} ft^{-1}) by several studies (Yager and Fountain, 2001).

The ramifications of representing changes in storage from the fluctuating water table near OU-1 was assessed using two alternative models. In the first model (A), an S_s value of 2.0×10^{-6} ft^{-1} was assigned to all hydrogeologic units. In the second model (B), the S_s value of Unit 1 (Qvr sediments), the uppermost hydrogeologic unit, was increased to 0.1 to approximate an unconfined storage value associated with specific yield. The larger S_s value in Model B overestimates storage in areas where the Qvr sediments span multiple model layers, however, because this larger value is operative in each layer, rather than only in the layer(s) in which the water table is fluctuating. The HUF2 package in MODFLOW-2005 does not allow the specification of different parameter values within the same hydrogeologic unit. A multiplicative scaling factor based on the Qvr unit thickness was applied to the S_s values of the Qvr sediments to compensate for this problem. The specified S_s values were smaller where Unit 1 was thicker and larger where the unit was thinner, such that the sum of S_s values in each stack of model cells representing Qvr sediments totaled to 0.1. This approach resulted in less overestimation of storage, but still overestimated S_s values in the deeper parts of the Qvr sediments where Unit 1 spanned multiple model layers.

Simulation Results

Parameter Values

Model A

Coefficients of variation (CV) for 8 of the 15 estimated parameters in Model A were less than 100 percent, indicating that the regression was relatively sensitive to these parameters and that these values are better estimated than those of the other parameters (table 4). Estimated hydraulic conductivity (K) values for the coarse-grained, permeable Qv sediments (Units 1, 4 & 6; Qvr, Qva and Qvinter) range from 0.9 to 1.7 ft/d, and are lower than the geometric mean values (3.3 to 4.1 ft/d) computed from 25 slug tests conducted in permeable Qv sediments near the OU-1 (URS Consultants, 1998). The estimated K value for the Unit 2 (Qestuary) was 1 ft/d; lower values had no effect on the regression. Estimated K values for the Unit 2 (Qmarsh) and Unit 3 (Qvt) are one order of magnitude lower than for the permeable units, with the exception of the till recharge area delineated around a small knoll in the lower part of the uplands southwest of the Keyport Peninsula (fig. 13). Water levels in two wells screened in shallow Qv sediments indicate that the slope of the water-table surface changes abruptly and becomes more gradual in this area. The hydraulic conductivity of Unit 3 was increased to 10 ft/d and recharge was reduced by a factor of 0.1 in this area to match the observed groundwater levels. These changes suggest that more permeable units occur in this area than those indicated by the hydrogeologic model. Values for vertical anisotropy (ratio of horizontal to vertical hydraulic conductivity) were specified from the literature, with the exception of anisotropy for Unit 3, which was estimated as 26:1.

The nonlinear regression decreased the recharge rates computed by the SWB model on the coarse-grained units by a factor of 0.65, and on Unit 3 (Qvt) by factors of 0.22 and 0.17 in the uplands and lowlands, respectively. The average recharge rate in the flow model domain in Model A is 4.2 in/yr. This value is much less than the average rate of 16.7 in/yr computed with the SWB model, but comparable to recharge rates estimated by Welch and others (2014) for the northern part of the Kitsap groundwater-flow model domain (4 in/yr). The recharge rates estimated for the Keyport groundwater-flow model predict base flow in the perennial stream draining to the shallow lagoon reasonably well, and higher recharge rates result in a simulated water table that is above land surface.

The lower recharge rates estimated by nonlinear regression for Model A suggests that the SWB model overestimates recharge to groundwater in uplands similar to those in the Keyport study area, where the topography dips steeply to sea level, and where relatively permeable soils at land surface are underlain by much lower permeability sediments at depth. Much of the precipitation that percolates through the soil root zone in the uplands likely discharges as interflow to local drainage features rather than infiltrating downward to the groundwater flow system. The recharge factors estimated by the nonlinear regression are correlated with the hydraulic conductivities estimated for Unit 3 (Qvt) and Unit 4 (Qva) at levels greater than 0.85, however, indicating that higher values could be specified for both recharge and K in these units with little change in model error.

Model B

Coefficients of variation (CV) for 8 of the 16 estimated parameters in Model B were less than 100 percent, although half of these parameters had CV values greater than or equal to 90 percent (table 4). Estimated hydraulic conductivity (K) values for some of the coarse-grained, permeable Qv sediments (Units 1, 2 & 6; Qvr, Qestuary and Qvinter) were higher than in Model A and range from 3.0 to 19 ft/d. Estimated K values for lowland till (Unit 3, Qvt) were an order of magnitude less, while the remainder of the K values were comparable to those

in Model A. Values for vertical anisotropy were estimated for Units 2, 3 and 5 (Qm, Qvt and Qvsemi, respectively), and were higher for Units 3 and 5, and lower for Unit 2 than in Model A. The higher *K* values estimated in Model B for the coarse-grained, permeable Qv sediments compensate for the higher storage values specified in Unit 2 (Qvr), so the hydraulic diffusivity (*D*) value remained unchanged at 5.35×10^5 ft²/d.

Estimated recharge rates were higher in Model B than in Model A. SWB recharge rates on the coarse-grained units were increased by a factor of 1.2 and decreased on Unit 3 (Qvt) by factors of 0.38 and 0.23 in the uplands and lowlands, respectively. The average recharge rate in the flow model domain in Model B is 7.3 in/yr, slightly less than half the SWB recharge rate. The larger recharge factors estimated in Model B are correlated in the nonlinear regression with the higher hydraulic conductivities, as noted above.

Model Fit

Errors associated with groundwater-flow Model A for groundwater levels, water-level fluctuations and pseudo water-table altitudes are depicted in a series of residual plots (figs. 15 and 16). The standard error in groundwater levels is 7.8 ft, which is 13 percent of the 60-ft measurement range, while the standard error in water-level fluctuations is 1.0 ft or 14 percent of the 7.3-ft measurement range. Errors in groundwater levels for the deeper hydrogeologic units below the Clover Park Aquitard (Units 7 & 9; QC1) show more scatter than for the Qv sediments. Groundwater levels in the vicinity of OU-1 are generally less than 20 ft where the agreement is quite good, although groundwater levels are overestimated in some areas at the base of the uplands south of the Keyport Peninsula. The standard error in pseudo water-table altitudes is 11.3 ft, which is 4 percent of the 320-ft measurement range. This indicates close agreement between the water tables computed by the MODFLOW-2005 and MODFLOW-NWT simulations.

Residual plots for Model A indicate little bias in model results for water-level fluctuations (fig. 16*B*), but there is a bias towards overestimating measured water levels and underestimating pseudo water-table altitudes (figs. 16*A* and *C*). These biases are in opposite directions and limit the ability of the nonlinear regression to further reduce model error. Additional groundwater-level data in the uplands would be required to better calibrate the groundwater-flow model.

Errors associated with groundwater-flow Model B for groundwater levels and pseudo water-table altitudes are similar to those with Model A, but the errors in water-level fluctuations are worse (fig. 15). The standard error in groundwater levels and pseudo water-table altitudes are 7.6 and 11.2 ft, respectively, while the standard error in water-level fluctuations is 1.3 ft. The biases in water levels and pseudo water-table altitudes are also similar in Model B to those observed in Model A, but there is a distinct bias towards underestimating water-level fluctuations (fig. 16). The higher storage values in Model B dampen the water-level fluctuations, although the higher vertical anisotropy values in Model B (especially in Unit 5, Qvsemi) ameliorate this condition to some extent by decreasing the hydraulic connection between the upper and lower parts of the Qv sediments.

The spatial distribution of residuals indicates that the water-table altitude is underpredicted in Model A in the uplands and on Keyport Peninsula, but overpredicted in lowland areas near the base of the uplands (fig. 17*A*). Water-level fluctuations are generally underpredicted near OU-1 but overpredicted near the tide flats. The spatial distribution of residuals in Model B is similar, but the water-table altitude is better predicted in lowland areas near the base of the uplands, and water-level fluctuations are underpredicted near OU-1. The directions of the three vertical hydraulic-gradient observations were simulated correctly in both models, downward beneath the uplands and upward beneath the Keyport Peninsula (fig. 17*B*). Errors in the simulated gradients ranged from 25 to 66 percent of the observed value. The simulated value of streamflow in the perennial stream that discharges to the shallow lagoon in Model A (0.18 ft³/s) was 70 percent less than the measured value of 0.6 ft³/s, while streamflow was 40 percent less than the measured value in Model B (0.33 ft³/s).

Simulated Groundwater Flow

The water table simulated by groundwater-flow Model A for the steady-state period indicates that groundwater enters the model domain from the western boundary and flows northward to Dogfish and Liberty Bays and southward to the southern boundary (fig. 17*B*). There are two high points on the water-table surface that are separated by the watershed of the perennial stream that drains to the shallow lagoon. Groundwater also flows eastward and discharges along the steep bluffs that border Port Orchard. Groundwater flows northeastward from the uplands to the base of the Keyport Peninsula, where it discharges to the tide flats and the marsh and its outlet creek (fig. 17*A*). Another high point is evident on water-table surface on the western side of the peninsula. Some groundwater on the peninsula flows south and southwestward beneath OU-1, but the hydraulic gradient is gradual. The simulated water table indicates that OU-1 is located adjacent to a regional discharge area that prevents the flow of groundwater from the landfill toward areas south and west of the tide flats and the marsh. The water table simulated by Model B is similar, but the maximum predicted altitudes are 10 ft higher under Virginia Point and 20 ft under the Keyport Peninsula, because of increased recharge.

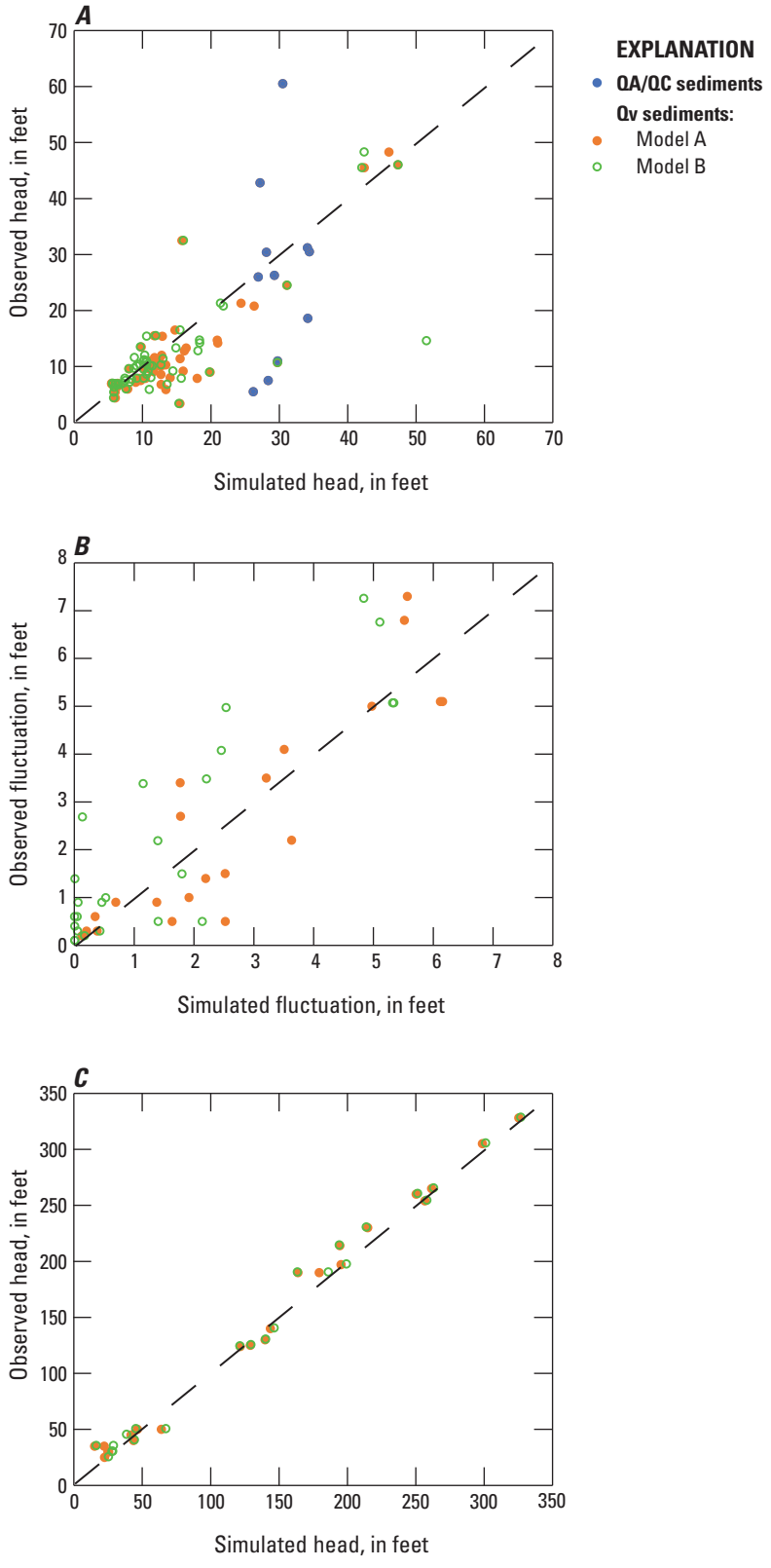

Figure 15. Residual plots showing relations between observed and simulated values in models A and B: *A*, water levels, *B*, water level fluctuations, and *C*, pseudo water-table altitudes.

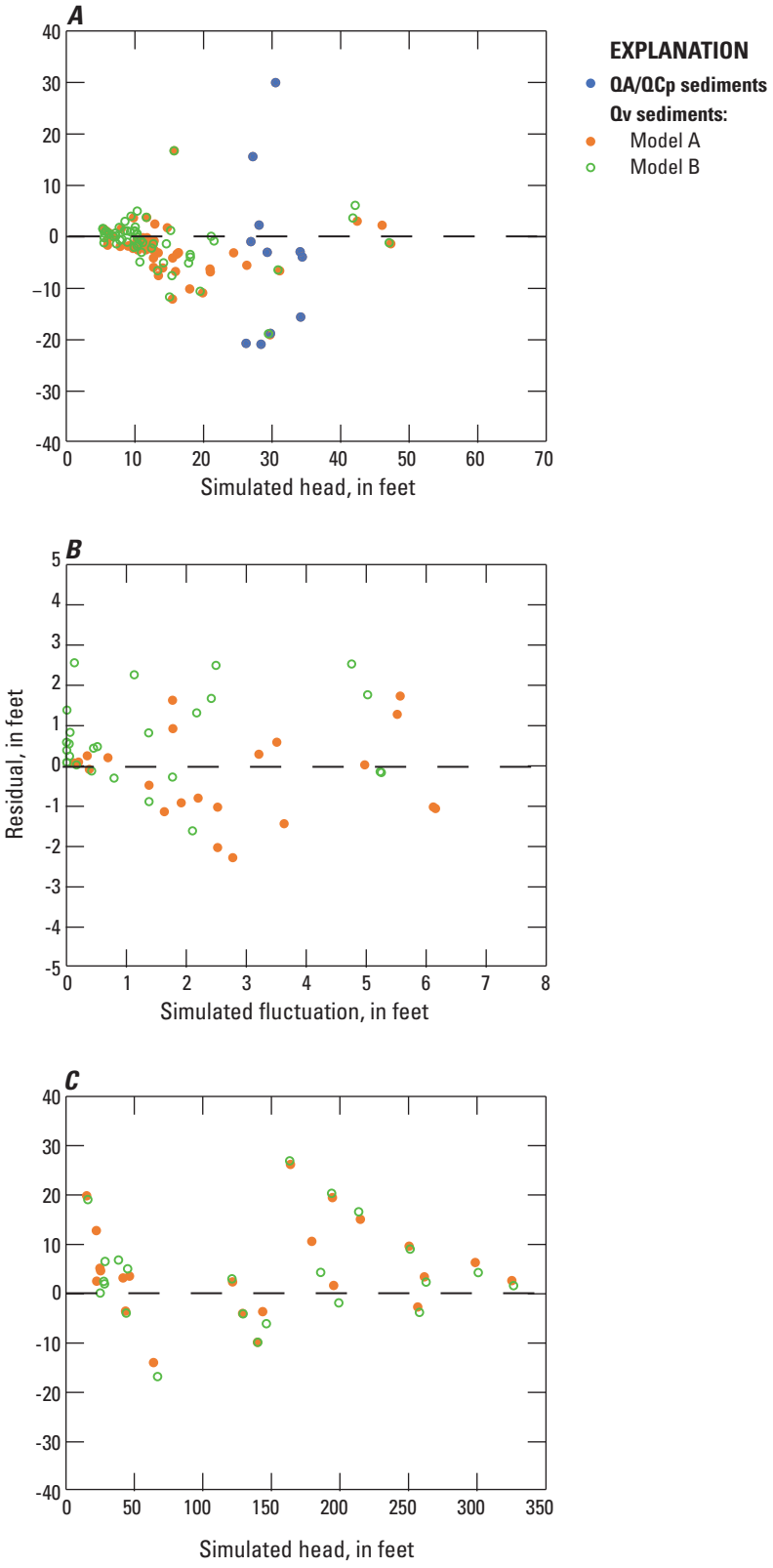

Figure 16. Residual plots showing relations between simulated values and residuals in models A and B: *A*, water levels, *B*, water level fluctuations, and *C*, pseudo water-table altitudes.

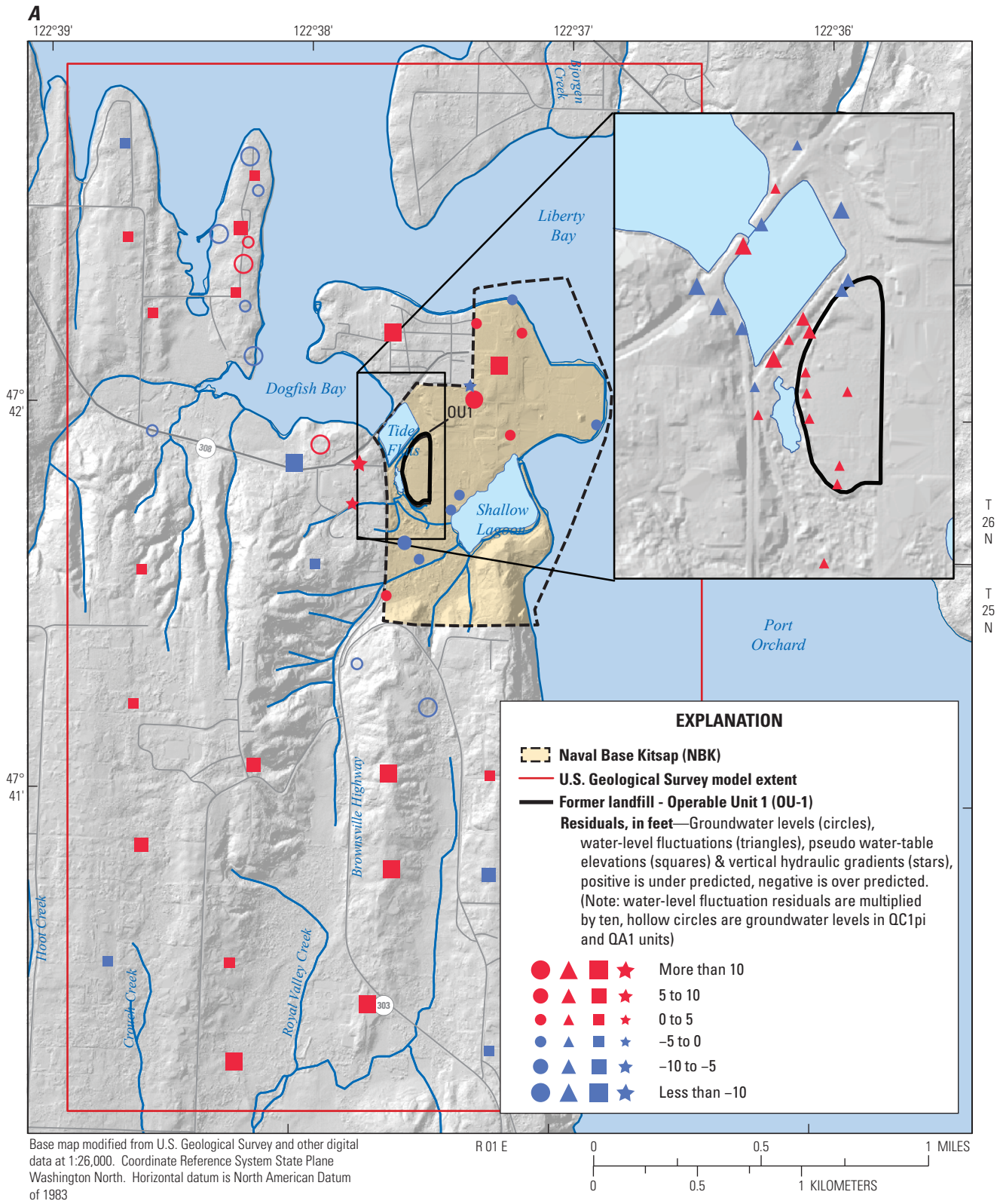

Figure 17. Keyport groundwater-flow model results: *A*, distribution of residuals in groundwater-level, water-level fluctuations, pseudo water-table altitudes and vertical hydraulic-gradient observations; and *B*, simulated water table.

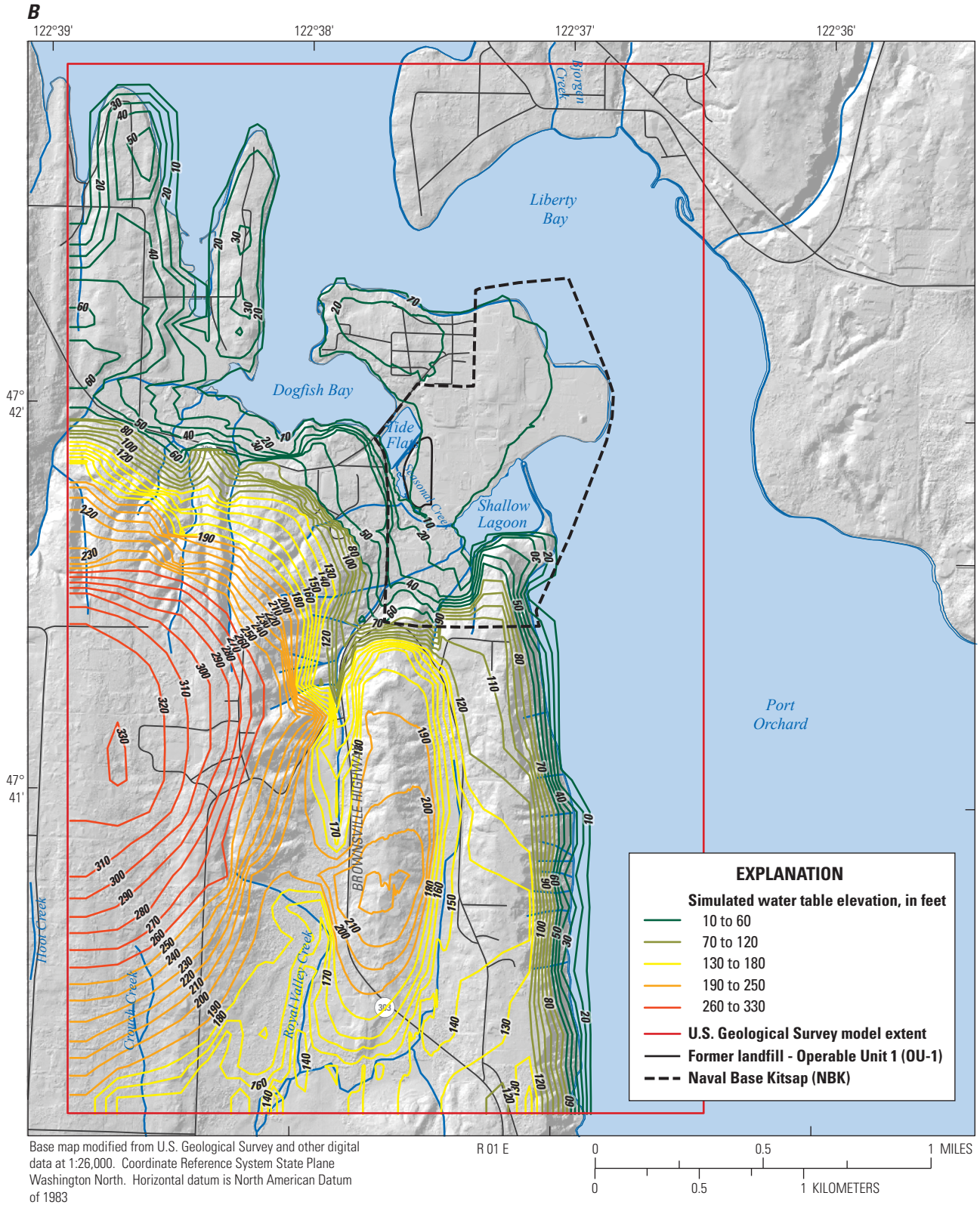

Figure 17.—Continued

The Clover Park Aquitard (Unit 7, QC1), which serves as a hydraulic barrier in both models A and B, limits the flow of groundwater from the Qv sediments to and from the deeper hydrogeologic units. Vertical groundwater flow is generally at least an order of magnitude less than horizontal flow, except along the western boundary of the model domain where the flows are nearly equal. Groundwater flow from the Qv sediments is downward beneath the uplands and upward beneath Keyport Peninsula and Dogfish and Liberty Bays and Port Orchard in Model A (fig. 18). A transition from downward to upward flow occurs southeast of the tide flats and marsh at the base of the peninsula. A similar distribution of flow is evident in Model B. The simulated distributions of vertical flow indicate that upward flow beneath the landfill would prevent the migration of dissolved contaminants from OU-1 toward deeper hydrogeologic units.

Water budgets simulated for the steady-state period in Model A by the confined MODFLOW-2005 and unconfined MODFLOW-NWT simulations for the groundwater-flow and transport model domains are shown in table 5. The water budgets generally agree closely, although there is more underflow from Model Boundaries in the confined MODFLOW-2005 simulation that overestimates the saturated thickness of Qv sediments. Most of the inflow to the groundwater-flow model domain is from recharge and underflow along the western model boundary. Most of the outflow is discharge to streams and underflow along the southern model boundary. The vertical flow to and from deeper hydrogeologic units is specified at the bottom model boundary in Unit 10 (QA1; sea-level aquifer). The pattern is similar for the transport model domain surrounding the Keyport Peninsula, but underflow from the uplands to the southern transport boundary is a smaller component of the overall budget. The vertical flow is through the Clover Park Aquitard (Unit 7, QC1) which underlies the transport model domain. Underflow from the uplands to transport model domain is overestimated by 35 percent by the confined MODFLOW-2005 simulation, and the simulated water table is as much as 8 ft above land surface in a 4-acre area south of the marsh. As a result, the magnitude of groundwater flow from the uplands to the marsh is overestimated in this area.

Most water-budget components for Model B are similar to those for Model A, although there is 75 percent more recharge and streamflow predicted in Model B. There is correspondingly more underflow predicted to the transport domain in Model B (9,360 ft^3/d) than in Model A (4,814 ft^3/d). The agreement between the confined MODFLOW-2005 simulation and the unconfined MODFLOW-NWT simulation with Model B is comparable to that of Model A. The water table simulated by Model B is at or below land surface in the 4-acre area south of the marsh, where Model A simulated the water table above land surface, suggesting a better model fit in this area.

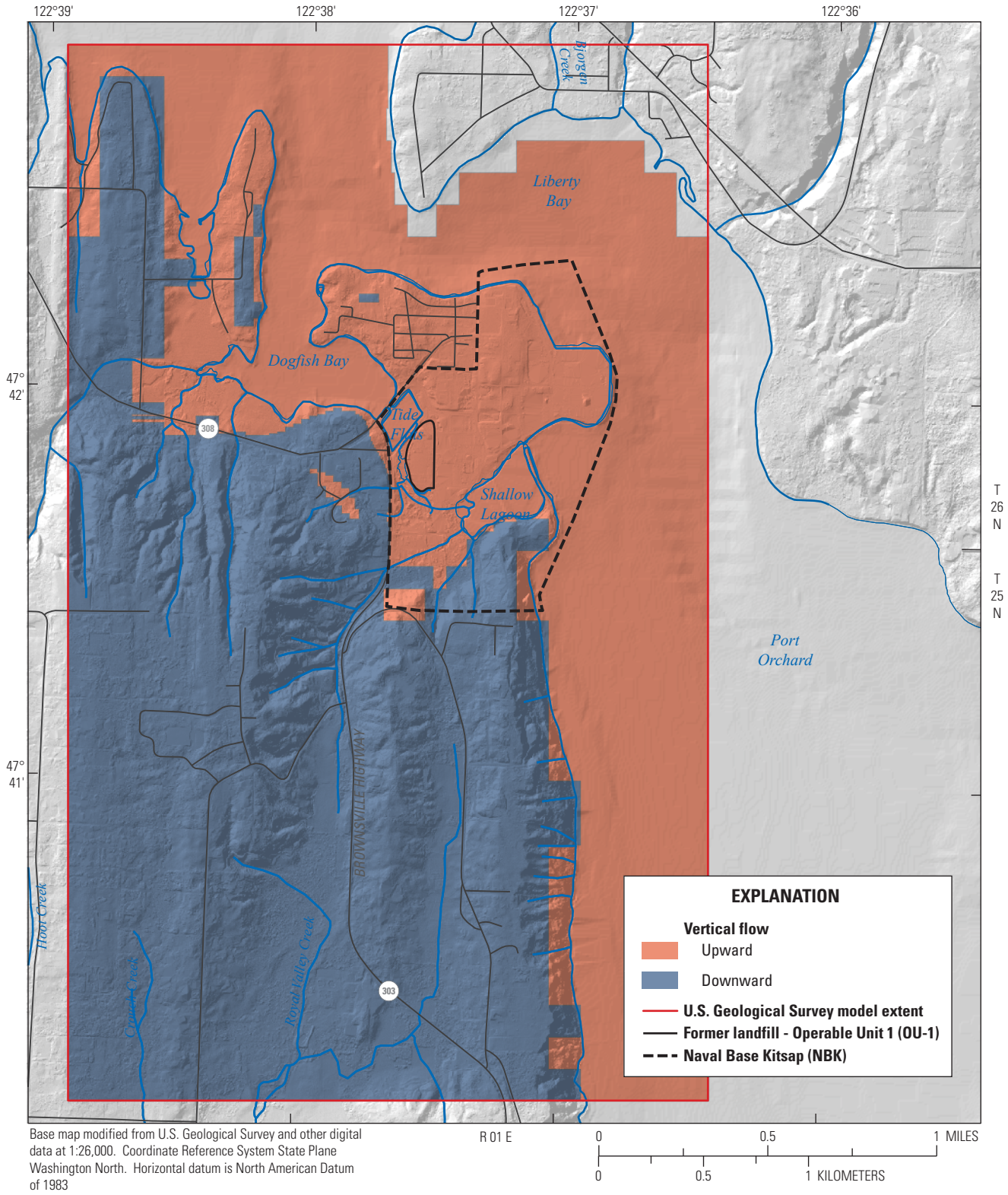

Figure 18. Vertical flow from (positive) to (negative) Qv sediments simulated by Keyport groundwater-flow Model A, Operable Unit 1, Naval Base Kitsap, Keyport, Washington.

Table 5. Water budgets for the groundwater-flow and transport model domains simulated for the steady-state period with Model A by the confined MODFLOW-2005 and unconfined MODFLOW-NWT simulations.

MODFLOW-2005 simulation				MODFLOW-NWT simulation			
Groundwater flow domain				Groundwater flow domain			
Source	Inflow volume (ft^3/d)	Discharge	Outflow volume (ft^3/d)	Source	Inflow volume (ft^3/d)	Discharge	Outflow volume (ft^3/d)
Recharge from precipitation	103,810	Streams	88,080	Recharge from precipitation	102,280	Streams	83,348
Underflow from upgradient areas	85,175	Underflow to downgradient areas	111,740	Underflow from upgradient areas	71,370	Underflow to downgradient areas	99,472
Vertical flow from deeper units	27,275	Vertical flow to deeper units	4,406	Vertical flow from deeper units	27,275	Vertical flow to deeper units	4,406
Seawater[1]	2,276	Seawater[1]	13,328	Seawater[1]	95	Seawater[1]	12,830
		Wells	982			Wells	982
Total	218,536	Total	218,536	Total	201,020	Total	201,038
Transport domain				Transport domain			
Source	Inflow volume (ft^3/d)	Discharge	Outflow volume (ft^3/d)	Source	Inflow volume (ft^3/d)	Discharge	Outflow volume (ft^3/d)
Recharge from precipitation	18,340	Streams	13,209	Recharge from precipitation	18,308	Streams	12,367
Underflow from upgradient areas	4,814	Underflow to downgradient areas	272	Underflow from upgradient areas	3,545	Underflow to downgradient areas	337
Vertical flow from deeper units	677	Vertical flow to deeper units	228	Vertical flow from deeper units	649	Vertical flow to deeper units	232
Seawater[2]	91	Seawater[2]	10,215	Seawater[2]	67	Seawater[2]	9,644
Total	23,922	Total	23,924	Total	22,570	Total	22,579

[1]Dogfish and Liberty Bays and Port Orchard.

[2]Dogfish and Liberty Bays.

Simulation of Variable-Density Flow and Transport of Chlorinated Ethenes

Two SEAWAT simulations of steady-state, variable-density flow and transient solute transport were conducted for the 1.3 mi² transport domain surrounding the Keyport Peninsula using models A and B. The first 5,000-yr simulation used a single solute (seawater) to establish the initial distribution of seawater for the second 50-yr simulation that consisted of two solutes, seawater, and CVOCs. Both SEAWAT simulations used the same model design and parameter distributions as in the MODFLOW-2005 groundwater-flow models A and B discussed previously but required the specification of additional model features to represent transport as described further on. The model input, output, and executable files are available from Yager (2020).

In the variable-density flow and transport simulations described herein, the flow and transport equations were explicitly coupled using a one time-step lag and solved alternately with a mass-balance error less than 0.01 percent. An implicit finite-difference (FD) method with upstream weighting was used to solve the advection-dispersion equation in the single-solute simulation of seawater. The selection of the FD method allowed the use of relatively large time steps (up to 100 days) in the 5,000-year simulation and resulted in run times of 4 hours on a 3.2-GHz Zeon processor. The total-variation-diminishing (TVD) method with a Courant number of 1.0 was used to solve the advection equation in the dual-solute simulation of seawater and CVOCs in order to minimize numerical dispersion. The TVD method required much smaller time steps (0.5 days) in the 50-yr simulation and resulted in run times of seven hours. The potential effect of numerical dispersion on model results was explored through alternative simulations discussed later in this report.

Model Design

The transport-model domain (fig. 19) extends from the top of the groundwater-flow model (model layer 1) to the upper part of the Clover Park Aquitard (Unit 7, QC1, model layer 12) (table 1). Solute concentrations predicted by transport simulations for Unit 7 are disregarded, however, because the thickness of model layer 12 is over 100 ft beneath OU-1, greater than the numerical dispersion criteria allows. Unit 7 would need to be discretized into several model layers in order to obtain accurate solute concentrations from transport simulations. Four additional model parameters (porosity and longitudinal, horizontal-transverse, and vertical-transverse dispersivities) were specified in both transport simulations. A porosity value of 0.2 was specified for all hydrogeologic units and a porosity of 1.0 was specified for surface water.

Longitudinal dispersivity parallel to the direction of groundwater flow was specified as proportional to the grid cell size, in accordance with the observation that measured values of dispersivity increase with the scale of observation (Zheng and Bennett, 2002). Longitudinal dispersivity α_l was computed for each grid cell as:

$$\alpha_l = \frac{(\Delta r^* \Delta c)^{1/2}}{2} \quad (4)$$

where

Δr and Δc are the row and column dimensions (L) of the cell.

The maximum α_l value was limited to 50 ft. The computed α_l value (12.5 ft) for the smallest grid cells (25 × 25 ft) is within the high portion of the range of reported field values in Gelhar and others (1992) and therefore conservative, as dispersion could be over-estimated. The computed α_l value (50 ft) for the largest cells (351 × 500 ft) falls within the trend of the data in Gelhar and others (1992). The largest grid cells are located at the eastern edge of the Keyport Peninsula and do not affect the simulated migration of CVOCs at OU-1. Values of horizontal-tranverse and vertical-tranverse dispersivity perpendicular to the direction of groundwater flow were specified as ratios to the longitudinal dispersivity. Ratios of 0.1 and 0.01 for the horizontal-tranverse and vertical-tranverse dispersivity, respectively, were specified in accordance with recommended values in Zheng and Bennett (2002).

Seawater Simulation

The transport equations solved by the SEAWAT simulations are written in terms of concentration (ML^{-3}), and additional boundary conditions regarding solute concentrations are specified for the transport-model domain. Seawater concentrations in both the single- and dual-solute simulations ranged from zero percent for fresh water with a specific gravity of 1.0 to 100 percent for seawater in surface-water bodies with a specific gravity of 1.022. Constant-concentration boundaries of 100 percent were specified in model layer 1 to represent seawater in Dogfish and Liberty Bays, the tide flats and Port Orchard (fig. 19). Constant-concentration boundaries of 50 percent were specified in model layer 2 to represent pore waters in mud flats surrounding Dogfish Bay. The initial seawater concentration in all other grid cells within the transport domain was specified as zero in the single-solute, seawater simulation. The computed seawater concentrations in model cells beneath the surface-water bodies increased during the 5,000-year simulation, and the computed distribution of seawater concentration at the end of the simulation served as the initial seawater-concentration distribution for the dual-solute, CVOC simulation.

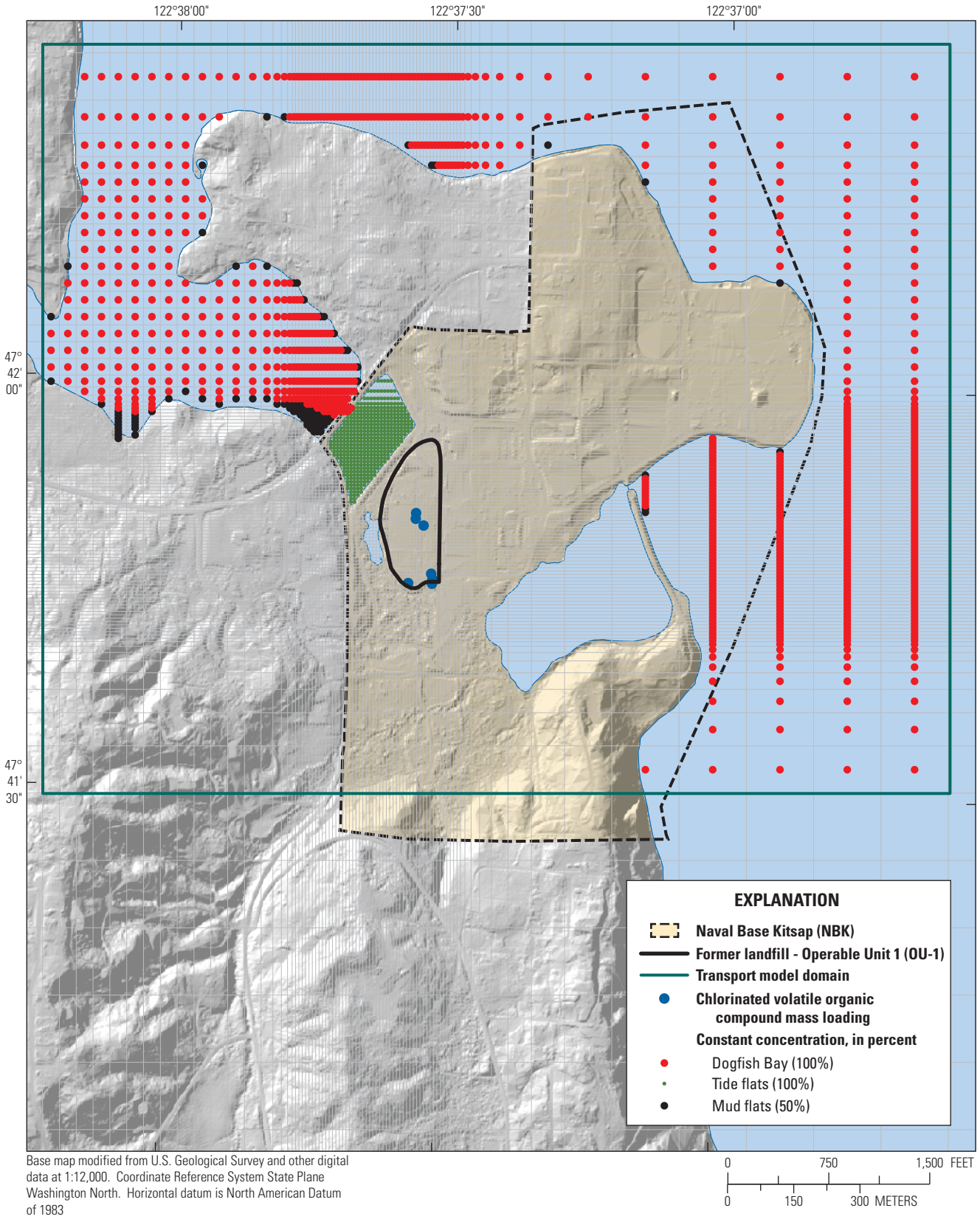

Figure 19. Domain and boundary conditions in transport simulations, Operable Unit 1, Naval Base Kitsap, Keyport, Washington.

CVOC Simulation

Inflow of CVOCs in the former landfill at OU-1 was represented though mass-loading rates (MT^{-1}) that remained constant throughout the dual-solute simulation. Concentration units of mg/L were chosen to represent CVOCs in the dual-solute simulation in order to facilitate comparison of model results with existing maps of the CVOCs distribution at OU-1 that use these concentration units. Units of mass in SEAWAT are defined as the product of concentration units and water volume. If inconsistent units are specified in the model (for example, concentration units of mg/L and length units of ft), then mass units are given in the unconventional units of milligram-cubic feet per liter [mg-ft^3/L]. A conversion factor of 2.832×10^{-5} milligram-cubic feet per liter (kg-L/mg-ft^3) is applied to convert the mass units computed by model simulations to kg (Christopher Neville, S.S. Papadopulos & Associates, Inc., written commun, 2009).

Mass-loading rates were specified at model cells identified through analysis of CVOCs concentration data collected from sediment cores and groundwater wells within the former landfill at OU-1 from 2015 to 2017. Molar concentrations of trichloroethene (TCE), 1-2-*cis*-dichloethene (DCE) and vinyl chloride (VC) were summed to obtain total CVOC concentrations at different depths at seven persistent contaminant sources in OU-1, including model cells corresponding to monitoring wells MW1-50, -56, -57-, and -58 and in the southern part of the landfill, and model cells corresponding to monitoring wells MW1-46, -47-, and -48 in the central part of the landfill (fig. 3). Mass-loading rates were adjusted in transport simulations to reproduce the maximum CVOC concentrations observed at these seven locations.

Complete, sequential reductive dechlorination of CVOCs has been demonstrated at OU-1 through the identification of redox conditions and the presence of ethene (Dinicola, 2006), and mass—degradation rates of total CVOC concentrations have been estimated from changes in concentration data along groundwater flow paths. Individual degradation rates between pairs of parent and daughter compounds in the degradation chain have not been estimated, however. For this reason, the expected degradation of CVOCs was neglected in the initial transport simulation described below, with the understanding that a considerable portion of the CVOCs generated through mass loading would be biodegraded to ethene and not discharge with groundwater at downgradient boundaries, as predicted by the simulation. The goal of the initial transport simulations was to reproduce the observed configuration of the CVOCs plume at OU-1, and thereby estimate both the mass-loading rates of CVOCs from persistent contaminant sources and the total mass of CVOCs in the contaminant plume. An additional simulation described further on addresses the potential effects of biodegradation of CVOCs at OU-1 using Model A.

Simulation Results

Seawater Simulation

The mass of seawater in the transport domain increases rapidly at the beginning of the 5,000-yr, single-solute transport simulation with Model A, but then increases gradually near the end of the simulation as it asymptotically approaches a limit of slightly less than 3×10^9 kg (fig. 20). The mass of seawater in the transport simulation with Model B is about 12 percent larger than with Model A. The increase in seawater mass at the end of the transport simulations results from the continued influx of higher-density seawater that displaces lower-density fresh water in low permeability sediments of the Clover Park Aquitard underlying Dogfish and Liberty Bays. A 3D depiction of the computed seawater distribution (fig. 21) indicates that seawater concentrations greater than 1 percent (about 340 mg/L) extend 100 ft beyond the tide flats, although the predicted penetration of seawater is farther on the western end of Keyport Peninsula where the model cells are larger.

A vertical section from the marsh pond north through the tide flats and the western arm of the Keyport Peninsula shows the extent of the transition zone between fresh water and seawater near OU-1 with Model A (fig. 22). The transition zone is about 100 ft wide and extends to the bottom of the Qv sediments. Saline water overlies fresh water at shallow depths south of the tide flats where groundwater in the deeper, permeable Qv sediments discharges into seawater. The transition zone with Model B is about 25 ft wider than with Model A as a result of the higher K values in Units 1 and 2 (Qvr and Qestuary). The computed distribution of saline water extends into the Clover Park Aquitard under the deeper part of the tide flats and Liberty Bay.

Chlorinated Volatile Organic Compounds Simulation

The mass of CVOCs beneath OU-1 increases rapidly at the beginning of the 50-yr, dual-solute transport simulation with Model A, but then increases gradually and approaches a dynamic equilibrium when the contaminant mass in groundwater reaches about 256 kg (fig. 23). Almost all the contaminant mass (134 g/d) discharges to small creeks draining the southern edge of OU-1, while most of the remainder discharges to the marsh pond and creek (1.7 g/d) and the tide flats (49 mg/d). The CVOC mass-loading rate is 150 g/d, of which about 95 percent sustains the southern plume. The mass-loading rate is within the range of biodegradation rates of 130–170 g/d estimated by Dinicola (2006) using CVOC concentration data from 1999 to 2000 and 2004, respectively. The actual mass-loading rate should be greater than the biodegradation rate, as a portion of CVOC mass discharges to surface waters adjacent to OU-1. Dinicola (2006) estimated that this mass flux ranged from 7 to 9 g/d in 2000 and 2004, respectively.

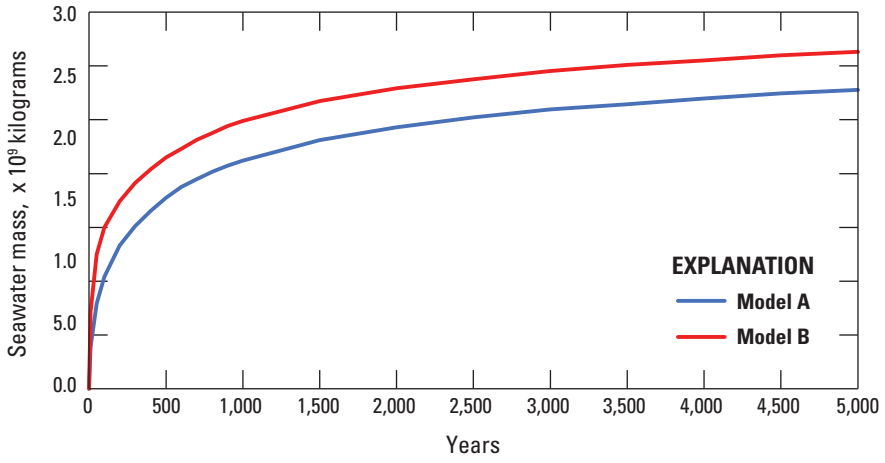

Figure 20. Computed mass of seawater during 5,000-year, single-solute simulations with models A and B, Operable Unit 1, Naval Base Kitsap, Keyport, Washington.

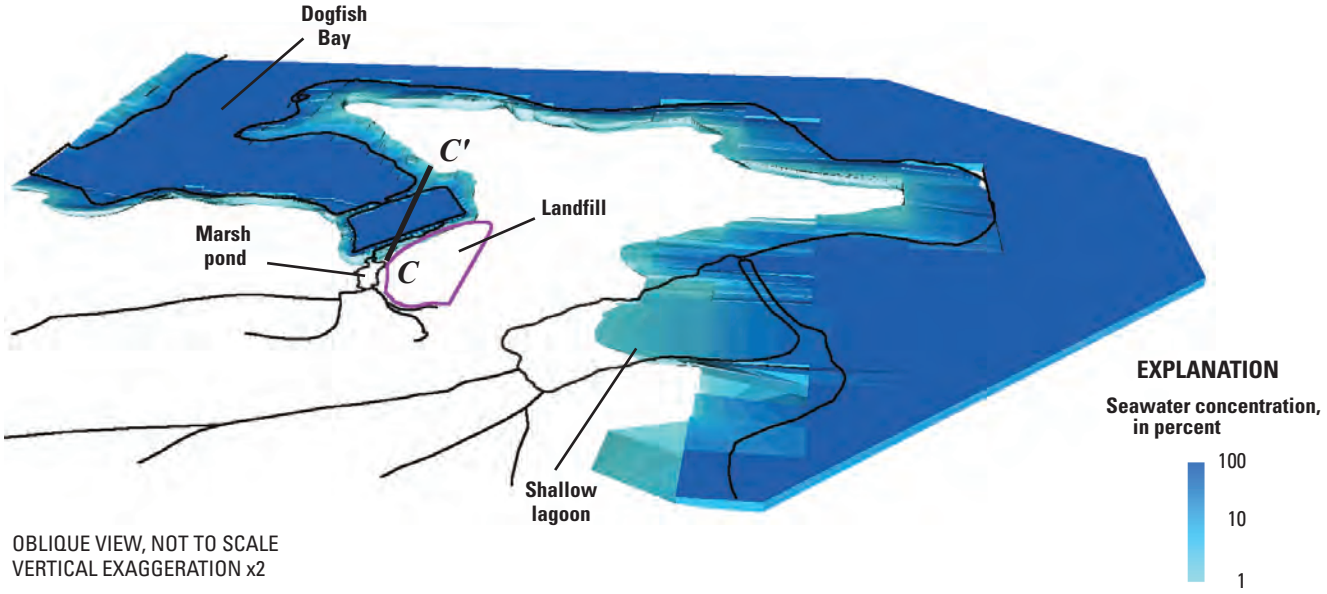

Figure 21. Computed seawater concentrations in the Qv sediments at the end of 5,000-year, single-solute simulation with Model A, Operable Unit 1, Naval Base Kitsap, Keyport, Washington.

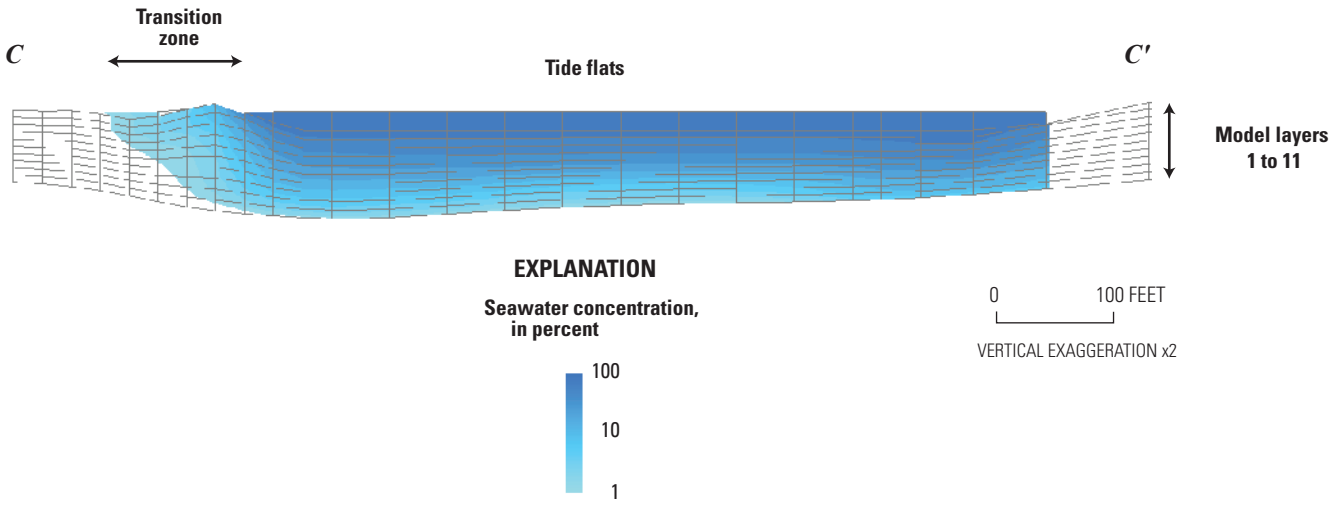

Figure 22. Vertical section C–C′ through tide flats showing computed seawater concentrations and transition zone between fresh water and seawater at the end of 5,000-year, single-solute simulation with Model A, Operable Unit 1, Naval Base Kitsap, Keyport, Washington.

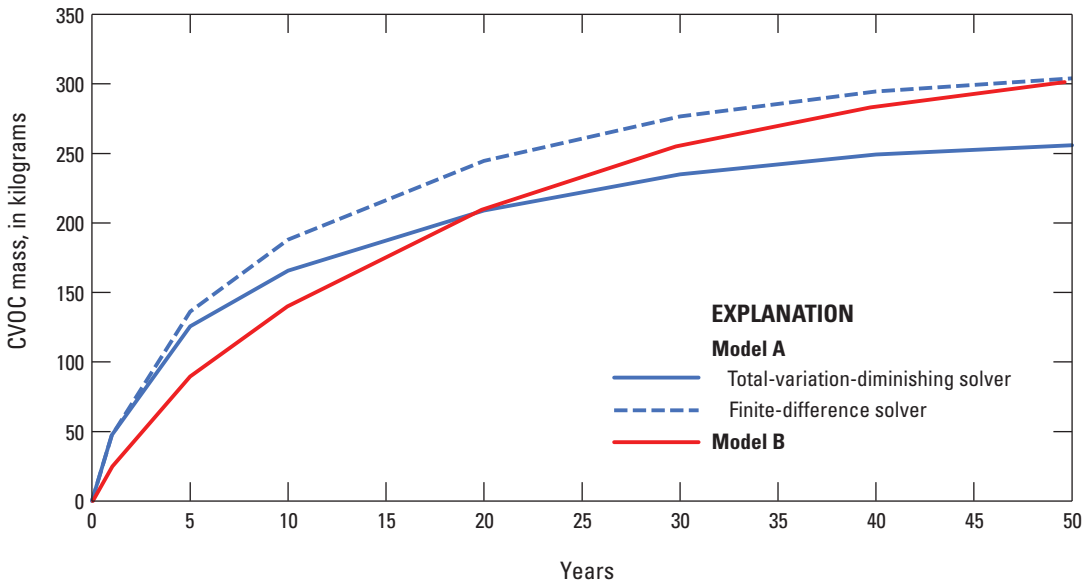

Figure 23. Computed mass of chlorinated volatile organic compounds (CVOCs) during 50-year, dual-solute simulations using total-variation-diminishing and implicit finite-difference solvers with Model A, and TVD solver with Model B, Operable Unit 1, Naval Base Kitsap, Keyport, Washington.

The mass of CVOCs beneath OU-1 is slightly greater with Model B (310 kg), but the CVOC mass-loading rate is only 73 g/d. The lower mass-loading rate results from the lower volume of groundwater flow in the deeper Qv sediments beneath OU-1 in Model B, in which the vertical anisotropy in Unit 5 (Qvsemi) is higher than in Model A. As a result, less contaminant mass (48 g/d) discharges to the small creeks draining the southern edge of OU-1 than in Model A. More CVOC mass discharges to the marsh pond and creek (7.8 g/d) and the tide flats (160 mg/d) in Model B, however, because the contaminant plumes are diverted westward to Dogfish Bay by the higher *K* values in Unit 2 (Qestuary).

Two distinct contaminant plumes emanate from the persistent sources in the transport simulation with Model A, a northern plume that migrates toward the marsh pond and creek, and a southern plume that migrates toward small creeks south of OU-1 (fig. 24). The extents of the simulated CVOC plumes agree favorably with those delineated from observed data (fig. 3), and the maximum CVOC concentrations for the northern and southern plumes (120 and 630 mg/L, respectively) are close to those estimated for the persistent contaminant sources. The southern plume accounts for about 70 percent of the total contaminant mass. Both CVOC plumes extend from the water table to the bottom of the Qv sediments. The CVOC plumes migrate downward to the base of the Qv sediments and then laterally before migrating upward to discharge in the marsh and creeks.

The two contaminant plumes emanating from the persistent sources intermingle in the transport simulation with Model B and become indistinguishable downgradient (fig. 25). Unfortunately, no contaminant data are available in locations between the two distinct plumes predicted by Model A, so the possibility that the Model B simulation is a more accurate depiction of actual CVOC migration cannot be either verified or ruled out on the basis of available data. The maximum CVOC concentrations at the northern and southern persistent sources with Model B are the same as those predicted by Model A (120 and 630 mg/L, respectively). As indicated above, the combined plumes in the Model B simulation migrate toward Dogfish Bay and less contaminant mass discharges to the small creeks at the southern edge of OU-1.

A vertical section from the marsh pond north through the tide flats shows the extent of the northern CVOC plume beneath Marsh Creek that discharges to the tide flats in the Model A simulation (fig. 26). The northern plume extends beneath the tide flats where it mixes with higher-density seawater. The seawater presents a hydraulic barrier that limits the upward discharge of CVOCs to the tide flats. As a result, most of the CVOCs in this area are forced to discharge to Marsh Creek. A vertical section through the CVOC contaminant distribution simulated with Model B is similar, but the combined plumes underlie the tide flats to the east of the plume simulated with Model A.

Application of the FD solver in place of the TVD solver in the 50-yr, dual-solute transport simulation with Model A produces a contaminant mass (304 kg) that is about 19 percent larger as a result of numerical dispersion (fig. 23). The increased dispersion generates larger CVOC plumes that overlap beneath the pond in the marsh (fig. 27). The difference in the extents of the CVOC plumes predicted by the TVD and FD solvers indicates that the magnitude of numerical dispersion associated with the FD solver ranges from 50 to 100 ft, or two to four grid-cell widths.

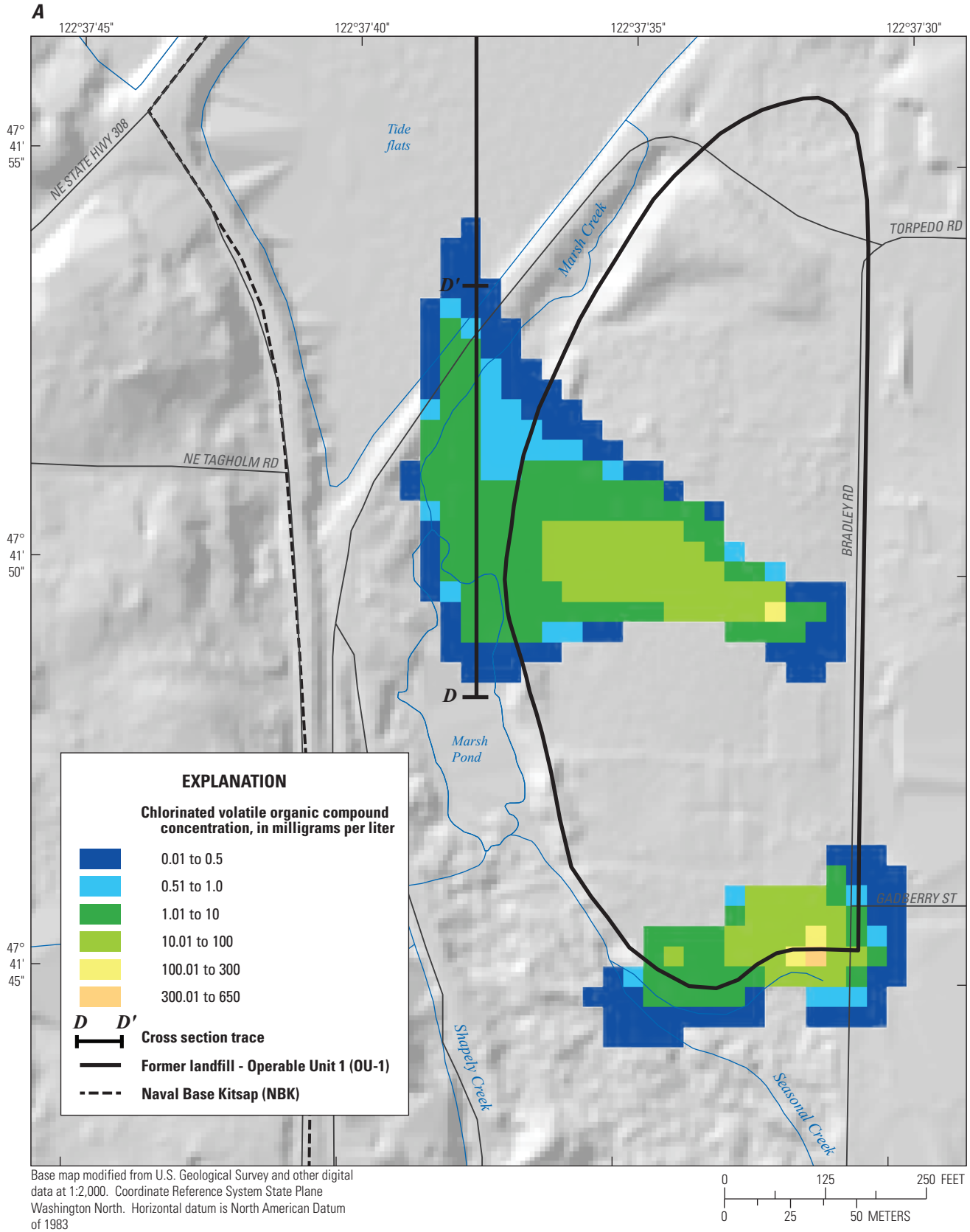

Figure 24. Computed chlorinated volatile organic compound (CVOC) concentrations in the Qv sediments at the end of 50-year, dual-solute simulation with Model A: *A*, plan view in Unit 6 (Qvinter), *B*, three-dimensional perspective view.

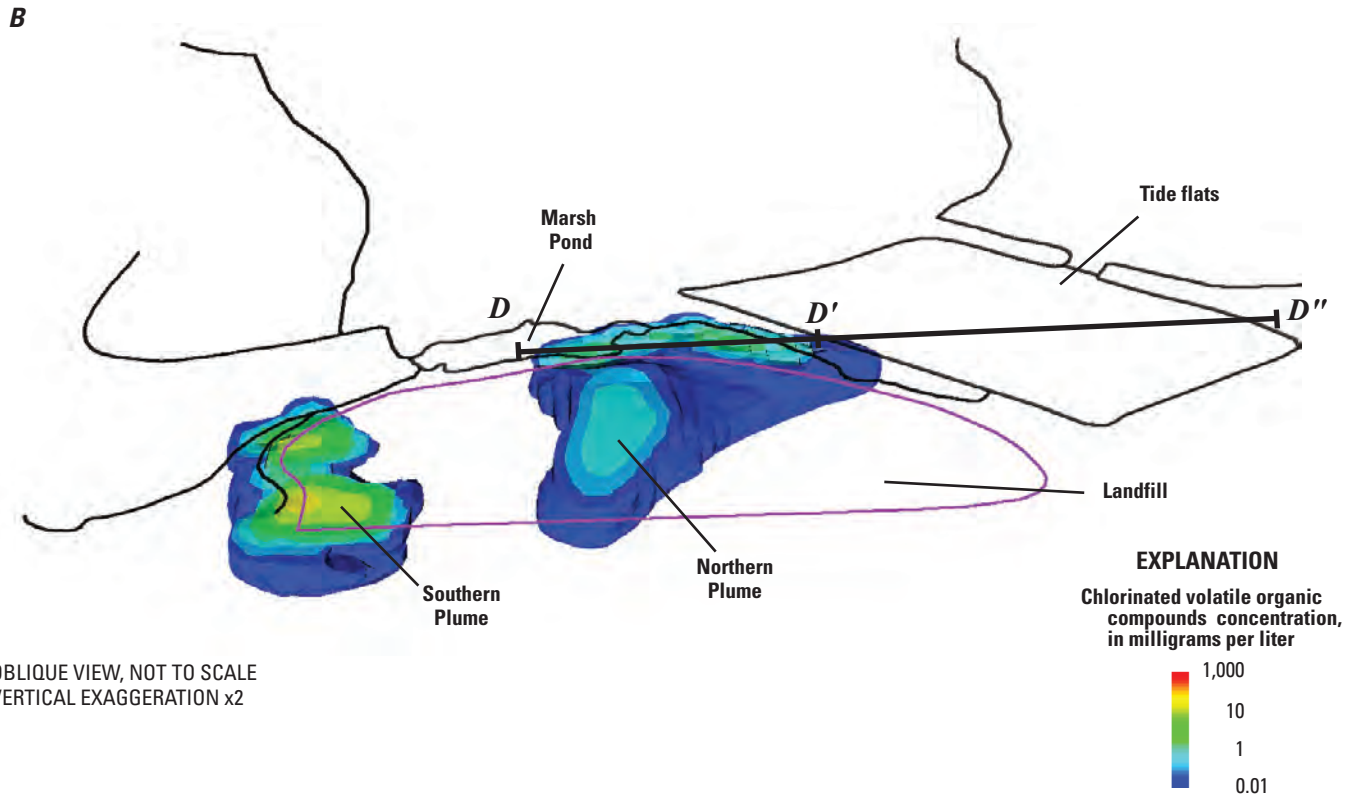

Figure 24.—Continued

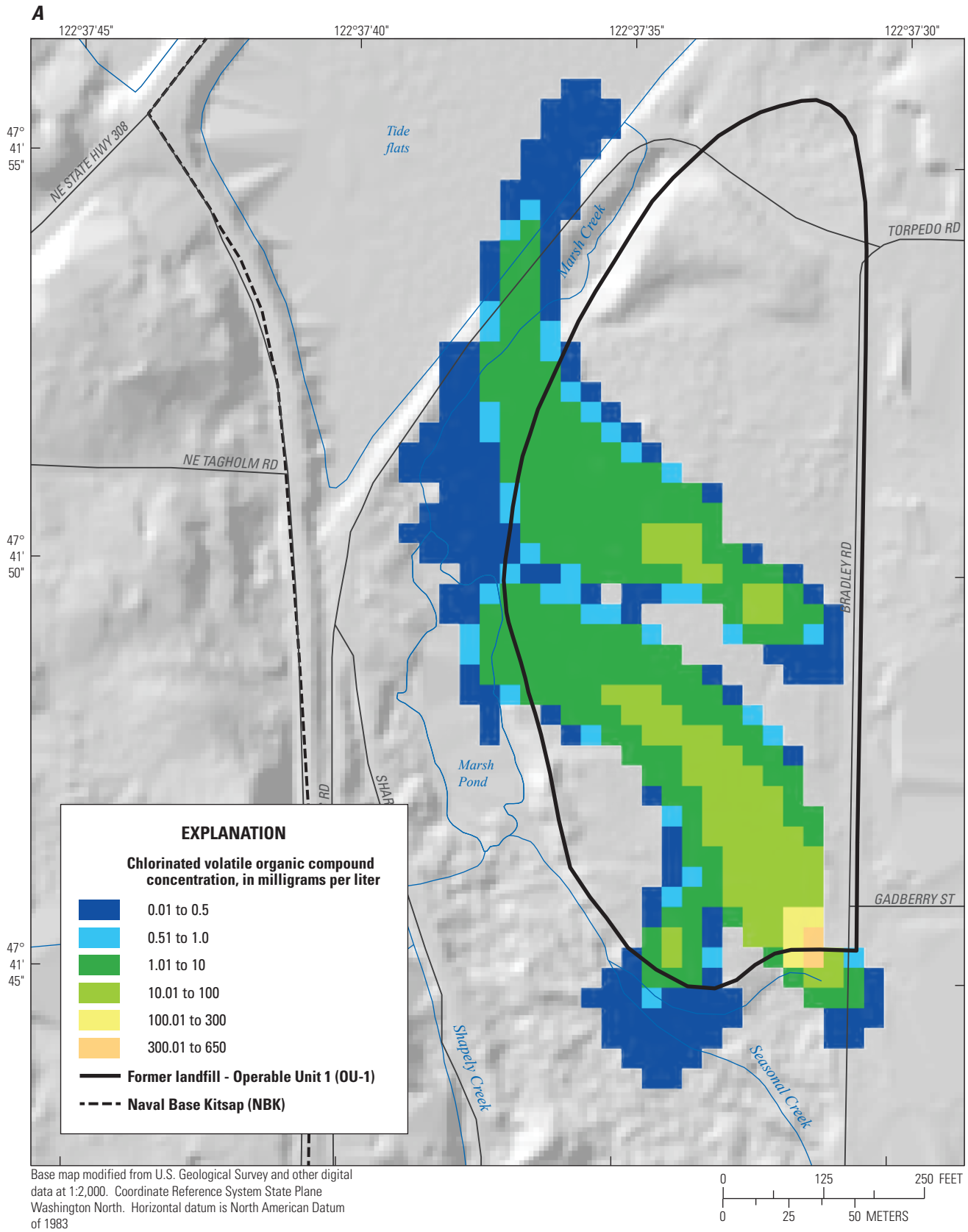

Figure 25. Computed chlorinated volatile organic compound (CVOC) concentrations in the Qv sediments at the end of 50-year, dual-solute simulation with Model B: A, plan view in Unit 6 (Qvinter), B, three-dimensional perspective view.

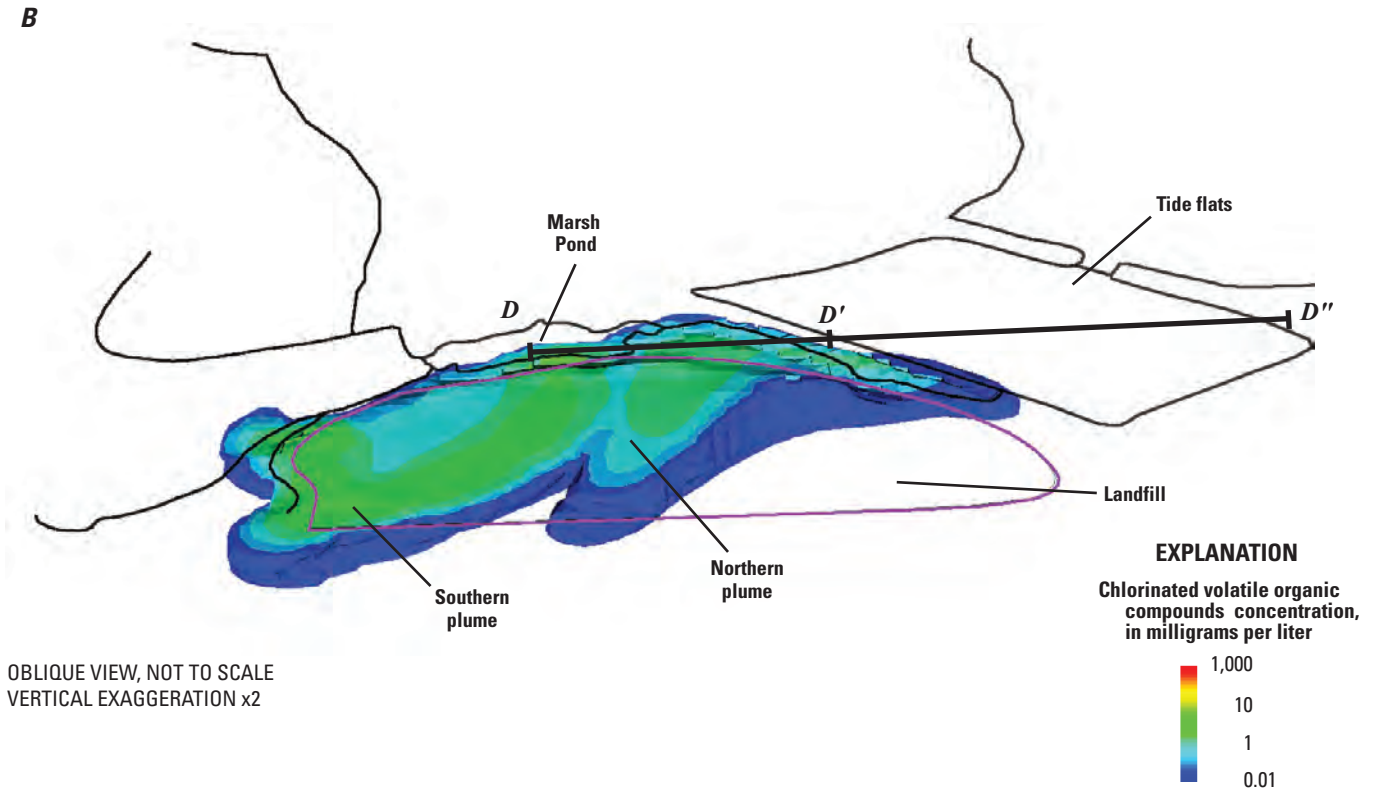

Figure 25.—Continued

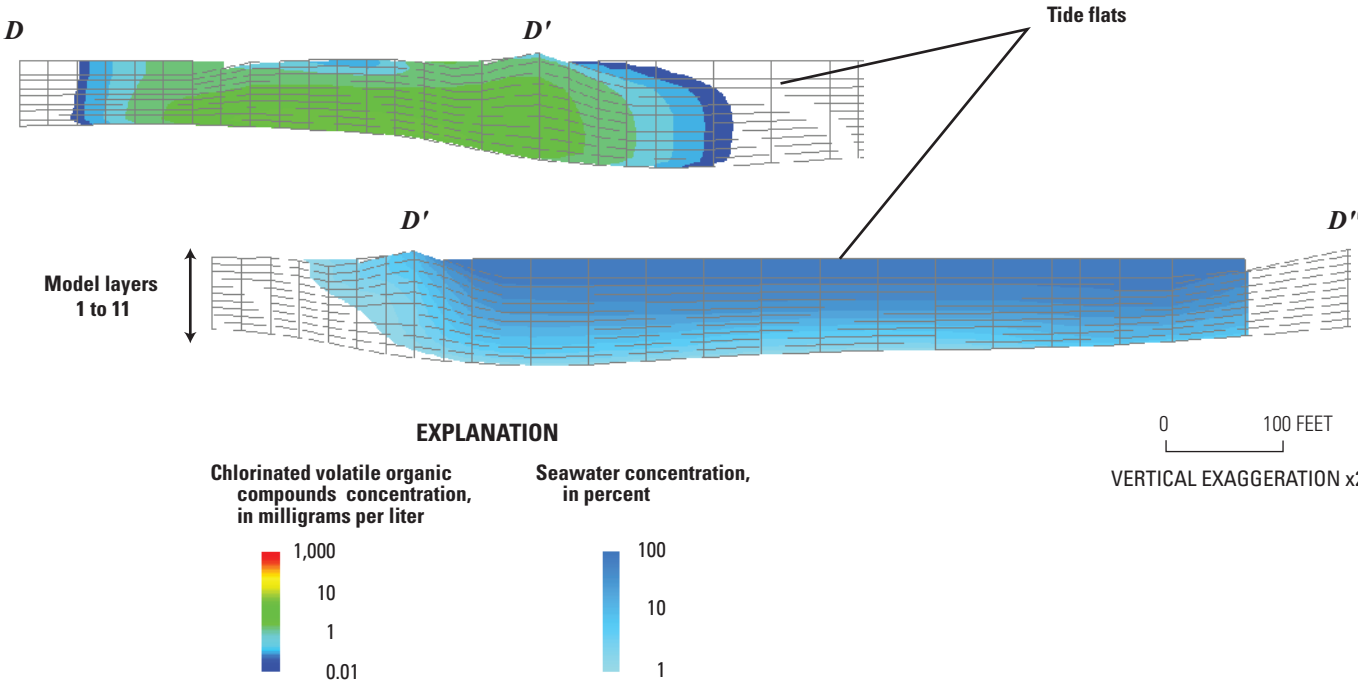

Figure 26. Vertical section from marsh pond through tide flats showing computed chlorinated volatile organic compound (CVOC) and seawater concentrations at the end of 50-year, dual-solute simulation with Model A.

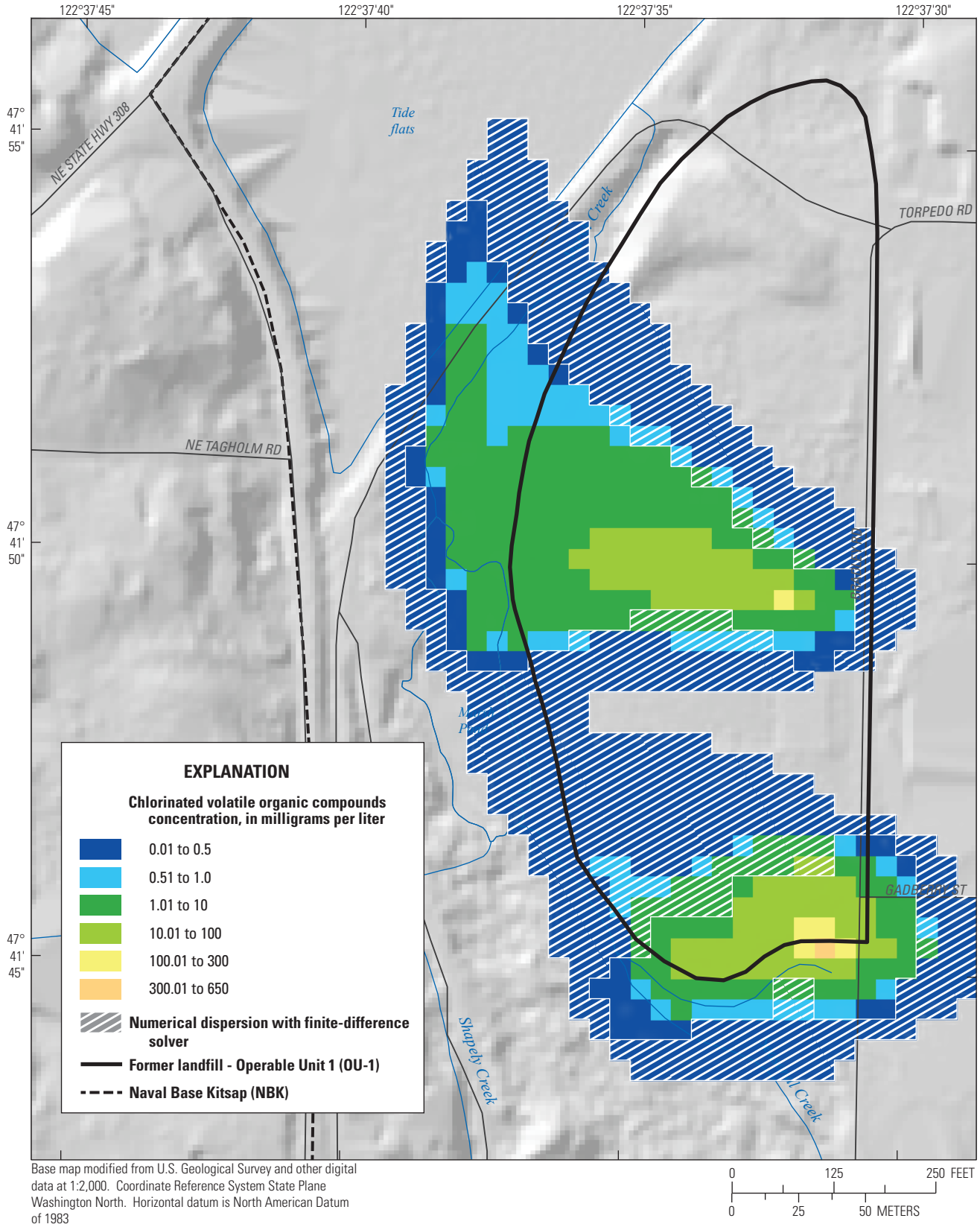

Figure 27. Comparison of the extents of chlorinated volatile organic compound (CVOC) migration with total-variation-diminishing and implicit finite-difference solvers with Model A showing effect of numerical dispersion.

Discussion of Simulation Results

Containment of Chlorinated Volatile Organic Compounds Contaminants

Results of the groundwater-flow and contaminant-transport simulations indicate that both geologic and hydraulic barriers limit the migration of CVOCs from the former landfill at OU-1. The CVOC contaminant plumes at OU-1 in both models A and B are largely contained within Naval Base Kitsap, although a small quantity of CVOCs discharges to the tide flats. The Clover Park Aquitard, a low-permeability geologic barrier that underlies the Keyport Peninsula and adjacent uplands, limits vertical groundwater flow between shallow, contaminated Qv sediments at OU-1 and deeper geologic units. Moreover, evidence from measured groundwater levels and simulated groundwater flow in both the regional Kitsap Model And Keyport model indicate that the hydraulic gradient is upward beneath the Keyport Peninsula, and presents an additional hydraulic barrier to the potential downward migration of CVOCs from OU-1 through the Clover Park Aquitard.

Underflow from upland areas south of the Keyport Peninsula discharges to the marsh at the base of the peninsula and presents an additional hydraulic barrier, limiting CVOC migration to the south. Contaminant transport simulations indicate that the CVOC plumes discharge mainly to the marsh pond and creeks. Only a very small portion of the simulated contaminant mass (less than 0.1 percent in Model A and 0.3 percent in Model B) discharges into seawater in the tide flats. It should be noted that neither of these simulations include the effects of biodegradation, which would decrease the predicted CVOC mass reaching the tide flats. The saline water that underlies seawater in the tide flats and in Dogfish and Liberty Bays west of OU-1 has a higher density than fresh groundwater and limits upward discharge of CVOCs into seawater. This saline water presents an additional hydraulic barrier that prevents westward CVOC migration beneath Dogfish Bay toward residential wells on Virginia Point.

Model Uncertainty

There are no shallow pumped wells on the Keyport Peninsula and, consequently, no data are available concerning the rate of groundwater flow through the Qv sediments in the area surrounding OU-1. Recharge to groundwater has been estimated by the SWB model described earlier, but the SWB recharge rates were adjusted downward during calibration of both models A and B to better match the observed base flow in the perennial stream that drains to the shallow lagoon, and to maintain the simulated water table below land surface. Estimated recharge rates are correlated with estimated hydraulic conductivities for hydrogeologic units in the Qv sediments, however. A combination of higher recharge rates and larger hydraulic conductivities would therefore yield higher groundwater flow rates with little change in model error. Uncertainty in the rates of recharge and groundwater flow produces uncertainty in the estimated mass-loading rate of CVOCs.

At higher rates of recharge and groundwater flow, the CVOCs entering the flow system are transported faster to discharge boundaries, requiring larger mass-loading rates to maintain a stable configuration of the contaminant plume. The CVOC mass-loading rate with Model B (73 g/d) was lower, however, because most of the increased recharge in that model flows through the upper part of the Qv sediments, due to the increased vertical anisotropy in Unit 5 (Qvsemi). Data on the rate of groundwater flow on the Keyport Peninsula and under OU-1, collected through cross-hole aquifer tests or additional measurements of base flow in perennial streams, could be used to narrow the 73–240 g/d range of uncertainty associated with the estimated CVOC mass-loading rate at the OU-1 site.

Neither Model A nor B predicted groundwater flow or contaminant transport from OU-1 to wells MW1-38 and -39 located on the State Route 308 causeway to the northwest of the tide flats because of the hydraulic barriers identified above. The contaminants 1,4-dioxane and vinyl chloride have been detected in one or both of those wells at low concentrations (maximum values of 4.1 and 2.7 µg/l). Dinicola and others (2002) could not determine whether groundwater at these causeway wells originated from OU-1, based on multiple lines of evidence from chemical isotope and common-ion geochemical data. There are no wells in the tide flats to provide data on the continuity of hydrogeologic units between the landfill and the causeway, so there is uncertainty as to whether the contaminants measured in those wells originated in the landfill or elsewhere.

Effect of Biodegradation

Previous studies (Dinicola and others, 2002; Dinicola, 2006) have established that reductive dechlorination of CVOCs is occurring at OU-1, and Dinicola (2006) estimated CVOC biodegradation rates ranging from 130 to 170 g/d. A first-order, removal rate-constant λ for CVOCs at OU-1 was computed from these rate estimates using the CVOC mass in the contaminant plume obtained from the 50-yr, dual-solute transport simulation with Model A. The rate constant λ (d^{-1}) is related to the reaction half-life $t_{1/2}$ as:

$$\lambda = \frac{\ln 2}{t_{\frac{1}{2}}} \qquad (2)$$

where

$t_{1/2}$ is the time required for the CVOC mass to decrease to half the original mass under the influence of biodegradation alone.

The half-life of the 256-kg contaminant plume predicted by the simulation is about 850 days at a biodegradation rate of 150 g/d, which is equivalent to a rate constant of about 8×10^{-4} d^{-1}. The comparable half-life and rate constant computed with

the CVOC mass predicted with transport simulation with Model B are 1,000 days and 7×10^{-4} d^{-1}. These estimated half-lives are within the range of $t_{1/2}$ values (35 to 3,600 days) for TCE, *cis*-DCE and VC reported for field sites by Wilson and others (1996).

An additional 50-yr, dual solute contaminant transport simulation with Model A was conducted in which CVOC biodegradation was represented as a first-order reaction with a rate constant of 10^{-3} d^{-1}. In this simulation the CVOC plume reached a stable mass of 77 kg within 10 years of migration, although the CVOC mass-loading rates and maximum CVOC concentrations were equivalent to those in the original contaminant-transport simulation described previously (fig. 28). About one half the CVOC mass was lost through biodegradation at a rate of 75 g/d, and nearly all the remainder (71 g/d) was discharged by the southern plume to a small creek south of OU-1. The CVOC mass discharged from the northern plume to the marsh and tide flats was 0.95 mg/d. The areas of the northern and southern plumes (fig. 29) are 67 percent and 32 percent less, respectively, than the areas computed by the original transport simulation (fig. 24), and the northern plume does not extend past the landfill boundary at concentrations exceeding 10 µg/L.

Refined estimates of CVOC mass-loading rates and biodegradation rates could be obtained in future transport simulations by matching CVOC concentrations at different locations within the contaminant plumes. Alternatively, individual biodegradation rates for components in the reductive dechlorination chain could be estimated by matching TCE, *cis*-DCE, and VC concentrations in a transport simulation that represents coupled sequential reactions. These simulations would also better estimate the mass-loading rates of CVOCs at OU-1. This effort was beyond the scope of the current study and would necessitate another variable-density, contaminant-transport program as SEAWAT Version-4 does not support coupled sequential reactions.

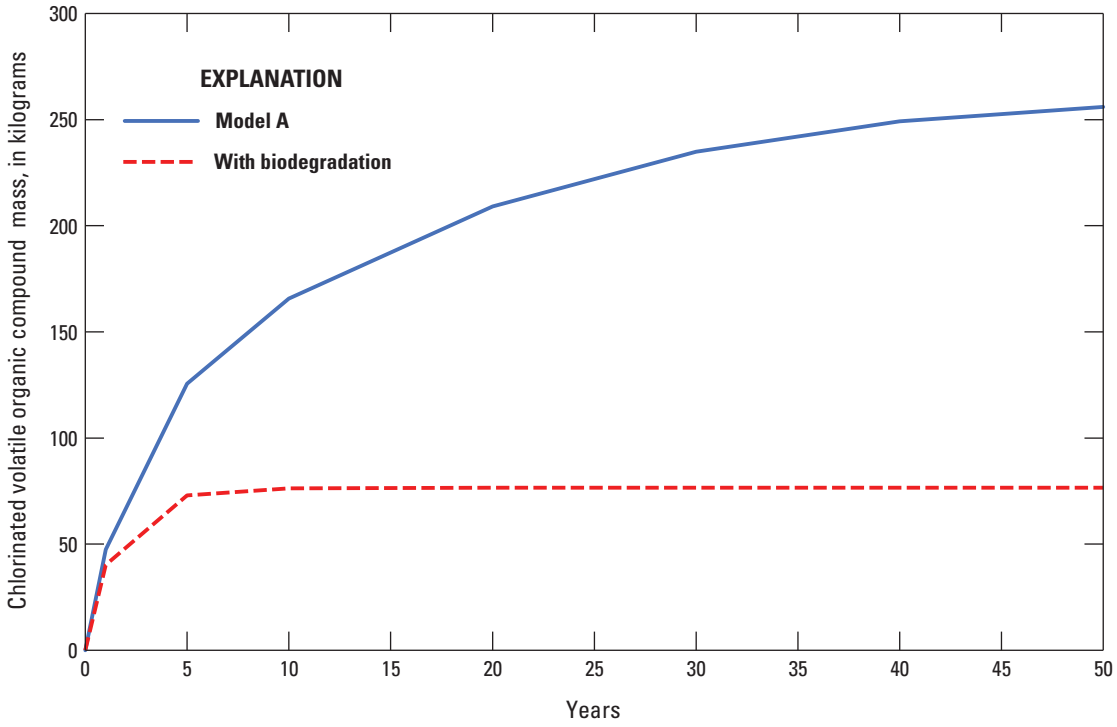

Figure 28. Computed mass of chlorinated volatile organic compounds (CVOCs) during original 50-year, dual-solute simulation with Model A, and alternate simulation with biodegradation.

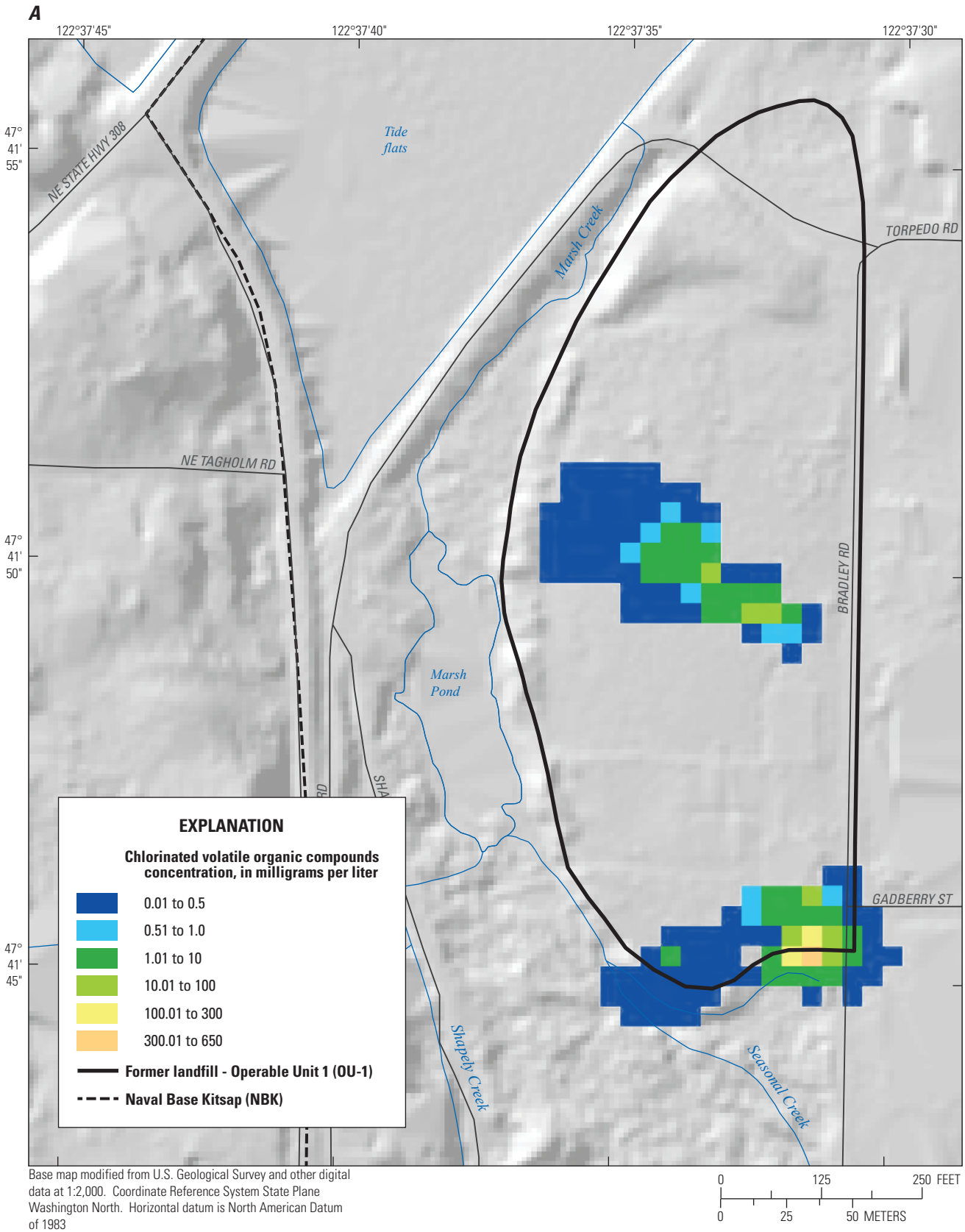

Figure 29. Computed chlorinated volatile organic compound (CVOC) concentrations in the Qv sediments at the end of 50-year, dual-solute simulation with Model A including biodegradation: *A*, plan view, *B*, three-dimensional perspective view.

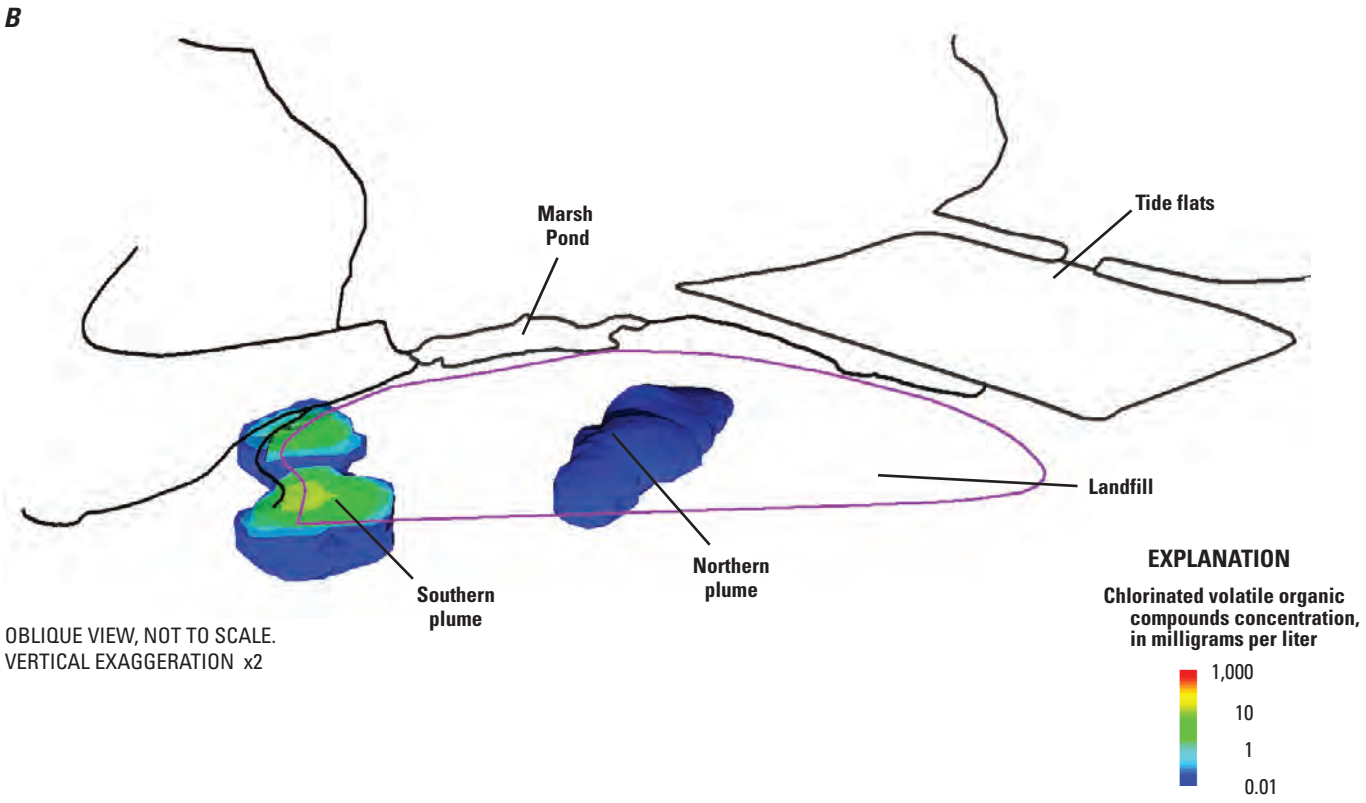

Figure 29.—Continued

Alternative Models

Two models (A and B) of groundwater flow and contaminant transport are presented that each provide an adequate fit to hydraulic and contaminant data. As indicated above, the determination as to which model more accurately predicts actual contaminant migration at OU-1 cannot be made without additional contaminant data. Both models predict similar contaminant masses and biodegradation rate constants and also predict that contaminant migration is limited by the same geologic and hydraulic barriers. Model predictions differ, however, in terms of the hydraulic parameters used in model simulations (recharge rates, and horizontal and vertical hydraulic conductivities) and in the CVOC mass-loading rates and contaminant plume configurations. The groundwater flow system simulated with Model B better represents the effects of tidal fluctuations on unconfined storage than does Model A and also uses recharge rates that are closer to those estimated with the SWB Model And predicts water table altitudes near OU-1 that are below land surface. Model B overestimates the effects of unconfined storage, however, and underpredicts the response of groundwater levels to tidal fluctuations and also overpredicts measured stream flow. In the following sections, Model A, which better represents the groundwater-level response to tidal fluctuations, is used to demonstrate the effects of the representation of tidal fluctuations and potential remedial activities. The effects illustrated using Model A would be similar if Model B were chosen instead, however.

A version of MODFLOW 6 will soon be available that supports variable-density flow and contaminant transport (C.D. Langevin, U.S. Geological Survey, written commun., 2019). Application of this MODFLOW 6 version could represent the distribution of discontinuous hydrogeologic units in the Keyport model domain directly (without using the HUF2 package), permit the use of the NWT solver and, therefore, better represent unconfined and confined storage. A single model could then be developed to simulate groundwater flow and CVOC contaminant migration at OU-1 and greatly simplify the modeling approach described in the current study.

Effect of Tidal Fluctuations

The 50-yr, steady-state, contaminant-transport simulations of CVOC migration with Model A discussed previously represent the mean (average of high and low tide) tidal conditions in Dogfish and Liberty Bays and Port Orchard based on predicted high and low tides in 2017. The depiction of mean tidal conditions was necessary in order to complete the simulations within a reasonable time, as determined by the small time increments required by the TVD solver. Two alternate simulations with Model A were conducted to assess the sensitivity of predicted CVOC migration from OU-1 to the depiction of tidal fluctuations. In the first simulation (C), the mean tide was computed for Dogfish and Liberty Bays, Port Orchard, and the tide flats and Marsh Creek, as the average of

water levels measured during the 31-day period in July and August 2018. The mean water levels in steady-state simulation A were lowered by 1.2 ft in Dogfish and Liberty Bays, 0.87 ft in the tide flats, and 0.1 ft in Marsh Creek. In the second simulation (D) the FD solver was applied in a 51-yr transient simulation that consisted of 600 repetitions of the 31.05-day transient periods used for calibration of the groundwater-flow model. In transient simulation B, tidal fluctuations were represented as shown in figure 11. The initial conditions for the simulation D were the same as those used in 50-yr, steady-state transport simulation computed with the TVD solver with Model A and required several days to complete.

The results of the steady-state TVD simulation C and the transient FD simulation D are compared with the original steady-state TVD and FD simulations with Model A depicted previously in figure 24. Under steady-state simulation C the CVOC mass in the contaminant plumes increased slightly faster than in the original TVD simulation, and the CVOC mass after 50 years (272 kg) was 6 percent higher (fig. 30). The simulated northern CVOC plume extended about 100 ft farther under the tide flats, and CVOC discharge to the tide flats increased from 49 mg/d under the original TVD simulation to 890 mg/d. CVOC discharge to Marsh Creek and pond were reduced by 46 percent from 1,700 to 770 mg/d. Under transient simulation D the CVOC mass in the contaminant plumes increased slightly slower than in the original FD simulation, and the CVOC mass after 50 years (297 kg) was 3 percent less (fig. 30). The simulated northern CVOC plume extended about 75 ft farther under the tide flats, and CVOC discharge to the tide flats increased from 67 mg/d under the original FD simulation to 75 mg/d. The extent of the transition zone between fresh water and seawater north of the marsh was increased from 100 ft in the original steady-state FD simulation to 125 ft in transient simulation B.

The results of these pairs of simulations indicate that the representation of tidal fluctuations has a small effect on the sizes and masses of the simulated CVOC plumes. Comparisons of the TVD and FD simulations must be considered separately because the effects of numerical dispersion are greater than the effects of tidal fluctuations on the simulated CVOC plumes. Representing the mean tidal stages in steady-state simulation C as the averages of water levels measured during the 31-day period in July and August 2018 predicts larger CVOC plumes than in the original TVD simulation, in which the mean tidal stages computed with the average of high and low tide stages are higher. The larger northern CVOC plume results in more CVOC discharge to the tide flats and less discharge to the marsh. Data required to compute the averages of water levels in all surface-water bodies are only available for the 31-day period in July and August 2018, however, which may not be representative of annual tidal fluctuations.

In contrast, representation of tidal fluctuations in transient simulation D results in smaller CVOC plumes and only slightly more CVOC discharge to the tide flats than in the original steady-state FD simulation. Simulated tidal stages in transient simulation D are more frequently higher than the mean stage, despite the representation of the low tide period. In both pairs of simulations, the increase in CVOC discharge from the northern CVOC plume to the tide flats is offset by a decrease in CVOC discharge to the marsh. It is important to note that neither of the pairs of simulations represents biodegradation, which was previously shown to reduce CVOC discharge to the tide flats and the marsh by a factor of 50.

The small effect of tidal fluctuations on the sizes and masses of the simulated CVOC plumes is expected because the period of the fluctuations (12 hr) is rapid compared with the groundwater velocity (20 ft/yr) beneath OU-1. The rapid tidal fluctuations slightly alter groundwater-flow paths and the representation of lower tidal stages causes the simulated northern CVOC plume to lengthen slightly under the tide flats. These results are consistent with those of La Licata and others (2007), who simulated the effect of tidal fluctuations on variable-density groundwater flow and contaminant transport in a coastal aquifer in Italy. They found that representing tidal fluctuations had little effect on the contaminant mass discharged to seawater. The principal effect of tidal fluctuations in their simulations was to increase the width of the transition zone between fresh water and seawater, thereby increasing dispersion of contaminants near the seashore. An increase in the transition zone was also noted in transient simulation D, indicating that tidal fluctuations could affect CVOC concentrations near the tide flats. These effects are likely small compared with the larger effects produced by biodegradation, however.

Implications for Remediation of Contaminant Sources

The U.S. Navy has conducted a comprehensive characterization program at the OU-1 site to delineate the locations of persistent contaminant sources in the former landfill (Battelle Memorial Institute, 2018). Current studies at the site are focused on potential remediation strategies to attenuate or isolate these contaminant sources. Three additional 50-yr, steady-state contaminant-transport simulations with Model A were conducted as a complement to these studies to predict the time required for potential source-control measures to diminish the mass of CVOCs in groundwater at OU-1. The initial conditions for the contaminant-transport simulations were taken from the end of the original 50-yr, steady-state simulation of CVOC migration with Model A without biodegradation discussed above. The mass-loading rates of CVOCs in the three simulations were reduced by factors of 50, 90 and 99 percent, respectively.

In each of the three contaminant source-control scenarios the mass of CVOCs decreased rapidly at first and then slowly approaches a new dynamic equilibrium (fig. 31). The reduction in CVOC mass in groundwater after 50 years in each scenario is slightly less than the magnitude of source reduction (table 6). The reductions of CVOC mass in groundwater after 50 years for the three scenarios are 46, 86, and 95 percent, respectively. The sizes of the contaminant plumes are largely unchanged from the original transport simulation (fig. 24), although the CVOC concentrations in each are reduced.

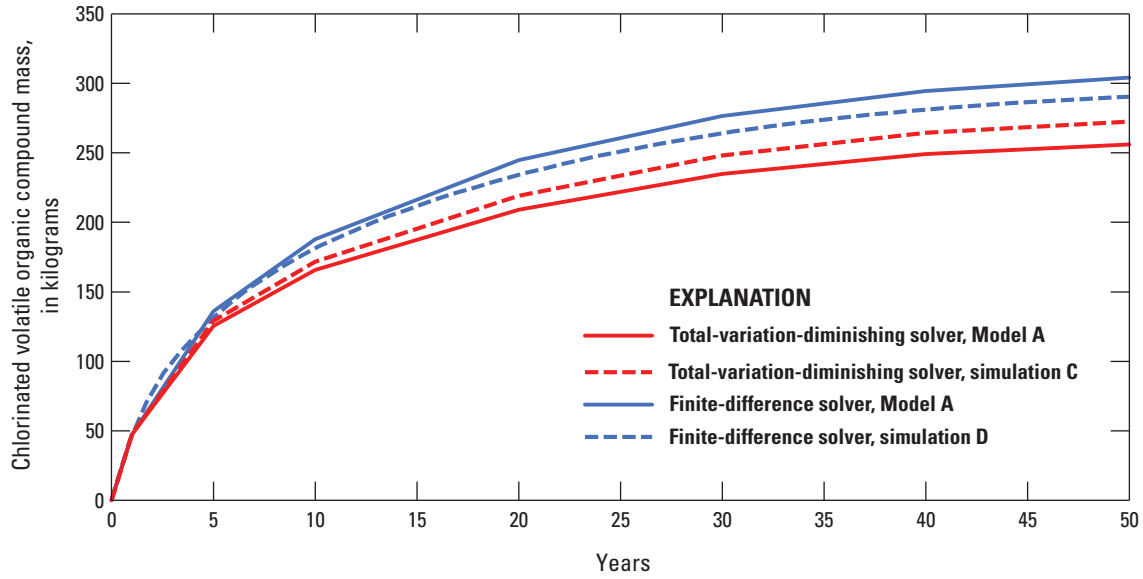

Figure 30. Computed mass of chlorinated volatile organic compounds (CVOCs) during original 50-year, dual-solute simulations using total-variation-diminishing and implicit finite-difference solvers with Model A, and alternate steady-state simulation C with lower tidal stages and alternate transient simulation D with transient representation of tidal fluctuations.

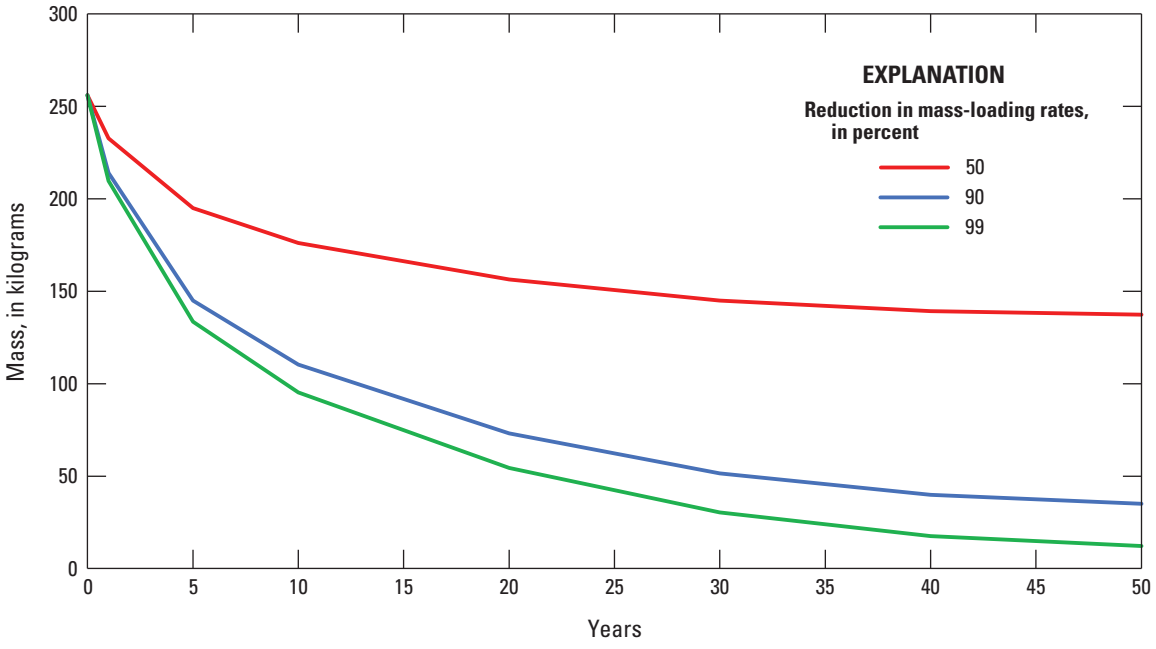

Figure 31. Reduction in chlorinated volatile organic compound (CVOC) mass with time resulting from three contaminant source-control scenarios with Model A that reduce CVOC mass-loading rates.

Table 6. Reduction in chlorinated volatile organic compounds mass after 50 years of contaminant source-control measures with Model A, Operable Unit 1, Naval Base Kitsap, Keyport, Washington.

[**Abbreviations:** g/d, gram per day; CVOC, chlorinated volatile organic compounds]

Scenario	Percentage reduction in mass-loading rate	Mass-loading rate (g/d)	Percentage reduction in CVOC mass in plumes
1	50	74	46
2	90	24	86
3	99	2.4	96

Summary

Chlorinated volatile organic compounds (CVOCs) have migrated to groundwater beneath a former 9-acre landfill at Operable Unit 1 (OU-1) of the Naval Base Kitsap on the Keyport Peninsula, in Kitsap County, Washington. Previous studies demonstrated that biodegradation of CVOCs in shallow groundwater at OU-1 is substantial and prevents most of the mass of dissolved-phase CVOCs in groundwater from discharging to surface water, but contaminant concentrations up to 630 milligrams per liter persist in localized areas, likely from the dissolution of residual, non-aqueous phase liquids. Variable-density groundwater-flow and contaminant-transport models were developed using SEAWAT-Version 4 to simulate the direction and rate of groundwater flow in a 5.9 mi^2 area surrounding the Keyport Peninsula, estimate the CVOC mass in groundwater and the rate of mass loading, and to assess possible remedial activities at OU-1.

The landfill at OU-1 is on a narrow strip of land connecting the Keyport Peninsula to the mainland and is adjacent to tide flats extending from Dogfish Bay, a segment of Liberty Bay connected to Puget Sound. The study area is underlain by Quaternary deposits consisting of alternating glacial and interglacial sediments from 500 to 1,500 ft thick. A sequence of six units was delineated in a hydrogeologic model within a relatively thin package (less than 100 ft) of recent sediments from the Vashon Stade (Qv) and younger deposition beneath the Keyport Peninsula. These Qv sediments are underlain by the much thicker (more than 300 ft) Clover Park Aquitard (QC1), which in turn overlies a confined, sea-level aquifer (QA1).

A shallow lagoon, tide flats, marsh (including a pond and outlet creek), and Dogfish Bay are the principal areas of groundwater discharge near OU-1. Water levels in these surface-water bodies fluctuate in response to tidal cycles, but manmade structures limit the extent of water-level fluctuations in the tide flats, marsh, and shallow lagoon. Groundwater flow at OU-1 is derived from lateral flows from the Keyport Peninsula to the northeast and from the Kitsap Peninsula uplands to the southwest and from vertical flow from the underlying sea-level aquifer (QA1).

Daily tidal fluctuations in Liberty Bay follow a semi-diurnal pattern that includes two high tides and two low tides each day, with a higher and lower high tide and a higher and lower low tide. The mean high-high tide in Liberty Bay in 2017 was 7.94 ft, and the mean low-low tide was -2.54 ft (based on tides predicted by NOAA at Poulsbo, Washington), resulting in a mean range of 10.53 ft. The daily tidal cycle had a mean length of 24.84 hr. The daily range in water-level fluctuations measured in July and August 2018 in the tide flats, marsh outlet creek and marsh pond were 8, 1.5, and 0.5 ft, respectively. Groundwater-level response to tidal fluctuations in monitoring wells in and near OU-1 was as much as 7.3 ft. The hydraulic diffusivity was estimated as 5.4×10^5 ft^2/d from the attenuation of tidal fluctuations measured in 12 monitoring wells.

The magnitude and distribution of groundwater recharge in the 5.9 mi^2 study area was computed using national spatial datasets and the SWB model using a modified Thornthwaite Mather, soil-water-balance approach at daily time steps for the period 1980 to 2015. The daily recharge rates were calculated on a 25-ft grid, summed and averaged to obtain spatially distributed, mean-annual recharge rates that reflect the spatial distribution of land cover and soil properties in the study area. The average recharge rate computed for the study area was 16.7 in/yr.

Constant-Density Groundwater-Flow Simulation

Three-dimensional (3D), constant-density groundwater flow in the 5.9 mi^2 study area was simulated using MODFLOW-2005 and MODFLOW-NWT models run alternately in an iterative sequence: a combined steady-state and transient simulation using MODFLOW-2005 followed by a steady-state simulation using MODFLOW-NWT. The HUF2 package was employed to represent the discontinuous hydrogeologic units beneath OU-1 in MODFLOW-2005, a program that requires the aquifer system to be treated as confined to obtain a numerical solution for hydraulic head in the study area, where steep slopes in the uplands transition abruptly to the level topography of the lowlands. In contrast, the MODFLOW-NWT program (which does not support the HUF2 package) can better simulate the transition in hydraulic head from the uplands to the lowlands while treating the aquifer system as unconfined and computes underflow from the uplands using a more realistic value of saturated thickness than does MODFLOW-2005. The water table computed by the MODFLOW-NWT simulation was used to specify as inactive the model cells in the MODFLOW-2005 simulation that were above the simulated water table, thereby reducing the simulated saturated thickness in the confined simulation.

The 3D groundwater-flow model encompasses a 5.9 mi^2 area that is divided into a variably spaced grid with 15 model layers, 120 rows, and 88 columns; cell widths ranged from 25 ft near OU-1 to 500 ft near model boundaries. The bottom 4 model layers correspond to 4 hydrogeologic units from the Clover Park Aquitard (Unit 7; QC1) to the sea-level aquifer (Unit 10; QA1), while 10 model layers represent the Quaternary Vashon Stade (Qv) or younger deposits. These Qv sediments were subdivided into 10 model layers to better represent flow through the surficial sediments beneath OU-1. The top model layer represents surface water. The thicknesses of the 10 model layers representing Qv sediments are equal within each vertical stack of model cells, and the mapping of hydraulic properties of the hydrogeologic units to model layers was computed using the HUF2 package.

The 3D groundwater-flow simulation included a steady-state period that provided initial conditions to a 31-day transient period that represented 30 tidal cycles. Tidal fluctuations in Dogfish and Liberty Bays and Port Orchard were approximated by a trapezoidal function with a period of 1.035 days that ranged from a single low-tide stage to a high-tide stage (the respective means of the low-low and high-high tides predicted for Liberty Bay at Poulsbo, Washington, in 2017), corrected for the specific gravity of seawater. The mean tide predicted for 2017 was specified for the model boundary during the steady-state period. Water levels specified in the tide flats were the same as in Dogfish Bay, with the exception of low tide when the water level was specified as the elevation of the sill connecting the two water bodies (0.3 ft). Water levels in the marsh pond and its outlet were specified as the average high, low and mean levels measured during July and August 2018.

Keyport model boundaries coincide with the model grid of the 3D Kitsap groundwater-flow model of Frans and Olsen (2016), and hydraulic heads and flow rates computed by the Kitsap model were used to set head and flow boundaries in the Keyport model. Hydraulic heads were specified at model boundaries in model layers 13 and 15 representing the permeable interbeds within the Clover Park Aquitard (Unit 8; QC1pi) and the sea-level aquifer (Unit 10; QA1), respectively, and vertical flows exchanged between the sea-level aquifer and deeper model layers in the Kitsap model were specified in model layer 15. Hydraulic heads were specified along southern and western boundaries in a single model layer within the Qv sediments. The elevation and head were computed as the top of the Clover Park Aquitard (Unit 7; QC1) plus one-third of the thickness of the Qv sediments to maintain the simulated water table below land surface. Hydraulic heads corresponding to the high, low and mean tide stages were also specified in model layer 1 along the northern and eastern boundaries where the model domain intersects Liberty Bay and Port Orchard.

The Drain (DRN) package was used to represent groundwater discharge to surface water at land surface, including perennial streams, seeps in the uplands and wet areas in the lowlands. Groundwater withdrawals from wells in model layers 15 (Unit 10; QA1) and 13 (Unit 8; QC1pi) were represented with the Well (WEL) package. Groundwater withdrawals from shallow domestic wells screened in Qv sediments and infiltration from domestic septic systems were accounted for by representing the net outflow (withdrawals minus infiltration) in the estimated recharge values. Recharge computed by the SWB model was applied to model layer 2 with the Recharge (RCH) package, and the model domain was divided into five areas to adjust the recharge values during model calibration, including a coarse-grained area, three fine-grained (Unit 3; Qvt) areas, and an area where the Clover Park Aquitard (Unit 7; QC1) is present at land surface.

Two alternative models (A and B) with differing storage properties were constructed to assess the ramifications of representing changes in storage from the fluctuating water table near OU-1 with a confined numerical model. An S_s value of 2.0×10^{-6} ft^{-1} was assigned to all hydrogeologic units in Model A, while in Model B, the S_s value of the uppermost Unit 1 (Qvr sediments) was increased to 0.1 to approximate an unconfined storage value associated with specific yield. A multiplicative scaling factor based on the Qvr unit thickness was applied in Model B to reduce the S_s values where Unit 1 spanned multiple model layers. Unconfined storage near the water table at OU-1 was underestimated in Model A and overestimated in Model B.

Both groundwater-flow models were calibrated by adjusting values of hydraulic properties and recharge to match 99 observations of four types of data: groundwater levels (69), water-level fluctuations in wells in response to tides (26), vertical hydraulic gradients (3), and streamflow (1). In addition, pseudo water-table altitudes computed by the MODFLOW-NWT simulation were specified as observations at 24 locations in the uplands. A subset of 15 of the 24 parameter values specified in the model were estimated through nonlinear regression using UCODE, while values for the remaining 9 parameters were assigned by trial and error or taken from the literature. Weights assigned to observations included in the regression were chosen to account for differences in units or ranges of measurements and adjusted such that the observations were weighted equally. Parameter values were initially estimated in a confined transient simulation using MODFLOW-2005 and then updated in an unconfined steady-state simulation using MODFLOW-NWT. The water table computed by the MODFLOW-NWT simulation was then used to update inactive model cells in the MODFLOW-2005 simulation, and parameter estimation was then reapplied to the MODFLOW-2005 simulation. This procedure was continued until the volumetric water budgets of both simulations were nearly equal.

Coefficients of variation (CV) for 8 of 15 estimated parameters were less than 100 percent in Model A, indicating that the regression was relatively sensitive to these parameters. Estimated hydraulic conductivity values for the coarse-grained, permeable Qv sediments (Units 1, 4, and 6; Qvr, Qva and Qvinter) ranged from 0.9 to 1.7 ft/d, slightly lower than the geometric mean values (3.3–4.1 ft/d) computed from 25 slug tests. Estimated hydraulic conductivity values for Unit 2

(Qmarsh) and Unit 3 (Qvt) were one order of magnitude lower than for the permeable units, and the estimated hydraulic conductivity for Unit 2 (Qestuary) was 1 ft/d. The hydraulic conductivity in the till recharge area delineated around a small knoll in the lower part of the uplands southwest of the Keyport Peninsula was estimated as 10 ft/d, indicating that more permeable units occur in this area than those mapped by the hydrogeologic model.

SWB recharge rates were reduced during nonlinear regression by factors of 0.65 for coarse-grained sediments, 0.22 and 0.17 for Unit 3 (Qvt) in the uplands and lowlands, respectively, and 0.1 for the small knoll in the uplands. The average recharge rate in the model domain was 4.2 in/yr, much less than the average rate of 16.7 in/yr computed with the SWB Model But comparable to recharge rates (4 in/yr) estimated for the northern part of the Kitsap groundwater-flow model domain. The lower recharge rates estimated by nonlinear regression suggest that the SWB model overestimates recharge to the groundwater in uplands where relatively permeable soils at land surface are underlain by much lower permeability sediments at depth. In these areas infiltration through the soil profile likely discharges as interflow to local drainage, rather than to the groundwater-flow system.

The CVs for 8 of the 16 parameters estimated with Model B were less than 100 percent, but half of these parameters had CV values greater than or equal to 90 percent. Estimated *K* values for Units 1, 2, and 6 (Qvr, Qestuary and Qvinter) were higher than in Model A (ranging from 3.0 to 19 ft/d), while *K* values Unit 3 (Qvt) were an order of magnitude less. Values for vertical anisotropy were estimated for Units 2, 3, and 5 (Qm, Qvt and Qvsemi) and were higher for Units 3 and 5, and lower for Unit 2 than in Model A. The average recharge rate in Model B was 7.3 in/yr, slightly less than half the SWB recharge rate, and 60 percent higher than in Model A.

The standard error in model fit in Model A is 7.8 ft for groundwater levels (13 percent of the 60-ft measurement range), 1.0 ft for water-level fluctuations (14 percent of the 7.3-ft measurement range), and 11.3 ft for pseudo water-table altitudes (4 percent of the 320-ft measurement range). The corresponding numbers for Model B are 7.6 ft and 11.2 ft for groundwater levels and pseudo water-table altitudes and 1.3 ft in water-level fluctuations because the higher storage values dampen the response to tidal fluctuations. Residual plots indicate little bias in water-level fluctuations in Model A, but offsetting biases in water levels (overestimated) and pseudo water-table altitudes (underestimated). Biases in Model B are similar, but there is a distinct bias towards under estimating water-level fluctuations The directions of the three vertical hydraulic-gradient observations were simulated correctly in both models, with errors ranging from 25 to 66 percent, while the simulated streamflow for a perennial stream (0.18 ft^3/s) was 70 percent less than the measured value in Model A and 40 percent less in Model B.

The hydraulic-head distribution simulated by both groundwater-flow models for the steady-state period indicates that OU-1 is just north of a regional discharge area that limits groundwater flow from the landfill toward uplands south and west of the tide flats and the marsh, and that the Clover Park Aquitard (Unit 7, QC1) is a hydraulic barrier limiting flow from the Qv sediments to and from the deeper hydrogeologic units. Vertical groundwater flow is generally at least an order of magnitude less than horizontal flow and downward beneath the uplands and upward beneath Keyport Peninsula, Dogfish and Liberty Bays, and Port Orchard.

Variable-Density Groundwater Flow and Contaminant-Transport Simulations

Two SEAWAT simulations of steady-state, variable-density flow and transient solute transport were conducted for models A and B in a 1.3 mi^2 transport domain surrounding the Keyport Peninsula. The first 5,000-yr simulation used a single solute (seawater) to establish the initial distribution of seawater in the second 50-yr simulation that consisted of two solutes, seawater and CVOCs. Both simulations used the same model design and parameter distributions as in the MODFLOW-2005 groundwater-flow model. The transport-model domain extends from surface water (model layer 1) to the upper part of the Clover Park Aquitard (Unit 7, QC1, model layer 12). A porosity value of 0.2 was specified for all hydrogeologic units. Longitudinal dispersivity was spatially distributed and proportional to the grid cell size (with a maximum value of 50 ft), and horizontal-transverse and vertical-transverse dispersivities were specified as ratios to the longitudinal dispersivity (0.1 and 0.01, respectively).

Seawater concentrations in both single- and dual-solute simulations ranged from 0 percent for fresh water (specific gravity 1.0) to 100 percent for seawater (specific gravity 1.022) in surface-water bodies. Constant-concentration boundaries of 100 percent were specified in model layer 1 to represent Dogfish and Liberty Bays, the tide flats and Port Orchard. An implicit finite-difference (FD) method with upstream weighting was used to solve the advection-dispersion equation in the single-solute simulation to allow the use of large time steps (up to 100 days) in the 5,000-year simulation. The mass of seawater increased rapidly at the beginning of both single-solute transport simulations, but then gradually near the end and asymptotically approached limits of 2.8×10^9 kg in Model A and 3.1×10^9 kg in Model B. The transition zone between fresh water and seawater near the tide flats west of OU-1 was about 100 ft wide in Model A and 125 ft wide in Model B and extended to the bottom of the Qv sediments. Saline water overlies fresh water at shallow depths in this area where groundwater in the deeper, permeable Qv sediments discharges into seawater.

Inflow of CVOCs within the former landfill at OU-1 was represented in the dual-solute simulations by using mass-loading rates (MT^{-1}) to depict total CVOC concentrations (TCE, *cis*-DCE, and VC) at different depths at seven persistent contaminant sources. The mass-loading rates were adjusted to reproduce the maximum observed CVOC concentrations in

2017. The expected biodegradation of CVOCs was initially neglected in the transport simulations, with the understanding that a considerable portion of the CVOCs generated through mass loading would be biodegraded to ethene and not discharge with groundwater at downgradient boundaries, as predicted by the simulations. The goals of the transport simulations were to reproduce the observed configuration of the CVOCs plume and to estimate the mass-loading rates of CVOCs and the total mass of CVOCs in groundwater. The total-variation-diminishing (TVD) method with a Courant number of 1.0 was used to solve the advection-dispersion equation in the dual-solute simulation to minimize numerical dispersion while using small time steps (0.5 days) in the 50-yr simulation.

The mass of CVOCs beneath OU-1 increased rapidly at the beginning of the dual-solute simulation with Model A, then increased gradually and approached a dynamic equilibrium with a contaminant mass of 256 kg. Almost all the contaminant mass (134 g/d) discharged to small creeks draining the southern edge of OU-1, while the remainder discharged to the marsh pond and creek (1.7 g/d) and the tide flats (49 mg/d). The CVOC mass-loading rate was 150 g/d, within the range of biodegradation rates of 130 to 170 g/d estimated by Dinicola (2006). The CVOC mass was 310 kg in Model B, but the mass-loading rate is only 73 g/d because there is a lower volume of groundwater flow in the deeper Qv sediments than in Model A, due to the higher vertical anisotropy in Unit 5 (Qvsemi). As a result, less CVOC mass (48 g/d) discharges to the small creeks draining the southern edge of OU-1. More CVOC mass discharges to the marsh pond and creek (7.8 g/d) and the tide flats (160 mg/d), however, because contaminant plumes are diverted westward in Model B to Dogfish Bay by the higher *K* values in Unit 2 (Qestuary).

Two distinct contaminant plumes were simulated in Model A: a northern plume with 30 percent of the contaminant mass that migrates toward the marsh pond and creek and a southern plume with 70 percent of the contaminant mass that migrates toward small creeks south of OU-1. Both CVOC plumes extend from the water table to the bottom of the Qv sediments where they migrate laterally and upward to discharge in the marsh and creeks. The northern plume extends beneath the tide flats where it mixes with higher-density saline water, which presents a hydraulic barrier that limits the upward discharge of CVOCs to the tide flats. The contaminant plumes emanating from two persistent sources intermingle in Model B and become indistinguishable downgradient, but contaminant data are lacking to determine whether either the two distinct plumes predicted by Model A, or the single plume predicted by Model B more accurately depicts actual CVOC migration at OU-1.

Discussion of Simulation Results

Results of groundwater-flow and contaminant-transport simulations with both models A and B indicate that geologic and hydraulic barriers limit the migration of CVOCs from the former landfill at OU-1 and contain the CVOC plumes on Naval Base Kitsap. The Clover Park Aquitard is a low-permeability geologic barrier that limits vertical groundwater flow between shallow, contaminated Qv sediments at OU-1 and deeper hydrogeologic units. In addition, hydraulic barriers limit downward migration of CVOCs through the Clover Park Aquitard and lateral migration of CVOCs into upland areas south of the Keyport Peninsula. Finally, saline water beneath the tide flats and in Dogfish and Liberty Bays limits westward CVOC migration toward residential wells on Virginia Point.

Uncertainty in the rates of recharge and groundwater flow produces uncertainty in the estimated mass-loading rate of CVOCs at OU-1. Higher rates of recharge and groundwater flow require larger mass-loading rates to maintain a stable configuration of the contaminant plume. The lower mass-loading rate in Model B (73 g/d), however, indicates that higher vertical anisotropy can restrict groundwater flow rates through deeper Qv sediments beneath OU-1. The estimated CVOC mass-loading rate, therefore, ranges from 73 to 240 g/d. Although the contaminants 1,4-dioxane and vinyl chloride have been detected at low concentrations on the State Route 308 causeway northwest of the tide flats, neither Model A nor B predicted groundwater flow or contaminant transport from OU-1 to this area. There is uncertainty as to whether the contaminants measured in this area originated in the landfill or elsewhere.

Previous studies established that reductive dechlorination of CVOCs is occurring at OU-1 with biodegradation rates ranging from 130 to 170 g/d. A first-order, removal rate-constant of 10^{-3} d^{-1} was computed from CVOC contaminant masses computed by the transport simulations of models A and B and the biodegradation rate (150 g/d) estimated by Dinicola (2006). An alternate 50-yr, dual-solute contaminant-transport simulation with Model A and a first-order reaction predicted that a stable 77-kg CVOC plume formed within 10 years of migration, using the same mass-loading rates as in the original transport simulation. One half the CVOC mass was lost through biodegradation (75 g/d), and nearly all the remainder (71 g/d) was discharged by the southern plume to a small creek south of OU-1. The CVOC mass discharged from the northern plume to the marsh and tide flats was 0.95 mg/d. The areas of the northern and southern plumes were 67 percent and 32 percent less, respectively, than the areas computed by the original transport simulation.

Both models A and B provide an adequate fit to hydraulic and contaminant data, but additional data are required to determine which model more accurately predicts actual contaminant migration at OU-1. Both models predict similar contaminant masses and biodegradation rate constants and also predict that contaminant migration is limited by the same geologic and hydraulic barriers. Model predictions differ in terms of the hydraulic parameters (recharge rates, and horizontal and vertical hydraulic conductivities), and in the CVOC mass-loading rates and contaminant plume configurations. Model B better represents the effects of tidal fluctuations on unconfined storage, uses recharge rates closer to the SWB estimated rates, and predicts water-table altitudes below land surface near OU-1. Model A better predicts the groundwater-level response to tidal fluctuations, however, and was chosen to demonstrate the effects representation of tidal fluctuations and potential remedial activities, although the effects would be the same if Model B were chosen instead. A soon-to-be-released version of MODFLOW 6 that supports variable-density flow and contaminant transport, and the distribution of discontinuous hydrogeologic units with the NWT solver would better represent unconfined and confined storage and greatly simplify the simulation of groundwater and contaminant transport at OU-1.

Two alternate 50-yr, contaminant-transport simulations assessed the sensitivity of predicted CVOC migration from OU-1 to the depiction of tidal fluctuations in the original transport simulation with Model A. In steady-state simulation C, which used the TVD solver, mean tides were lowered by 1.2 ft in Dogfish and Liberty Bays, 0.87 ft in the tide flats, and 0.1 ft in Marsh Creek (the averages of water levels measured during the 31-day period in July and August 2018). In transient simulation D, the FD solver was applied to compute 600 repetitions of the 31.05-day transient periods that represented diurnal tidal fluctuations used for calibration of the groundwater-flow model.

Both alternative representations of tidal fluctuations in simulations C and D had a small effect on the sizes and masses of the simulated CVOC plumes, when compared with the results of the original, steady-state TVD and FD simulations with Model A. The lower high and low tide stages in simulation C predicted larger CVOC plumes (272 kg) than in the original TVD simulation. The northern CVOC plume extended about 100 ft farther under the tide flats and CVOC discharge to the tide flats increased (from 49 to 890 mg/d) and CVOC discharge to Marsh Creek and pond decreased (from 1,700 to 770 mg/d). Representation of transient tidal fluctuations in simulation D predicted smaller CVOC plumes (297 kg), and the northern CVOC plume extended about 75 ft farther under the tide flats. The CVOC discharge to the tide flats increased (from 67 mg/d to 75 mg/d), and the width of the transition zone between fresh water and seawater north of the marsh also increased (from 100 ft to 125 ft). The effect of tidal fluctuations on the predicted CVOC plumes is small because the period of the fluctuations (6 hr) is rapid compared with the groundwater velocity (20 ft/yr) beneath OU-1, and tidal fluctuations only slightly alter groundwater-flow paths and lengthen the northern CVOC plume under the tide flats.

Three 50-yr, steady-state contaminant-transport simulations with Model A predicted the effects of potential source-control scenarios on the contaminant plumes by reducing CVOC mass-loading rates by factors of 50, 90, and 99 percent, respectively. Under each scenario, the mass of CVOCs decreased rapidly and then slowly approached a new dynamic equilibrium. The reductions of CVOC mass in groundwater were 46, 86, and 95 percent, respectively, but sizes of the contaminant plumes were largely unchanged.

References Cited

Anderman, E.R., and Hill, M.C., 2000, MODFLOW-2000, the U.S. Geological Survey Modular Ground-Water Model—Documentation of the Hydrogeologic-Unit Flow (HUF) Package: U.S. Geological Survey Open-File Report 00–342, 89 p. [Also available at https://doi.org/10.3133/ofr00342.]

Battelle Memorial Institute, 2018, 2017 Site recharacterization, Phase II, Operable Unit 1, Naval Base Kitsap, Keyport, Washington: Prepared by Battelle Memorial Institute, Columbus, Ohio for Naval Facilities Engineering Command Northwest, Silverdale, Wash., variously paged.

Collias, E.E., McGary, Noel, and Barnes, C.A., 1974, Atlas of physical and chemical properties of Puget Sound and its approaches: Seattle, Wash. and London, Washington Sea Grant Publication distributed by the University of Washington Press, 235 p.

Department of the Navy, 1993, Remedial Investigation Report, NUWC Keyport: Prepared by URS Consultants and Science Applications International Corporation for EFA NW under CLEAN Contract No. N62474-89-D-9295, CTO 10.

Department of the Navy, 2015, Fourth Five-Year Review, Naval Base Kitsap, Keyport, Washington—Prepared by Naval Facilities Engineering Command Northwest: Washington, Silverdale, 444 p.

Dinicola, R.S., Cox, S.E., Landmeyer, J.E., and Bradley, P.M., 2002, Natural attenuation of chlorinated volatile organic compounds in ground water at Operable Unit 1, Naval Undersea Warfare Center, Division Keyport, Washington: U.S. Geological Survey Water-Resources Investigations Report 2002–4119, 115 p. [Also available at https://pubs.er.usgs.gov/publication/wri024119.]

Dinicola, R.S., 2006, Continued biodegradation of chloroethene compounds in ground water at Operable Unit 1, Naval Undersea Warfare Center, Division Keyport, Washington: U.S. Geological Survey Scientific Investigations Report 2006–5056, 42 p. [Also available at https://doi.org/10.3133/sir20065056]

Frans, L.M., and Olsen, T.D., 2016, Numerical simulation of the groundwater-flow system of the Kitsap Peninsula, west-central Washington (ver. 1.1, October 2016): U.S. Geological Survey Scientific Investigations Report 2016–5052, 63 p. [Also available at https://pubs.er.usgs.gov/publication/sir20165052.]

Garling, M.E., Molenaar, Dee, and others, 1965, Water resources and geology of the Kitsap Peninsula and certain adjacent islands: Olympia, Washington, Washington Department of Conservation, Washington Division of Water Resources Water-Supply Bulletin 18, 309 p.

Gelhar, L.W., Welty, C., and Rehfeldt, K.W., 1992, A critical review of data on field-scale dispersion in aquifers: Water Resources Research, v. 28, no. 7, p. 1955–1974, https://doi.org/10.1029/92WR00607.

Gendaszek, A.S., and Welch, W.B., 2018, Water budget of the upper Chehalis River Basin, southwestern Washington: U.S. Geological Survey Scientific Investigations Report 2018–5084, 17 p. [Also available at https://doi.org/10.3133/sir20185084.]

Harbaugh, A.W., Banta, E.R., Hill, M.C., and McDonald, M.G., 2000, MODFLOW-2000, the U.S. Geological Survey modular ground-water model—User guide to modularization concepts and the ground-water flow process: U.S. Geological Survey Open-File Report 00–92, 121 p. [Also available at https://doi.org/10.3133/ofr200092.]

Harbaugh, A.W., 2005, MODFLOW-2005, The U.S. Geological Survey modular ground-water model—the Ground-Water Flow Process: U.S. Geological Survey Techniques and Methods 6–A16, variously paged. [Also available at https://pubs.usgs.gov/tm/2005/tm6A16/.]

Hargreaves, G.H., and Samani, Z.A., and the George H. Hargreaves, and the Zohrab A. Samani, 1985, Reference crop evapotranspiration from temperature: Applied Engineering in Agriculture, v. 1, no. 2, p. 96–99, https://doi.org/10.13031/2013.26773.

Headman, A.O, 2020, Soil water balance (SWB) model of Keyport, Washington: U.S. Geological Survey data release, https://doi.org/10.5066/P95WQ7TM.

Jones, M.A., 1999, Geologic framework of the Puget Sound aquifer system, Washington and British Columbia: U.S. Geological Survey Professional Paper 1424–C, 31 p. [Also available at https://doi.org/10.3133/pp1424C.]

La Licata, I., Langevin, C.D., and Dausman, A.M., 2007, Effect of tidal fluctuations on contaminant transfer to the ocean: A New Focus on Groundwater–Seawater Interactions, Proceedings of Symposium HS1001 at IUGG2007, Perugia, July 2007, IAHS Publ. 312, 2007.

Langevin, C.D., Thorne, D.T., Jr., Dausman, A.M., Sukop, M.C., and Guo, Weixing, 2007, SEAWAT Version 4—A computer program for simulation of multi-species solute and heat transport: U.S. Geological Survey Techniques and Methods, book 6, chap. A22, 39 p. [Also available at https://pubs.er.usgs.gov/publication/tm6A22.]

Keller, C.K., van der Kamp, G., and Cherry, J.A., 1989, A multiscale study of the permeability of a thick clayey till: Water Resources Research, v. 25, no. 11, p. 2299–2317, https://doi.org/10.1029/WR025i011p02299.

Miller, D.A., and White, R.A., 1998, A conterminous United States multilayer soil characteristics dataset for regional climate and hydrology modeling: Earth Interactions, v. 2, no. 2, p. 1–26, https://doi.org/10.1175/1087-3562(1998)002<0001:ACUSMS>2.3.CO;2.

Niswonger, R.G., Panday, Sorab, and Ibaraki, Motomu, 2011, MODFLOW-NWT, A Newton formulation for MODFLOW-2005: U.S. Geological Survey Techniques and Methods 6–A37, 44 p. [Also available at https://pubs.usgs.gov/tm/tm6a37/.]

National Oceanic and Atmospheric Administration, 2018, Tides and currents: National Oceanic and Atmospheric Administration, web, accessed August 2018 at https://tidesandcurrents.noaa.gov/noaatidepredictions.html?id=9445719&units=standard&bdate=20180712&edate=20180808&timezone=LST/LDT&clock=12hour&datum=MLLW&interval=hilo&action=data.

Opatz, C.C., and Dinicola, R.S., 2019, Analysis of groundwater response to tidal fluctuations, Operable Unit 1, Naval Base Kitsap, Keyport, Washington: U.S. Geological Survey Open-File Report 2019–1098, 36 p. [Also available at https://doi.org/10.3133/ofr20191098.]

Poeter, E.P., and Hill, M.C., 1998, Documentation of UCODE, a computer code for universal inverse modeling: U.S. Geological Survey Water-Resources Investigations Report 98–4080, 116 p.

U.S. Geological Survey, 2014, Hydrography—National hydrography dataset, watershed boundary dataset: U.S. Geological Survey Web site, accessed August 27, 2018, at https://nhd.usgs.gov/index.html

URS Consultants Inc, 1997, Final summary data assessment report for Operable Unit 1 Naval Undersea Warfare Center Division Keyport, Washington—Prepared by URS Consultants, Seattle, Washington, for Engineering Field Activity 3 vols: Poulsbo, WA, Northwest, Naval Facilities Engineering Command.

URS Consultants Inc, 1998, Final record of decision for Operable Unit 1 Naval Undersea Warfare Center Division Keyport, Washington—Prepared by URS Consultants, Seattle, Wash., for Engineering Field Activity: Poulsbo, Wash., Northwest, Naval Facilities Engineering Command, 111 p.

Vaccaro, J.J., Hansen, A.J., Jr., and Jones, M.A., 1998, Hydrogeologic framework of the Puget Sound aquifer system, Washington and British Columbia: U.S. Geological Survey Professional Paper 1424–D, 77 p. [Also available at https://doi.org/10.3133/pp1424D

Welch, W.B., Frans, L.M., and Olsen, T.D., 2014, Hydrogeologic framework, groundwater movement, and water budget of the Kitsap Peninsula, west-central Washington: U.S. Geological Survey Scientific Investigations Report 2014–5106, 44 p. [Also available at https://doi.org/10.3133/sir20145106.]

Westenbroek, S.M., Kelson, V.A., Dripps, W.R., Hunt, R.J., and Bradbury, K.R., 2010, SWB—A modified Thornthwaite-Mather soil-water balance code for estimating groundwater recharge: U.S. Geological Survey Techniques and Methods, book 6, chap. A31, 60 p. [Also available at https://pubs.usgs.gov/tm/tm6-a31/.]

Wilson, J.T., Kampbell, D.H., and Weaver, J.W., 1996: Environmental chemistry and the kinetics of biotransformation of chlorinated organic compounds in ground water, in U.S. Environmental Protection Agency, Symposium in natural attenuation of chlorinated organics in ground waters, September 11–13, 1996: Dallas, Texas, EPA/540/R-96/509.

Yager, R.M., and Fountain, J.C., 2001, Effect of natural gas exsolution on specific storage in a confined aquifer undergoing water level decline: Ground Water, v. 39, no. 4, p. 517–525. https://doi.org/10.1111/j.1745-6584.2001.tb02340.x.

Yager, R.M., and Kappel, W.M., 1998, Infiltration and hydraulic connections from the Niagara River to a fractured-dolomite aquifer in Niagara Falls, New York: Journal of Hydrology (Amsterdam), v. 206, no. 1-2, p. 84–97, https://doi.org/10.1016/S0022-1694(98)00088-2.

Yager, R.M., 2020, MODFLOW-2005, MODFLOW-NWT, and S EAWAT V.4 models used to simulate variable-density groundwater flow and contaminant transport at Naval Base Kitsap, Keyport, Washington: U.S. Geological Survey data release, https://doi.org/10.5066/P9YNPPNL.

Zheng, Chunmiao, and Bennett, G.D., 2002, Applied contaminant transport modeling: John Wiley and Sons, Inc., New York, 621 p.

Zheng, C., and Wang, P.P., 1999, MT3DMS—A modular three-dimensional multispecies transport model for simulation of advection, dispersion and chemical reactions of contaminants in ground-water systems–Documentation and user's guide: U.S. Army Corps of Engineers Contract Report SERDP-99-1.

Appendix 1. Soil-Water Balance (SWB) Model

The Soil-Water-Balance (SWB) computer program (Westenbroek and others, 2010) provides estimates for groundwater recharge by calculating water-balance components at daily time steps for each model cell using a modified Thornthwaite Mather soil-water-balance approach. The model documented in this report utilizes SWB ver1.2. The model input, output, and executable files are available from Headman (2020).

Soil-Water Balance (SWB) Model Spatially Distributed Datasets

Five spatially distributed (gridded) datasets were used in the SWB recharge simulations. All datasets were in ASCII format (with the exception of the climate data, which was in NetCDF format), and cover the 5.9 mi2 study area with a uniform cell size of 25 ft. The input datasets include daily climate data (precipitation, maximum and minimum air temperature), land cover, flow direction, hydrologic soil group and available soil-water capacity (table 1.1).

Daily Climate Data

Daily climate data required for the SWB recharge calculation include precipitation (inches) and maximum and minimum temperature (Fahrenheit). Daily evapotranspiration is computed using the method of Hargreaves and Samani (1985). Daily climate data were obtained from the Daymet dataset available from Oak Ridge National Laboratory (http://daymet.ornl.gov). The Daymet climate data is computed through interpolation from spatially referenced observation stations and available in 2-degree areas at a resolution of 0.62 mi for all of North America. Daily Daymet climate data were obtained for the study area for the period 1980 through 2015.

Land Cover

The 2011 National Land Cover Database (NLCD; Homer and others, 2015) was used to characterize land cover for the study area (table 1.2). The NLCD is produced by the Multi-Resolution Land Characteristics consortium (http://www.mrlc.gov) to describe land-cover characteristics across the United States using a 16-class classification schema at a resolution of 100 ft. The NLCD was obtained from https://www.mrlc.gov/nlcd11_data.php using an Albers Conical Equal Area projection (NAD83). The NLCD data was resampled to the 25-ft cell size of the SWB model using a

Table 1.1. Spatial data assigned to parameters in the soil-water balance model for Keyport study area.

[NLCD, National Land Cover Database; STATSGO, State Soil Geographic Database; ft, feet; --, not applicable (vector data)]

Type	Data source	Resolution	Soil-water balance parameters
Land Cover	NLCD 20111	100 ft	Land Cover
Soils	gSSURGO2 or STATSGO23	–	Runoff Curve number
			Root depth
			Maximum Recharge
			Available Water Capacity
Flow Direction	Puget Sound LiDAR	6 ft	D8 Flow Direction
Climate	Daymet	0.62 mi	Temperature
			Precipitation
			Evapotranspiration

[1]Homer and others (2015).

[2]National Resources Conservation Service, 2018

[3]Miller and White (1998).

Table 1.2. Distribution of land cover in the Keyport study area in 2011.

[mi², square mile]

Land use code	Description	Area (mi²)	Percentage of study area
11	Open water	1.85	31.3
21	Developed, open space	1.06	17.8
22	Developed, low intensity	0.64	10.9
23	Developed, medium intensity	0.16	2.7
24	Developed, high intensity	0.10	1.7
31	Barren land	0.15	2.5
41	Deciduous forest	0.49	8.3
42	Evergreen forest	0.45	7.6
43	Mixed forest	0.56	9.5
52	Shrub and scrub	0.07	1.1
71	Grassland/herbaceous	0.04	0.7
81	Pasture/hay	0.04	0.7
90	Woody wetlands	0.14	2.4
95	Emergent herbaceous wetlands	0.15	2.6

majority sampling technique in ArcGIS. A comparison of the two gridded datasets indicates that the spatial pattern for the principal land-cover classes in the study area is similar. Most of the land area is either developed or covered by forest.

Flow Direction

A flow-direction grid to route surface runoff between SWB model cells used the D8 flow-routing convention of Lehner and others (2008). The flow-direction grid was generated from Lidar elevation data at a 6 ft resolution obtained from Puget Sound Lidar (http://pugetsoundlidar.ess.washington.edu/). Individual Lidar files were combined and resampled to the 25-ft cell size of the SWB model using a majority sampling technique in ArcGIS. The resulting elevation grid was processed to smooth over small sinks that were artifacts of data processing and the D8 flow-direction grid was then generated with the ArcGIS "flow direction" tool.

Hydrologic Soil Group and Available Soil-Water Capacity

Two gridded datasets of soil properties, hydrologic soil group (HSG) and available water capacity (AWC), are required for the SWB model. HSG and AWC data are compiled by the U.S. Department of Agriculture Natural Resource Conservation Service (NRCS) for the entire United States. NRCS classifies HSGs in four groups (A, B, C and D) on a continuum from high infiltration capacity with low runoff potential to low infiltration capacity with high runoff potential. AWC is the amount of water a particular soil column can hold at various depths; the AWC for the top meter of soil was used for the SWB model described in this report. Data for HSG and AWC were mostly obtained from the NRCS Gridded Soil Survey Geographic (gSSURGO) database (National Resources Conservation Service, 2018). Some areas for which gSSURGO data were not available used the NRCS State Soil Geographic (STATSGO2) database (Miller and White, 1998). HSG and AWC grids were resampled to 25-ft cells using the majority technique for HSG data and the mean sampling technique for AWC data.

Tabular Input Datasets

Tabular information, which includes runoff curve numbers, vegetation routing depths, maximum infiltration rates, and maximum daily recharge rates, are also required for SWB model for each combination of HSG and Land Cover type. The table was populated with values used by Gendaszek and Welch (2018), Tillman (2015) and Westenbroek (2010) (table 1.3).

Table 1.3. Tabular data for soil-water balance (SWB) model of Keyport study area.

Land use code	Description	Impervious area (percent)	Curve numbers				Maximum recharge rate (inches/day)				Interception		Root zone depth (ft)			
			A[1]	B[1]	C[1]	D[1]	A[1]	B[1]	C[1]	D[1]	Growing season	Non-growing season	A[1]	B[1]	C[1]	D[1]
11	Open Water	0	100	100	100	100	2	0.6	0.12	0.24	0	0	0	0	0	0
21	Developed, Open Space	0	49	69	79	84	2	0.6	0.12	0.24	0.0835	0	8.53	8.53	8.53	8.53
22	Developed, Low Intensity	30	77	86	91	94	2	0.6	0.12	0.24	0.0835	0	8.53	8.53	8.53	8.53
23	Developed, Medium Intensity	60	89	92	94	95	2	0.6	0.12	0.24	0.0835	0	8.53	8.53	8.53	8.53
24	Developed, High Intensity	90	98	98	98	98	2	0.6	0.12	0.24	0.0835	0	8.53	8.53	8.53	8.53
31	Barren Land	0	77	86	91	94	2	0.6	0.12	0.24	0	0	1	1	1	1
41	Deciduous Forest	0	32	48	57	63	2	0.6	0.12	0.24	0.0835	0	9.5	9.5	9.5	9.5
42	Evergreen Forest	0	39	58	73	80	2	0.6	0.12	0.24	0.0835	0	12.8	12.8	12.8	12.8
43	Mixed Forest	0	46	60	68	74	2	0.6	0.12	0.24	0.0835	0	11.15	11.15	11.15	11.15
52	Shrub/Scrub	0	49	68	79	84	2	0.6	0.12	0.24	0.0835	0	3.5	3.5	3.5	3.5
71	Grassland/Herbaceous arid	0	64	71	81	89	2	0.6	0.12	0.24	0.0835	0	8.53	8.53	8.53	8.53
81	Pasture/Hay fair	0	49	69	79	84	2	0.6	0.12	0.24	0.0835	0	8.53	8.53	8.53	8.53
82	Cultivated Crops SR+CR poor	0	71	80	87	90	2	0.6	0.12	0.24	0.0835	0	2	2	2	2
90	Woody Wetlands	0	88	89	90	91	2	0.6	0.12	0.24	0.0835	0	4.5	4.5	4.5	4.5
95	Emergent Herbaceous Wetlands	0	89	90	91	92	2	0.6	0.12	0.24	0	0	4.5	4.5	4.5	4.5

[1]Hydrologic soil group (HSG).

References Cited

Carslaw, H.S., and Jaeger, J.C., 1959, Conduction of heat in solids (2nd ed.): New York, Oxford University Press, 510 p.

Gendaszek, A.S., and Welch, W.B., 2018, Water budget of the upper Chehalis River Basin, southwestern Washington: U.S. Geological Survey Scientific Investigations Report 2018–5084, 17 p. [Also available at https://doi.org/10.3133/sir20185084.]

Hargreaves, G.H., and Samani, Z.A., and the George H. Hargreaves, and the Zohrab A. Samani, 1985, Reference crop evapotranspiration from temperature: Applied Engineering in Agriculture, v. 1, no. 2, p. 96–99, https://doi.org/10.13031/2013.26773.

Headman, A.O, 2020, Soil water balance (SWB) model of Keyport, Washington: U.S. Geological Survey data release, https://doi.org/10.5066/P95WQ7TM.

Homer, C.G., Dewitz, J.A., Yang, L., Jin, S., Danielson, P., Xian, G., Coulston, J., Herold, N.D., Wickham, J.D., and Megown, K., 2015, Completion of the 2011 National Land Cover Database for the conterminous United States—Representing a decade of land cover change information: Photogrammetric Engineering and Remote Sensing, v. 81, no. 5, p. 345–354.

Lehner, B., Verdin, K., and Jarvis, A., 2008, New global hydrography derived from spaceborne elevation data: Eos (Washington, D.C.), v. 89, no. 10, p. 93–94, https://doi.org/10.1029/2008EO100001.

Miller, D.A., and White, R.A., 1998, A conterminous United States multilayer soil characteristics dataset for regional climate and hydrology modeling: Earth Interactions, v. 2, no. 2, p. 1–26, https://doi.org/10.1175/1087-3562(1998)002<0001:ACUSMS>2.3.CO;2.

National Oceanic and Atmospheric Administration, 2020, Tides and currents: National Oceanic and Atmospheric Administration, web.

National Resources Conservation Service, 2018, Web Soil Survey: United States Department of Agriculture, web, accessed March 19, 2018, at https://websoilsurvey.sc.egov.usda.gov/.

Tillman, F.D., 2015, Documentation of input datasets for the soil-water balance groundwater recharge model of the Upper Colorado River Basin: U.S. Geological Survey Open-File Report 2015–1160, 17 p. [Also available at https://doi.org/10.3133/ofr20151160.]

Westenbroek, S.M., Kelson, V.A., Dripps, W.R., Hunt, R.J., and Bradbury, K.R., 2010, SWB—A modified Thornthwaite-Mather soil-water balance code for estimating groundwater recharge: U.S. Geological Survey Techniques and Methods, book 6, chap. A31, 60 p., https://pubs.usgs.gov/tm/tm6-a31/

Publishing support provided by the U.S. Geological SurveyScience Publishing Network, Tacoma Publishing Service Center

For more information concerning the research in this report, contact the
Director, Washington Water Science Center
U.S. Geological Survey
934 Broadway, Suite 300
Tacoma, Washington 98402
https://wa.water.usgs.gov

ISSN 2328-0328 (online)
https://doi.org/10.3133/sir20205066